UNIVERSITÀ DEGLI STUDI DI PALERMO

Dottorato di ricerca in Ingegneria dei Materiali
Dipartimento di Ingegneria Civile, Ambientale, Aerospaziale e dei Materiali
Settore Scientifico Disciplinare: ING-IND 24

AN INTEGRATED TISSUE ENGINEERING APPROACH TO HUMAN BRONCHIAL MODELS: BIODEGRADABLE SCAFFOLD AND MICROFLUIDICS PLATFORM

IL DOTTORE
ING. SALVATORE MONTESANTO

IL COORDINATORE
PROF. ING. MARIO DI PAOLA

IL TUTOR
PROF. ING. VALERIO BRUCATO

CICLO XXIX – 2014/2016.
ANNO CONSEGUIMENTO TITOLO 2016

UNIVERSITÀ DEGLI STUDI DI PALERMO

Dedico questo mio modesto lavoro
Che si pone a conclusione di un lungo e faticoso cammino
Alle persone che nella vita mi hanno sostenuto tanto

mia mamma, mio papà, mia sorella e alla mia futura SPOSA.

Abstract

Tissue engineering is the use of a combination of cells, engineering and materials methods, together with suitable biochemical and physical-chemical factors to improve or replace biological functions of damage/deficient tissues [1, 2]. With this respect polymeric porous structures and microfluidics systems are used for tissue engineering purposes. Biodegradable polymeric scaffolds have been harnessed as temporal structural supports to regenerate various tissues such as bone, cartilage, nerve, ligament, skin and liver. An open porous geometry with interconnected channels is a prerequisite for high density cell growth as well as for a sustained mass transport of nutrients, oxygen, and metabolic waste; as a matter of fact, a high cell density and efficient mass transport contribute to cell viability, proliferation, and ultimate rehabilitation into functional tissues [3-5].

A wide range of biodegradable scaffolds with different morphologies have been fabricated by conventional methods such as solid porogen leaching, gas foaming, emulsion/ freeze drying, expansion in supercritical fluid and phase separation techniques [6,7].

The most widely adopted phase separation techniques are known with the acronyms TIPS (thermally induced phase separation) and DIPS (diffusion induced phase separation). More specifically, the production of polymeric scaffolds and membranes via DIPS has been widely studied and applied for a number of model systems. Various researchers investigated systematically the structure, porosity and crystallization behaviour of poly(L-lactic acid), blend of poly(L-lactic acid)/polyurethane and poly(L-lactic acid)/ polycaprolactone triol membranes, prepared from ethanol/dioxane and ethanol/water coagulation baths via phase separation [8-11], finding interesting correlations between phase behaviour, kinetics of demixing and the resulting membrane morphology. Other authors showed that mechanical properties of foams are mainly controlled by the gas pressure, material properties, manufacturing methods, and cell geometry. With this respect, the geometrical features influencing the mechanical properties were determined: number of open cells, relative foam density, cell size and cell shape [12,13].

A well designed tissue engineering scaffold should provide initial support to the seeded cells, localise the cells in the appropriate spaces, and provide physical and biological cues for adhesion, migration, proliferation, differentiation and eventually formation of model tissues and organs [14-16].

Microfluidic cell culture platforms combine the advantages of miniaturization and real-time microscopic observation with the ability to pattern cell culture substrates [17] to vary the composition of culture medium over space using gradient generators [18], and to create cell culture conditions that are more physiological than those found in other in vitro systems, in terms of nutrients exchange rates and to unable mechanical stimulation [19]. Microfluidic systems can be used as platforms to control and run cell and tissue growth analysis.

In this thesis, the attention is focused on the DIPS process, commonly used for the production of membranes for various applications and scaffolds for tissue engineering purposes. The target system selected in this work is constituted by poly-L-lactic acid (PLLA), dioxane and water. This ternary solution was adopted for the production of both thin membranes scaffolds for tissue engineering and biodegradable mechanical support.

As a first step to the characterization of the system PLLA-dioxane-water, sets of experimental parameters were characterized to obtain skinless membrane. A particular attention was paid to coagulation bath concentration, coagulation bath number, immersion time and drying environment. SEM, DSC and DMA analysis were used to characterize the series of thin membranes obtained changing experimental parameters. The results are in line with those available in literature for similar systems.

As a second step to the application of thin membranes is based on human cellular models realization for tissue engineering. Two kinds of human model were employed: the cellular model by NCI-H441 and A549. The experimental campaign was mainly dedicated to evaluate and compared the models realized on PLLA thin membranes than models realized on standard polyester (PE) membrane. Immunocytochemical, TEER (TransEpithelial Electrical Resistance) and ELISA were used to evaluate the results obtained.

As a third step to the application of thin membranes is based on design and development of a microfluidic devices in which the membranes are integrated. Soft lithography technique is used to build silica mold and electrical characterization technique was development to monitoring the tissue growth. A549 cell was used to set up the most important experimental parameters. The results are in line with those available in literature for similar systems.

The last thin membranes application is based on method of coating humans or/and animals decellularized biological tissues with poly-L-lactic acid (PLLA) for the preparation of a natural/synthetic hybrid tissues. Poly-L-lactic acid is a biodegradable, biocompatible, bioresorbable polymer whose degradation product is lactic acid via lactacid anaerobic metabolism. Decellularized tissue is coated with poly-L-lactic acid and foamed. The proposed technological method allows: the realization of a natural/synthetic three-dimensional scaffold

capable of supporting growth and differentiation of the cells implanted; the upswing of mechanical property of the biological tissue lost during the decellularization process; the mechanical support to improve and make easy the transplant of the bioengineered tissues; the protection against external environment to keep a aseptic environment when the tissue is exposed to outdoor environments.

Sommario

L'ingegneria tissutale è la combinazione di cellule, materiali e metodi di ingegneria, insieme con opportuni fattori biochimici e fisico-chimici, volta a migliorare o sostituire le funzioni biologiche di tessuti danneggiati [1, 2]. A tal proposito supporti porosi e sistemi microfluidici sono utilizzati per scopi di ingegneria tissutale. Scaffold polimerici biodegradabili sono stati sfruttati come supporti strutturali per rigenerare vari tessuti quali ossa, cartilagini, nervi, legamenti, pelle e fegato. Una geometria porosa aperta con canali interconnessi è un prerequisito per la crescita cellulare ad alta densità e per un trasporto di nutrienti, ossigeno e prodotti di scarto metabolici. Infatti, una elevata densità cellulare e un efficiente trasporto di massa contribuiscono alla vitalità cellulare, alla proliferazione e alla riabilitazione finale nei tessuti funzionali [3-5].

Una vasta gamma di scaffold biodegradabili con diverse morfologie è stata fabbricata con metodi convenzionali quali lisciviazione di un porogen solido, schiumatura gas, emulsione/ liofilizzazione, espansione di fluido supercritico e tecniche di separazione di fase [6,7].

Le tecniche di separazione di fase più ampiamente adottate sono note con l'acronimo TIPS (Thermally Induced Phase Separation) e DIPS (Diffusion Induced Phase Separation). Più in particolare, la produzione di supporti polimerici e membrane tramite DIPS è stata ampiamente studiata e applicata per un certo numero di sistemi modello. Vari ricercatori hanno studiato sistematicamente la struttura, la porosità e la cristallizzazione del poli (acido L-lattico), miscela di poli (acido L-lattico) / poliuretano e poli (acido L-lattico) / policaprolattone membrane triolo, preparati da etanolo / diossano e bagni di etanolo / acqua coagulazione attraverso la separazione di fase [8-11], trovando interessanti correlazioni tra il comportamento di fase, la cinetica di demixing e la morfologia della membrana risultante. Altri autori hanno dimostrato che le proprietà meccaniche delle schiume sono controllate principalmente dalla pressione del gas, dalle proprietà dei materiali, dai metodi di fabbricazione e dalla geometria della cella. Con questo proposito, sono state determinate le caratteristiche geometriche che influenzano le proprietà meccaniche: numero di cellule aperte, densità relativa, dimensione delle celle e forma delle cellule [12,13]. Affinché uno scaffold sia idoneo per applicazioni di ingegneria tissutale deve fornire: supporto iniziale e localizzazione delle cellule seminate negli appositi spazi, spunti fisici e biologici per l'adesione, migrazione, proliferazione, differenziazione e, infine, la formazione di tessuti e organi [14-16] .

Dispositivi di coltura cellulare microfluidici combinano i vantaggi di miniaturizzazione, semplicità di gestione e di osservazione microscopica (in tempo reale). La microfluidica

fornisce la possibilità di variare la composizione del terreno di coltura usando generatori di gradiente [17, 18] al fine di creare condizioni di coltura cellulare che sono fisiologicamente più vicine rispetto ai tradizionali sistemi in vitro (velocità di scambio sostanze nutritive, capacità di stimolazioni meccaniche) [19]. I sistemi microfluidici possono essere utilizzati come piattaforme per controllare e gestire analisi di crescita cellulare e del tessuto.

In questa tesi, l'attenzione è focalizzata sul processo DIPS, comunemente utilizzato per la produzione di membrane per varie applicazioni e di scaffold per scopi di ingegneria tissutale. Il sistema selezionato in questo lavoro è costituito da acido poli-L-lattico (PLLA), diossano e acqua. Questa soluzione ternaria è stata usata per la produzione di membrane sottili da usare sia come scaffold per l'ingegneria tissutale che come supporto meccanico biodegradabile. La presente tesi è articolata in più fasi.

Come primo passo per la caratterizzazione del sistema PLLA-diossano-acqua, un set di parametri sperimentali sono stati caratterizzati al fine di ottenere membrane porose su entrambi le superfici. Una particolare attenzione è stata dedicata alla concentrazione e al numero dei bagni di coagulazione, al tempo di immersione per singolo bagno e all'ambiente di essiccazione. Analisi SEM, DSC e DMA sono state realizzate per caratterizzare la serie di membrane ottenute modificando parametri sperimentali. I risultati sono in linea con quelli disponibili in letteratura per sistemi simili.

La seconda fase di questo lavoro, che punta all'applicazione delle membrane sottili, si basa sulla realizzazione di modelli cellulari umani per l'ingegneria tissutale. Due modelli umani sono stati riprodotti: il modello cellulare da NCI-H441 o A549 e il modello di outgrowth da biopsia umana. I due diversi percorsi seguiti in questo lavoro, vale a dire l'indagine sperimentale del modello cellulare e del modello outgrowth sulle membrane di PLLA, sono complementari. La campagna sperimentale è stata principalmente dedicata a valutare e confrontare i modelli realizzati su membrane sottili di PLLA rispetto ai modelli realizzati su membrane standard di polietilene (PE). Analisi di immunocitochimica, TEER (TransEpiteliale Electrical Resistance) ed ELISA sono state impiegate per valutare i risultati ottenuti.

Il terzo passo per l'applicazione delle membrane sottili si basa sulla progettazione e sullo sviluppo di dispositivi microfluidici in cui le membrane sono integrate. Tecniche di soft-litografia sono state utilizzate per costruire lo stampo di silicio per la fabbricazione del dispositivo microfluidico. Successivamente sono state sviluppate tecniche di caratterizzazione elettrica per il monitoraggio della crescita dei tessuti. Colture cellulari di A549 sono state

utilizzate per settare i principali parametri sperimentali. I risultati sono in linea con quelli disponibili in letteratura per sistemi simili.

L'ultima applicazione delle membrane riprodotte in questo lavoro di tesi si basa sul rivestimento di tessuti biologici umani e/o animale per la preparazione di un tessuto ibrido naturale/ sintetico. Il PLLA (Acido Poli-L-lattico) è un polimero biodegradabile, biocompatibile e bioassorbibile il cui prodotto di degradazione è l'acido lattico, ottenuto dal metabolismo anaerobico lattacido. I tessuti decellularizzati (trachee suine) sono state rivestite con membrane di PLLA e testati meccanicamente. Il metodo tecnologico proposto permette: la realizzazione di uno scaffold sintetico-naturali-tridimensionale in grado di sostenere la crescita e la differenziazione delle cellule impiantate; la ripresa delle proprietà meccaniche del tessuto biologico perse durante il processo di decellularizzazione; il supporto meccanico per migliorare e rendere facile il trapianto di tessuti biotecnologici; la protezione contro l'ambiente esterno al fine di mantenere un ambiente asettico quando il tessuto è esposto ad ambienti esterni.

References

[1] D. F. Stamatialis, B. J. Papenburg, M. Girones, S. Saiful, S. N. M. Bettahalli, S. Schmitmeier, and M. Wessling. Medical applications of membranes: Drug delivery, artificial organs and tissue engineering. Journal of Membrane Science (2008) 308:1–34.

[2] J. Jagur-Grodzinski. Polymers for tissue engineering, medical devices, and regenerative medicine. Concise general review of recent studies. Polymers for Advanced Technologies (2006) 17:395–418.

[3] S. J. Hollister. Porous scaffold design for tissue engineering, Nat. Mater 4 (2005) 518–524.

[4] J. J. Marler, J. Upton, R. Langer, J. P. Vacanti. Transplantation of cells in matrices for tissue regeneration, Advanced Drug Delivery Reviews 33 (1998) 165–182.

[5] H. J. Sung, C. Meredith, C. Johnson, Z.S. Galis. The effect of scaffold degradation rate on three-dimensional cell growth and angiogenesis, Biomaterials 25 (2004) 5735–5742.

[6] V. Thomas, D. R. Dean, Y. K. Vohra, Nanostructured biomaterials for regenerative medicine, Curr. Nanosci 2 (2006) 155–177.

[7] H. J. Chung, T. G. Park, Surface engineered and drug releasing pre-fabricated scaffolds for tissue engineering, Advanced Drug Delivery Reviews 59 (2007) 249–262.

[8] P. Van De Witte, H. Esselbrucce, P. J. Dijkstra, J. W. A. Van Den Berg, J. Feijen, Morphological study of membranes obtained from the systems polylactide–dioxane–methanol, polylactide–dioxane–water, and polylactide–N-methyl pyrrolidone–water, J. Polym. Sci. B Polym. Phys 34 (1996) 2569–2578.

[9] M. S. Huang, J. Coudane, S. Li, M. Vert, Methylated and pegylated PLA–PCL–PLA block copolymers via the chemical modification of di-hydroxyl PCL combined with the ring opening polymerization of lactide, J. Polym. Sci. A Polym. Chem 43 (2005) 4196–4205.

[10] D.V. Mistura, A.D. Messias, E.A.R. Duek, M.A.T. Duarte, Development, characterization, and cellular adhesion of poly(L-lactic acid)/poly(caprolactone triol) membranes for potential application in bone tissue regeneration, Artif. Organs 37 (2013) 978–984.

[11] H. Chen, M. Pyda, P. Cebe, Non-isothermal crystallization of PET/PLA blends, Thermochim. Acta 492 (2009) 61–66.

[12] V. Shulmeister, Modelling of the Mechanical Properties of Low-density FoamsPhD Thesis (1998).

[13] F. Ramsteiner, N. Fell, S. Forster, Testing the deformation behaviour of polymer foams, Polym. Test 20 (2001) 661–670.

[14] R. Langer, J.P. Vacanti, Tissue engineering, Science 260 (1993) 920–926.

[15] Y. Kimura, Y. Tabata, Experimental tissue regeneration by DDS technology of bio-signalling molecules, J. Dermatol. Sci 47 (2007) 189–199.

[16] I. O. Smith, X. H. Liu, L. A. Smith, P. X. Ma, Nanostructured polymer scaffolds for tissue engineering and regenerative medicine, Wiley Interdiscip. Rev. Nanomed. Nanobiotechnol 1 (2009) 226–236.

[17] S. W. Rhee, A. M. Taylor, C. H.Tu, D. H. Cribbs, C. W. Cotman, N. L. Jeon, Patterned cell culture inside microfluidic devices, Lab Chip (2005) 102-7.

[18] S. Kim, H. J. Kim, N. L. Jeon, Biological applications of microfluidic gradient devices, Integr Biol (Camb) (2010) 2:584–603. doi: 10.1039/c0ib00055h.
[19] J. Zhou and L. E. Niklason, Microfluidic artificial "vessels" for dynamic mechanical stimulation of mesenchymal stem cells, Integr Biol (Camb) (2012) 4(12):1487-97.

Pubblications

Some ideas and figures have appeared previously in the following publications:

ISI Pubblications

- S. Montesanto, G. A. Mannella, F. Carfì Pavia, V. La Carrubba, V. Brucato. Coagulation bath composition and desiccation environment as tuning parameters to prepare skinless membranes via diffusion induced phase separation; J. Appl. Polym. SCI. 2015, DOI: 10.1002/APP.42151
- S. Montesanto, V. Brucato, V. La Carrubba. Evaluation of mechanical and morphologic features of PLLA membranes as supports for perfusion cells culture systems; Materials Science and Engineering C 69 (2016) 841–849.
- A. Liga, S. Montesanto, G. Mannella, V. La Carrubba, V. Brucato. Study on heat transfer coef cients during cooling of PET bottles for food beverages. Heat and Mass Transfer, SCI.2015, DOI:10.1007/so00231-015-1652-x.

International Conference Paper

- S. Montesanto, F. Conforti, N. P. Smithers, F. Bucchieri, V. Brucato, V. La Carrubba, D. E. Davies. Pulmonary epithelial barrier formation on biodegradable poly-L-lactic-acid (PLLA) membranes. ERS International Congress – London, september3-7, 2016
- S. Montesanto, O. Fici, A. Pitruzzella, F. Bucchieri, M. Cammarata, V. Brucato, V. La Carrubba, M. Zingales. Effect of decellularization process on the mechanical bahaviour of porcine trachea rings. 22nd Congress of the European Society of Biomechanics, July 10 - 13, 2016, Lyon, France.
- A. Fucarino, S. Montesanto, A. Pitruzzella, F. Baronea, F. Carfì Pavia, F. Bucchieri, V. Brucato, and V. La Carrubba. Use of PLLA Scaffold to Reproduce Tubular Cell Cultures in Vitro: A Preliminary Study. XXXII LIAC Meeting, Ustica, September 14-17, 2016.
- S. Montesanto, O. Fici, M. Cammarata, V. Brucato, V. La Carrubba and M. Zingales. Comparison of mechanical properties of neat, decellularized and coated thacheal tissues. GNB2016, June 20th-22nd 2016, Naples, Italy.
- G. A. Mannella, F. Carfì Pavia, S. Montesanto, G. Conoscenti, V. La Carrubba, V. Brucato.

Poly- L-lactide (PLLA) membranes and foams for biomedical applications. Euromembrane Conference, Aachen (Germany), 7–10 September 2015.

- S. Montesanto, A. Fucarino, F. Bucchieri, V. La Carrubba, V. Brucato. Biological evaluation of PLLA membranes, with different pore diameters, to stimulate cell adhesion and growth in vitro. GT70 Conference, Salerno (SA), 15-17 ottobre 2015.
- S. Montesanto, G. Calò, M. Cruciata, L. Settanni, V. Brucato, V. La Carrubba. Optimization of environmental conditions for kefiran production by Kefir grain as scaffold for tissue engineering, Conference on Industrial Biotechnology, Bologna (BO), 10-13 April 2016.

- F. Bucchieri1, A. Fucarino, S. Montesanto, A. Pitruzzella, A. Marino Gammazza, R. Abbate, R. Marchese, F. Farina, F. Cappello, V. Brucato, V. La Carrubba, G. Zummo.
Tissue engineering for the development of three- dimensional in vitro models of human mucosa. Italian Journal OF Anatomy and Embryology, Vol. 119, n. 1 (Supplement): 25, 2014.
- S. Montesanto, G. A. Mannella, F. Carfì Pavia, V. La Carrubba, V. Brucato.
Design, build-up and optimization of a fast quenching device for polymeric thin films, 29th Annual Conference of the Polymer Processing; July 15-19, 2013 Nuremberg (Germany).

Patent

- 102016000033555

Acknowledgements

Perdonatemi questa libertà, ma penso che non sarei in grado di esprimere in maniera altrettanto precisa quanto segue, non usando la mia lingua natia.

Non posso che partire da dove tutto ha avuto origine, cioè dalle persone e dai fatti che volontariamente e involontariamente mi hanno spinto a fare questa esperienza. Prima della fine della mia tesi magistrale la vita mi ha condotto a studiare e analizzare cosa fosse un leiomioma metastatizzante. Sono stati giorni duri, passati tra una scrivania, un pc, una biblioteca e un ospedale. Lui, il cui nome dice tanto, è stato per me il nulla, il vuoto e la paura, fortunatamente oggi è solo un ricordo. Penso che in quel periodo è scattata la molla, è nata così la sfida, la voglia, il desiderio di mettere a disposizione le mie conoscenze in abito ingegneristico alla medicina. I dubbi sono stati tanti ma la sfida è stata veramente interessante. Sapevo che non sarei stato solo, c'erano loro, i prof. La Carrubba e V. Brucato.

I prof. tanto temuti durante il corso di studi diventano i miei compagni di viaggio, punti di riferimento dentro e fuori i luoghi di lavoro. Un grazie per quello che mi avete insegnato sia dal punto di vista professionale che umano.

In questa fase è sicuramente doveroso ringraziare quelli del gruppo "MONTE caffè": Gianluca Mannella, Francesco Carfì Pavia, Gioacchino Conoscenti e Giuseppe Scaglione. Siete stati compagni di avventura con cui ho condiviso gioie e dolori, patemi e successi, ma soprattutto incredibili esperienze. Grazie a tutti voi, amici in tutto e per tutto: "io due stigliole le metterei sul fuoco".

Grazie agli amici del Policlinico: Fabio e Alberto. Sui nostri discorsi, fatti dietro una scrivania, vicino una macchinetta del caffe o dentro il freddo laboratorio tra un muco e l'altro, c'è veramente poco da dire, ma tanto su cui ridere.

Un grande grazie va al Prof. N. Elvassore e al suo team: Onelia, Alessandro, Francesco, Sebastian, Giovanni, Camilla, Elena, etc., per l'opportunità data. E' stato un periodo lungo ed intenso ma sicuramente ricco di momenti belli passati dentro e fuori il laboratorio, tra uno spritz, un cinese, un vinello e una gita in barca. L'amicizia nata tra il "terrone" e i "verdi" veneti è stata un grande dono. Tra tutte le splendide persone conosciute nella città di Padova, non posso che ringraziare l'amico delle mille sventure, Federico Piscopo. Un grazie è veramente poco per descrivere la nostra amicizia, i caratteri di word non basterebbero per esprimere la mia gratitudine nei tuoi confronti.

Grazie Prof. Donna e grazie Natalie, vi siete presi cura di me in maniera meticolosa. Qualche giorno prima di partire per Southampton ero terrorizzato per la lingua, per le persone e anche

per il clima. Il giorno in cui vi ho incontrato ho capito subito che la lingua e il clima non sarebbero stati un problema e che le meravigliose persone che siete mi avrebbero arricchito. Grazie Franco, Carolina, Francesco e Sofia. Abbiamo vissuto assieme brevi momenti ma intensi. La vostra famiglia è stata sin da subito la mia, motivo per il quale non abbiamo mai smesso di sentirci.

La lista delle persone da ringraziare, che hanno permesso la realizzazione di questo lavoro di tesi, è veramente lunga: il Prof. M. Zingales, Marcello Cammarata, il Prof. G. Ghersi e i numerosi tesisti, ma so già che mi sono dilungato troppo e concesso fin troppe licenze.

Giunti al termine ringrazio i miei amici, la mia famiglia e la mia ragazza. Purtroppo il dedicare tanto al lavoro ha necessariamente tolto il tempo da poter dedicare allo stare insieme. Per quanti lunghi siano stati questi mesi, oggi siate ancor di più i miei punti fermi e il mio sostegno. La lontananza non ci ha indeboliti ma consolidati.

Vi lascio alla lettura, ma era giusto che sapeste che senza il contributo di tutte queste meravigliose persone, questa tesi, oggi, non sarebbe qui.

Contents

Chapter 1

Tissue Engineering and Biodegradable scaffolds

The artificial generation of tissues, organs, or even more complex living organisms was throughout the history of mankind a matter of myth and dream. During the last decades this vision became feasible and has been recently introduced in clinical medicine.

Tissue engineering has to do with the transformation of these fundamental ideas to practical approaches. Several aspects of generating new tissues and organs out of small pieces of living specimens are now scientifically solved, but at this point it is unknown how much impact these new approaches will have on clinical medicine in the future. In this respect it seems important to recapitulate from where the visions and the work came, in order to speculate or predict where tissue engineering and regenerative medicine will head.

Since the beginning of time, man has nurtured the idea of recreating parts of the human body. In the animal kingdom, several species have retained the ability to re-grow limbs if severed or traumatically amputated. For example the blindworm can lose the distal part of its tail but it will re- develop in some time. The tail lies flopping on the ground, or in the predator's mouth, distracting the harasser while the snake gets away. Another example is the salamander that can regenerate whole limbs in a matter of a few weeks if severed in a fight.

The genetic information to regenerate tissues and organs must also be retained in humans since the fetus, during the first two trimesters in utero, has the ability not only to heal wounds without scarring, but also to re-grow limbs if, for some reason, injured. This genetic information is, later in the pregnancy, either lost or hidden since we as full-born babies no longer possess these excellent properties.

Today, the current therapeutic modalities to treat tissue or organ loss include total artificial or mechanical devices, biological processed tissues, transplanting organ from one individual into another, surgical reconstruction, autologous transfer of tissue to the diseased-site or supplementing metabolic products of the lost tissue. Although these traditional forms of tissue replacement have rescued millions of patients and have improved countless lives, they suffer from problems of scarce supply, increased susceptibility to infection, immunological rejection, as well as uncertain long-term interaction with the patients, however still remain imperfect solutions.

Therefore, constructing a tissue-engineered replacement in vitro can be an excellent alternative to direct transplantation of donor organs.

Tissue engineering is an emerging multidisciplinary field involving biology, medicine, and engineering that is likely to revolutionize the ways we improve the health and quality of life for millions of people worldwide by restoring, maintaining, or enhancing tissue and organ function. In addition to having a therapeutic application, where the tissue is either grown in a patient or outside the patient and transplanted, tissue engineering can have diagnostic applications where the tissue is made in vitro and used for testing drug metabolism and uptake, toxicity, and pathogenicity. The foundation of tissue engineering for either therapeutic or diagnostic applications is the ability to exploit living cells in a variety of ways.

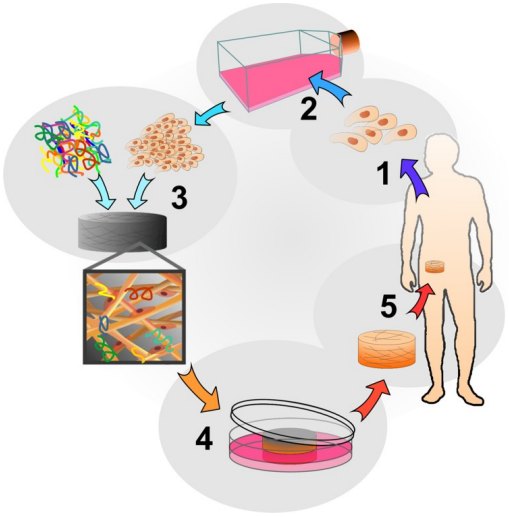

Figure 1: Tissue Engineering scheme.

The term 'Tissue Engineering' can be tracked back to a bioengineering panel meeting in Washington D.C. in the spring of 1987, held by the National Science Foundation. In 1988, at the first meeting devoted specifically to TE, at Lake Tahoe in California, USA, one definition of the expression 'Tissue Engineering' was coined;

"*Tissue engineering is the application of the principles and methods of engineering and the life sciences toward the fundamental understanding of structure/function relationships in normal and pathological mammalian tissues and the development of biological substitutes to restore, maintain, or improve functions".*

The essence of Tissue Engineering was well defined by Langer and Vacanti that described it as "*an interdisciplinary field that applies the principles of engineering and the life sciences toward the development of biological substitutes that restore, maintain or improve tissue function*".

Over the last two decades, the concept of cell guidance in tissue regeneration has been extensively discussed and progressively revised as new knowledge of the complex features of cell-material interaction have been disclosed and elucidated. Part of this evolution has been the development of novel scaffold materials, compatible with the cell guidance concept and resulting from contemporary advances in the fields of materials science and molecular biology [1]. Tissue regeneration, whenever it occurs for example, in response to physiological conditions or to trauma is a result of a complex cascade of events. These events are coordinated in spatial and temporal modalities, and each of them is governed by biophysical and biochemical signals. In turn, these signals are triggered by the extracellular microenvironment. Therefore, the final outcome of cell life for most connective tissue depends on the dynamic and reciprocal interaction between the cell and the extracellular matrix (ECM). It is this interaction that ultimately determines cell fate and ECM degradation or remodelling.

Three basic strategies have evolved over the past few years to engineer new tissues. The first approach involves the stimulation of endogenous cells to induce neo-tissue formation. This is achieved via delivery of tissue inducing substances to targeted locations including growth and differentiation factors. The second strategy involves transplantation of cells encapsulated in a semipermeable membrane to augment limited biochemical functions of a tissue or organ. (e.g. Transplantation of encapsulated islets of Langerhans to treat Type I [2]. Cell transplantation on porous synthetic matrices to create new tissues that integrate with the host tissue and are capable of replacing all the functions of deficient tissue represents the third approach [3]. Figure 1 shows the basic idea of tissue engineering.

Scaffolds for tissue engineering

Numerous scaffolds produced from a variety of biomaterials and manufactured using a plethora of fabrication techniques have been used in the field in attempts to regenerate different tissues and organs in the body. Regardless of the tissue type, a number of key considerations are important when designing or determining the suitability of a scaffold for use in tissue engineering.

The very first criterion of any scaffold for tissue engineering is that it must be biocompatible; cells must adhere, function normally, and migrate onto the surface and eventually through the scaffold and begin to proliferate before laying down new matrix. After implantation, the scaffold or tissue engineered construct must elicit a negligible immune reaction in order to

prevent it causing such a severe inflammatory response that it might reduce healing or cause rejection by the body.

The objective of tissue engineering is to allow the body's own cells, over time, to eventually replace the implanted scaffold or tissue engineered construct. Scaffolds and constructs, are not intended as permanent implants. The scaffold must therefore be biodegradable so as to allow cells to produce their own extracellular matrix [4]. The by-products of this degradation should also be non-toxic and able to exit the body without interference with other organs. In order to allow degradation to occur in tandem with tissue formation, an inflammatory response combined with controlled infusion of cells such as macrophages is required. Now that tissue engineering strategies are entering clinical practice more routinely, the field of immunology is a playing a role of increasing prominence in the research area [5,6].

Ideally, the scaffold should have mechanical properties consistent with the anatomical site into which it is to be implanted and, from a practical perspective, it must be strong enough to allow surgical handling during implantation. While this is important in all tissues, it provides some challenges for cardiovascular and orthopaedic applications specifically. Producing scaffolds with adequate mechanical properties is one of the great challenges in attempting to engineer bone or cartilage. For these tissues, the implanted scaffold must have sufficient mechanical integrity to function from the time of implantation to the completion of the remodelling process [7]. A further challenge is that healing rates vary with age; for example, in young individuals, fractures normally heal to the point of weight-bearing in about six weeks, with complete mechanical integrity not returning until approximately one year after fracture, but in the elderly the rate of repair slows down. This too must be taken into account when designing scaffolds for orthopaedic applications. However, as the field has evolved, it could be argued that too much focus has been placed on trying to develop scaffolds with mechanical properties similar to bone and cartilage. Many materials have been produced with good mechanical properties but to the detriment of retaining a high porosity and many materials, which have demonstrated potential in vitro have failed when implanted in vivo due to insufficient capacity for vascularization. It is clear that a balance between mechanical properties and porous architecture sufficient to allow cell infiltration and vascularization is key to the success of any scaffold.

The architecture of scaffolds used for tissue engineering is of critical importance. Scaffolds should have an interconnected pore structure and high porosity to ensure cellular penetration and adequate diffusion of nutrients to cells within the construct and to the extra-cellular matrix formed by these cells. Furthermore, a porous interconnected structure is required to

allow diffusion of waste products out of the scaffold, and the products of scaffold degradation should be able to exit the body without interference with other organs and surrounding tissues. The issue of core degradation, arising from lack of vascularization and waste removal from the centre of tissue engineered constructs, is of major concern in the field of tissue engineering [8,9]. Another key component is the mean pore size of the scaffold. Cells primarily interact with scaffolds via chemical groups (ligands) on the material surface. Scaffolds synthesized from natural extracellular materials (e.g. collagen) naturally possess these ligands in the form of Arg-Gly-Asp (RGD) binding sequences, whereas scaffolds made from synthetic materials may require deliberate incorporation of these ligands through, for example, protein adsorption. The ligand density is influenced by the specific surface area, i.e. the available surface within a pore to which cells can adhere. This depends on the mean pore size in the scaffold. The pores thus need to be large enough to allow cells to migrate into the structure, where they eventually become bound to the ligands within the scaffold, but small enough to establish a sufficiently high specific surface, leading to a minimal ligand density to allow efficient binding of a critical number of cells to the scaffold [10,11]. Therefore, for any scaffold, a critical range of pore sizes exists [12,13] which may vary depending on the cell type used and tissue being engineered.

In order for a particular scaffold or tissue engineered construct to become clinically and commercially viable, it should be cost effective and it should be possible to scale-up from making one at a time in a research laboratory to small batch production [14].

The development of scalable manufacturing processes to good manufacturing practice (GMP) standard is critically important in ensuring successful translation of tissue engineering strategies to the clinic [15]. Another key factor is determining how a product will be delivered and made available to the clinician. This will determine how either the scaffold or the tissue engineered construct will be stored. Clinicians typically prefer off-the shelf availability without the requirement for extra surgical procedures in order to harvest cells prior to a number of weeks of in vitro culture before implantation. However, for some tissue types, this is not possible and in vitro engineering prior to implantation is required.

The final criterion for scaffolds in tissue engineering, and the one which all of the criteria listed above are dependent upon, is the choice of biomaterial from which the scaffold should be fabricated.

Biomaterials

There are two procedures used for the treatment of the failure or loss of tissues and organs: transplants and implants. In the case of transplants, tissues or organs are obtained from living donors (e.g., heart or kidneys) or from cadavers (e.g., lyophilized and frozen bone). In some cases, immunosuppressive drugs are necessary to prevent rejection of the transplanted organ, or other medications that minimize possible microbial contamination [16]. In addition, transplants have the disadvantage of raising a series of ethical and even religious issues. In contrast, devices developed to serve as implants do not present many of the problems reported above and are designed to act at the recipient tissue interface in the organism, interacting with these tissues [16,17].

Biomaterials were first developed to remain inert in the organism. Thus, studies were aimed at investigating how to prevent or minimize undesired tissue reactions. At present, new materials are designed to elicit an effective interaction with tissues, provoking physiological responses such as cell growth and/or differentiation at the site of implantation [18].

Significant advances have been made over the past decades in the understanding of the mechanisms underlying the interaction of animal cells with their natural environment, i.e., the extracellular matrix, as well as of the influence of this matrix on cell growth and differentiation [19,20]. This knowledge is frequently being used for the development of polymers that mimic the characteristics of extracellular matrix, thus playing an active role in tissue restoration.

The biomaterials used can be classified into permanent or temporary materials (figure 2). Permanent materials are used to replace damaged tissue for an undetermined period of time and are therefore designed to retain their mechanical and physicochemical properties for prolonged periods of time [21].

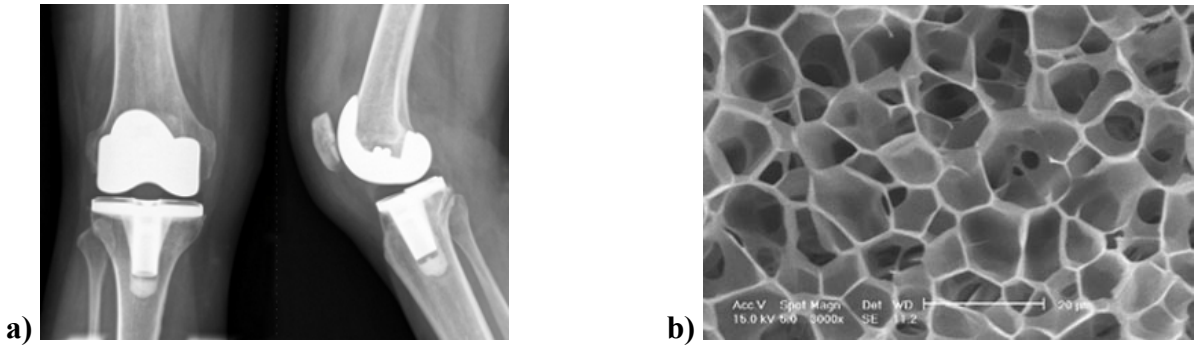

Figure 2: Biomaterials: a) permanent b) temporary (Boltorn based hydrogel).

These types of devices are commonly employed experimentally as prostheses, replacing damaged joints, heart valves and intraocular lenses, among others. On the other hand, in some

situations the support only needs to fill the damaged region temporarily until tissue regeneration is completed, or guides the regeneration process. Temporary biomaterials are an alternative in this case.

"Biodegradable" is a term that can be applied to polymers and solid devices that undergo dispersion in vivo as a result of macromolecular degradation, but without elimination of products and sub products by the organism. Biodegradable polymers can be attacked by biological elements in such a way that the integrity of the system is affected, forming fragments and other degradation products that can be removed from the site of action but not necessarily from the organism. "Bioabsorbable" is a term that can be applied to polymeric materials and devices that dissolve in body fluids without breakdown of the macromolecular chain or a reduction in molecular mass [22]. One example is the slow dissolution of soluble implants in organic fluids. "Bioresorbable" materials are polymers and solid devices that degrade through a reduction in size and that are resorbed in vivo, i.e., materials that are eliminated by metabolic pathways of the organism. Bioresorption is a concept that reflects the complete elimination of the material and of degradation products (compounds of low molar mass) in the absence of residual side effects. The term "bioresorption" is applied when complete elimination occurs. A polymer can be bioresorbable if its macromolecules are excreted [22,23]. Bioresorbable polymeric materials are preferentially used as temporary devices.

Fabrication techniques

In the body, cells and tissue are organized into three-dimensional architecture. To engineer these functional tissue and organs, scaffolds have to be fabricated by different methodology to facilitate the cell distribution and guide their growth into three-dimensional space. The main techniques for scaffolds fabrication are: 3D printing, solvent casting, particulate-leaching techniques, gas foaming, electrospinning, freeze drying and phase separation.

Solvent casting

Solvent casting property for the scaffold preparation is very simple, easy and inexpensive. It does not require any large equipment; it is totally based upon the evaporation of some solvent in order to form scaffolds by one of the following two routes. The first method is to dip the mold into polymeric solution and allow sufficient time to draw off the solution; as a result a layer of polymeric membrane is created. Another method is based on pouring he polymeric solution into a mold and awaiting sufficient time for solvent evaporation, thus forming a

polymeric membrane, which adheres to the mold [24]. As there is the possibility that the scaffolds designed by these techniques may retain some small amounts of organic solvents, scaffolds are fully dried by vacuum process to completely remove toxic solvent(s). However, this is very time consuming technique. Some researchers have combined the aforementioned protocol with particulate leaching [25-27].

Particulate-leaching techniques

Particulate leaching is one of the popular techniques that are widely used to fabricate scaffolds for tissue engineering applications [28,29]. Salt, wax or sugars known as porogens are used to create the pores or channels. Here salt is grounded into small particles and particles that have desired size are poured into a mold filling it. A polymer solution is then cast into the salt-filled mold. After the evaporation of the solvent, the salt crystals are leached away using water to form the pores of the scaffold. The process is easy to carry out. The pore size can be controlled by controlling the amount of porogen added, the size and shape of the porogen [30]. The particulate leached scaffold possesses pore size (~500 μm), percentage porosity (around 94-95%) and the desired crystallinity. One of the advantages of this method is the requirement of very low amount of polymer to fabricate the scaffold. However, certain critical variables such as pore shape and inter-pore openings are not controlled. To conquer these drawback new technologies, are being developed.

Gas foaming

The gas foaming scaffold fabrication techniques does not require the utilization of organic solvents and high temperature. This technique uses high pressure carbon dioxide gas for the fabrication of highly porous scaffolds. The porosity and porous structure of the scaffolds depend upon the amount of gas dissolved in the polymer. This process involves exposing the polymer to carbon dioxide at high pressure (800 psi) to saturate it with the gas [31]. After rapid depressurization, the dissolved carbon dioxide becomes unstable and will separates from the polymer. The carbon dioxide molecule undu clustering to minimize the free energy and as a result pore nucleation take place. These pores cause the significant expansion of polymeric volume and decrease in material density.

Electrospinning

The electrospinning technique for the scaffolds designing utilizes the electrostatic force for the production of polymeric fiber ranging from nanoscale to microscale. This process is controlled by a high intensity electric field imposed between two electrodes having electric

charges of opposite polarity. One electrode is the polymer solution nozzle and the other is the collector. Generally, when a polymer solution is pumped trough a thin nozzle leads to dropping.

When the electric field is present, it can exerts a force on the polymer, due to charging by the nozzle, that can overcome the surface tension of the solution. A jet of polymer solution is then ejected and stretched, while the solvent evaporate, leading to nanofibers that deposit on the collector. The process is very versatile, does not require the use of coagulation chemistry or high temperature for fiber generation and can produce very thin fibers.

Freeze drying

This technique is based upon the principle of sublimation. Polymer is first dissolved in a solvent to form a solution of the desired concentration. The solution is then frozen and the solvent is removed by lyophilization under vacuum leading to scaffold with high porosity and inter connectivity [32,33]. The pore size can be controlled by the freezing rate and pH; a fast freezing rate produces smaller pores. Controlled solidification in a single direction has been used to create a homogenous 3D-pore structure [34]. The drawback of this technique is smaller pore size and long processing time [35].

Phase separation

Phase separation of polymer solutions can be induced in several ways. Before discussing these phase separation processes used in this thesis in detail, a short survey of the four main techniques for the preparation of polymeric membranes by controlled phase separation is presented [36-38].

• Thermally induced phase separation (TIPS). This method is based on the instability of some polymeric solution when the temperature is decreased. After liquid-liquid demixing is induced the solution is frozen and the solvent is removed by extraction, evaporation or freeze drying.

• Air-casting of a polymer solution [39,40]. In this process, the polymer is dissolved in a mixture of a volatile solvent and a less volatile non-solvent. During the evaporation of the solvent, the solubility of the polymer decreases, and then phase separation can take place.

Precipitation from the vapour phase. During this process, phase separation of the polymer solution is induced by penetration of non-solvent vapour in the solution.

• Diffusion induced phase separation (DIPS). A polymer solution is cast as a thin film on a support or extruded through a die, and is subsequently immersed in a non-solvent bath.

Precipitation can occur because the good solvent in the polymer solution is exchanged with non- solvent.

The differences between the four techniques originate from differences in desolvation mechanisms. Phase diagrams can predict, whether or not a solution of a certain polymer in a certain solvent or solvent mixture is suitable for membrane formation. Binary and more frequently ternary phase diagrams - showing the phase boundaries as a function of temperature and composition - provide useful information for all phase separation processes.

Diffusion induced phase separation – DIPS

Membrane formation by DIPS has been studied much less intensively than thermally induced phase separation. Nevertheless, a good picture of the process is now available. A schematic representation of membrane formation by immersion precipitation is presented in figure 3. DIPS process is more complicated than thermally induced phase separation, because at least three components are involved, and because complex diffusion and convection processes play an important role.

It is clear that a large number of phase transitions and combinations of phase transitions can play a role. Introducing a third component will make the phase diagrams even more complex. Fortunately, the complexity is reduced by the fact that the DIPS process can be regarded as an isothermal process being heats of mixing negligible in almost all cases.

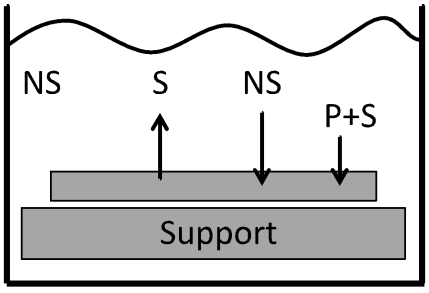

Figure 3: Schematic depiction of the immersion DIPS process where P, S and NS are polymer, solvent and nonsolvent respectively.

All of the possible solution composition of three components can be plotted in a triangle. The corners represent the pure components, the axes the three binary combinations and a point in the triangle a ternary composition (Fig. 4). Two types of phase transitions, combined or not each other phase transition, have general relevance for membrane formation: liquid-liquid and solid-liquid demixing. The phase diagram is divided into a homogeneous region, and an area representing a liquid-liquid or solid-liquid demixing gap. The liquid-liquid gap is entered when a sufficient amount of non-solvent is present in the solution. In principle, the same three

parts of the demixing gap are present as in the binary diagram. A metastable area exists between the spinodal and the binodal at low polymer concentrations, an unstable area is enclosed by the spinodal, and a second metastable area at higher polymer concentrations. The phase separation proceeds analogously with binary solutions.

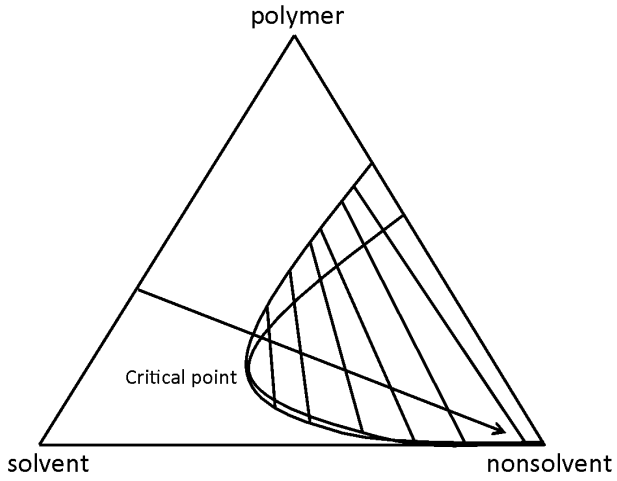

Figure 4: Example of an isothermal phase diagram for mixtures of a polymer, a solvent and a nonsolvent. The arrow connects the initial composition of the casting solution to the final average composition of the entire system (nascent membrane + coagulation bath). The shaded tie line connects the final composition of the bath with the final composition of the polymer rich phase in the film.

A line is plotted in the phase diagram, which connects the initial composition of the film to the final averaged composition of the film and the coagulation bath. The arrow does not represent the compositional change in the solution as a function of time. The components in the polymer solution will take a different composition path to the end condition.

In the framework of the Flory-Huggins description of polymer solutions, the size and location of the de-mixing gap depends on the molar volumes of the components, the polymer/solvent interaction parameter, the polymer/non-solvent interaction parameter, and the solvent/non-solvent interaction parameter [41].

The influence of these variables, the effect of polydispersity of polymer on the resulting phase diagrams has been discussed in detail by many authors [41-43]. The influence of the parameters can be summarized as follows.

A polymer/non-solvent interaction parameter (χ_{13}) determines, to a great extent, the surface area of the liquid-liquid de-mixing gap. High polymer/non-solvent interaction parameters imply that the point of intersection of the demixing gap with the polymer/non-solvent axis is located at very high polymer concentrations. Polymers and solvents with low mutual affinity (high χ_{23}) increase the magnitude of the de-mixing gap, especially at low values of χ12.

Low compatibility of polymer/non-solvent mixtures (high χ_{12}) results in large differences in solvent/non-solvent ratio in the equilibrium phases. Solvents and non-solvents with high mutual affinity (low χ_{12}) strongly increase the magnitude of de-mixing gaps.

In a first approximation (minor) changes in molecular weights, molecular weight distributions and molar volumes are negligible compared to the influence of interaction parameters. For liquid-liquid de-mixing three types of phase separation mechanisms can be distinguished [44]. At low polymer concentrations (between the binodal and the spinodal) phase separation takes place by nucleation and growth of a polymer-rich phase and finally polymer spheres will be obtained. At intermediate polymer concentrations spinodal de-mixing processes give rise to bi-continuous network structures. At high polymer concentrations (between the binodal and the spinodal) phase separation takes place by nucleation and growth of a polymer-poor phase and spongy structures can be obtained.

Solid–liquid de-mixing processes can give rise to the formation of single lamellae at very low polymer concentrations or supramolecular assemblies of lamellae-like axialities and spherulites at high polymer concentrations [45-50, 51,52,53].

In figure 5 has shown some composition paths for a fixed composition of the casting solution. A composition path describes the time and place dependent composition of the polymer solution between immersion and phase separation.

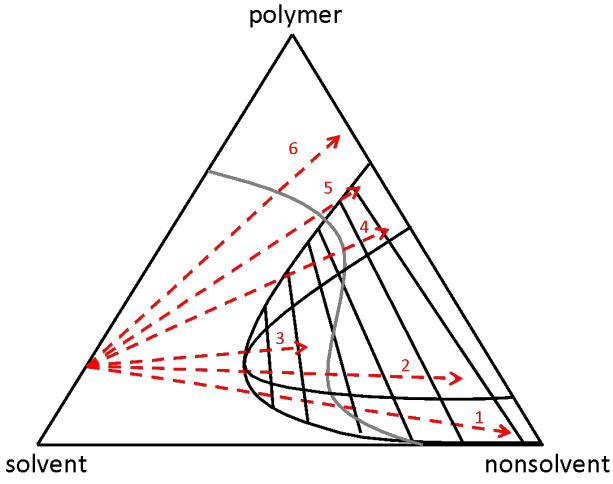

Figure 5: Nonequilibrium phase diagram for a ternary system.

In cases 1, 2, and 4 crystallization will only take place after liquid-liquid de-mixing. In case 1 first liquid-liquid de-mixing will take place by nucleation and growth of polymer-rich phase followed by crystallization of the polymer-rich droplets. In case 2 liquid-liquid de-mixing proceeds by spinodal decomposition, while in case 4 the liquid–liquid de-mixing proceeds by nucleation and growth of a polymer-poor phase followed by crystallization of the matrix.

Two reasons are responsible for this [54]. Unstable solid-liquid equilibria increase the free energy of mixing. For metastable solid-liquid equilibria the decrease in free energy of mixing for crystallization is smaller than for liquid-liquid de-mixing. In addition the activation energy for liquid-liquid de-mixing is much lower than for crystallization.

In case 5 crystallization takes place first; however, in the course of the de-mixing process the polymer solution will be pushed in the miscibility gap. These phenomena were recently reported by van de Witte et al. for the immersion precipitation of poly-L-lactide [51]. Spherulites surrounded with porous shells could be obtained. This morphology was attributed to a cascade of phase transitions. First solid-liquid de-mixing induced the formation of spherulites. Due to the spherulite growth liquid-liquid de-mixing was induced in the medium surrounding the spherulite. Crystallization occurred again in the polymer-rich phase generated during the liquid-liquid de-mixing process.

In case 6 only the solid-liquid miscibility gap is entered and in case 3 only the liquid-liquid miscibility gap is entered. The structure generation under these conditions is well established.

Mechanical properties of Membrane and governing parameters

The important characteristics of polymeric foams are lightweight and show: resilience, , stiffness, high porosity, high crushability, and good energy absorption capacity [54]. Polymeric foam possesses unique physical, mechanical, and thermal properties, which can be attributed to polymer matrix. This matrix is formed by a cellular structure filled by a gas and its properties are dependent on the ingredients and their distribution. Properties of gaseous mixtures are predominantly governed by volumetric characteristics of constituents. Thermodynamic properties, such as specific heat, equilibrium constant, etc., are governed by the molecular weight of individual participating components [55]. Mechanical properties of foams are broadly controlled by the gas pressure, base material properties, cell geometry, and manufacturing methods. Foams can be differentiated as open-cell foam and closed-cell foam, based on cell type. Structure–property relationship is discussed in the following two sections:

1. Modulus and effect of foam density;
2. Geometrical constitution of foam and its effect.

Modulus and effect of foam density

Like any other design parameter, foam density also needs to be optimized as per the targeted application. Gibson and Ashby [56] explained that at lower density, densification zone is reached quickly which results in very high force prior to full energy dissipation. On the other

hand, in case of high-density foam, force exceeds the critical value way before adequate energy absorption, resulting in partially utilized compressive strains. Higher density foams of the same type experience higher permanent deformation, whereas compression stresses are lower than that of the indentation stresses. This behavior suggests the role of shear and tensile strength in providing additional resistance to the deformation [57]. Internal structure plays a vital role in defining foam's mechanical properties. For any given amount of energy, low-density foam sustains a large deformation due to the quick densification and low value of plateau. On the other hand, high-density foam sustains low deformation for the same amount of energy [58], which clearly points that ideal foam should be of intermediate density. Young's Modulus and yield stress follow power law dependence with respect to density of foam shown in Eq. (1):

$$E = (\rho)^n \quad \textbf{(1)}$$

where **E**, **ρ**, and ***n*** are the modulus, density, and density exponent of foam.

Density exponent is found to be 1.5 and 4 for yield stress and Young's Modulus, respectively, though bulk modulus varies linearly with density [59–61]. It is well established that yield is controlled by the maximum principal stress for polystyrene and polyurethane foams [62, 63]. Effect of density, filler size, impregnation, cell structure, cell orientation, testing temperature, and crush behavior has been studied in detail [64–73].

Polymeric foams have always exhibited lower values of maximum force when compared with solid material block of the same material [58]. At higher strains, even at 80 %, stress increases very rapidly. At strains as high as 95 %, foam density is not equal to that of solid foam and becomes very stiff [74]. Higher density foams have higher yield strength, breaking strength, and Young's modulus, where stress and strain follow a linear relationship within the range of 20 % of tensile strain. Resilient foams can sustain strains up to 50 % before fracture, while crushable foams can take only 20 % strain before fracture [57]. In most of the cases, dynamic stress levels were higher than their static counterpart at the same strain level. Gibson and Ashby [74, 75] derived the modulus of a closed-cell foam which contained three terms that reflect the effect of strut bending, membrane (cell face) stretching [76, 77], and the internal gas pressure of closed cells. The stiffness of closed-cell foam can be attributed to these three contributions as in Eq. (2).

$$\frac{E^*}{E_S} \approx \phi^2\{\frac{\rho^*}{\rho_S}\}^2 + (1-\phi)\frac{\rho^*}{\rho_S} + (\frac{\rho_o}{\rho_S})\frac{(1-2\nu^*)}{1-(\frac{\rho^*}{\rho_S})} \quad \textbf{(2)}$$

where E* and E_s are the modulus of foam and solid polymer, respectively; ρ* and ρ_s are the density of foam and solid polymer; and n is the density exponent. On the other hand, Goods [59] simplified Gibson and Ashby's model [75, 76] by modeling foam as an array of cubic cells of length ''l, and struts of thickness t, as shown in Fig. 6a (open-cell foam) and Fig. 6b (closed-cell foam). The cells were staggered in such a way so that corners of one cell rest upon the midpoint of adjacent cells. Such structure neither matched to the actual geometric characteristics of real foam nor could be reproduced to fill the space. It is supposed to capture the critical physical processes of deformation and structural stability of a cellular structure.

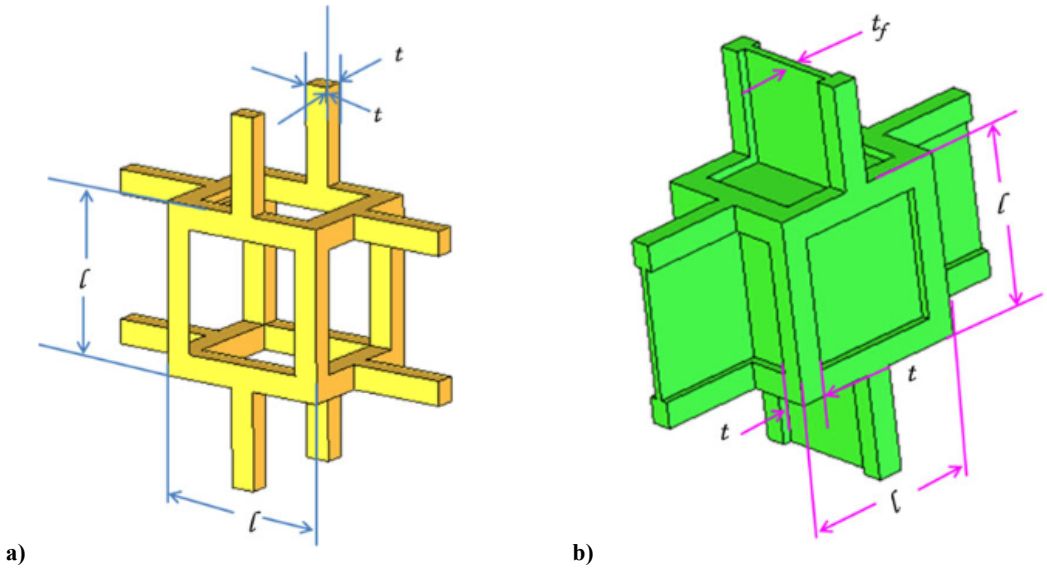

Figure 6: Unit cell of cubic symmetry: a) open-cell foam, b) closed-cell foam.

This unit cell assumption resulted in Eq. (3), which describes density dependence of the elastic modulus of open-cell foam, valid only at small displacements [74,75]:

$$\frac{E^*}{E_S} \approx \left\{\frac{t^4}{l^4}\right\} \approx \left\{\frac{\rho^*}{\rho_S}\right\}^2 \qquad (3)$$

Substantial amount of effort has been put to relate the mechanical response of foams and cell deformation mechanics. Zhu et al. [60] derived a relationship for Young's modulus, shear modulus, and Poisson's ratio as a function of edge cross section and foam density. A significant amount of work on cellular solids was based on incorrect assumptions. For instance, bending stiffness is a better representative of elastic behavior of foams instead of axial extensions of cell walls [75,79,80]. Initially, cell wall bent was attributed to elastic behavior of foams which was later not accepted [81,82]. Later, Menges and Knipschild [83]

found the correct mechanism, which was cell wall bending, and explained that open-cell and closed-cell foams have similar stiffness. Cell wall struts are responsible for a major part of load and contribute significantly to foam stiffness rather than thin cell wall. Ko [84] worked out the relationship between cell wall bending and modulus and so did Patel and Finnie [77].
Multiple variables are known to affect properties of foam like: structure of the foam, matrix material of the foam, density of the foam, cell orientation, and testing temperature [73]. There is a well-established direct relationship between the internal structural traits (e.g., porosity, cell shape and size, strut length and thickness) and the mechanical characteristics [75, 76] that are governed by cell wall material [85]. The structural variables, necessary to describe plastic foams, are density, cell size, cell geometry, polymer phase composition, and gas-phase composition [86]. It has been suggested that cell structure can be assumed oval and with some approximation it can be modelled by ratio of radius, area, and thickness of cell wall [87]. It has also been represented by many complex shapes, and various mechanical properties have been predicted by these approximate shapes [88–90]. Most of the work for plastic deformation of foams deal with cell corporeal like strut shape, size, and their effect on properties of periodic arrangement of cells, isotropy (effect of disorder), and cellular interaction at microscopic scale [91]. Most of the foam material is distributed, either in cell walls or cell ribs, and affects compression behavior of cellular foam. Energy dissipation mechanism is likely through cell bending, buckling, or fracture, but stress is generally limited by the long and flat plateau of the stress–strain curve 38]. Properties of foam are closely linked to its structural parameters. Berlin and Shutov [92] listed the following important parameters affecting the properties of foam:

1. Relative number of open cells;
2. Relative foam density;
3. Cell size;
4. Cell shape or geometrical anisotropy;
5. Cell walls thickness and distribution of solid between struts and faces;
6. Geometry of a foam cell and its constituents.

Relative number of open cells

According to their morphology, foams are subdivided in open-cell and closed-cell foams. The main difference between these two foam classes is absence of the membranes in the open-cell foam. But in most cases foam contains closed as well as open cells. This causes a necessity to

introduce the degree to which cells are closed or open, because it influences the properties of cellular materials significantly. A study of closed-cell foams performed by Berlin and Shutov [92] suggests, that the fraction of open cells, θ , is a function of the foams relative density. In the region of the low-density foams ($\rho_f / \rho_s < 0.06$, where ρ_s is the density of the solid material), the factor θ is approximately equal to 0.3 and decreases for foams of higher densities. They explain this effect by the fact, that in the low-density foams the membranes become very thin and can easily rupture during or after processing. However, the rheological behaviour of the foaming liquid will be important and possibly even dominate θ.

It is expected that the relative content of open cells in closed-cell foam will play a considerable role in the physical properties of cellular materials.

A recent study of the morphological features of closed-cell PUR foam [93] showed the importance of the amount of cell opening for the properties of closed-cell foam. The cell walls have been classified as:

- ✓ Closed;
- ✓ pin holes;
- ✓ partially open (less than 50% area open);
- ✓ open.

All these features are shown at the example of closed-cell glass foam in Fig. 7.

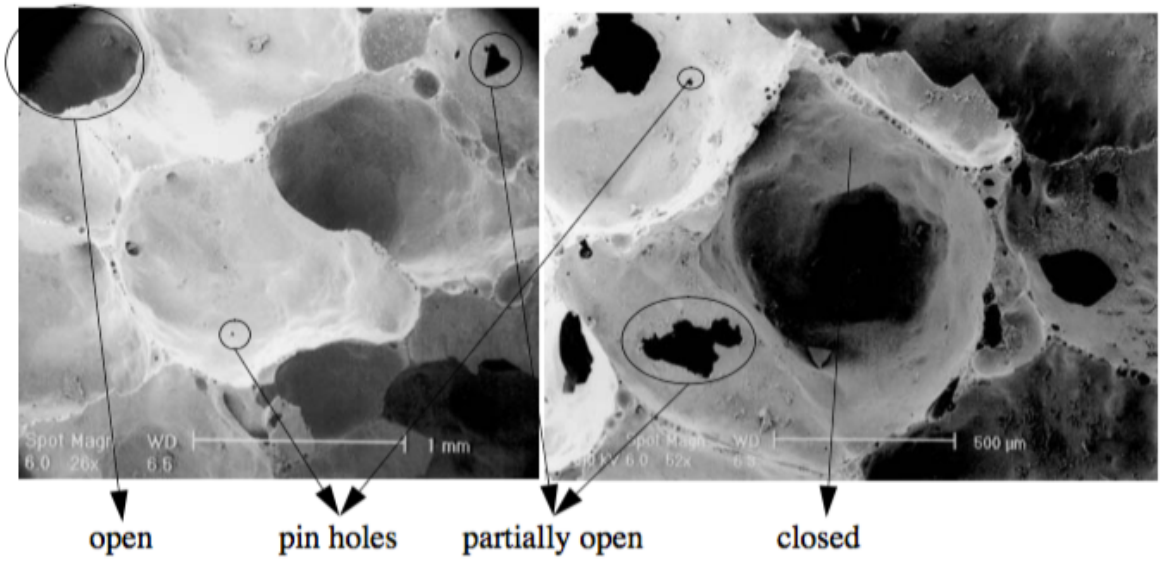

Figure 7: Scanning electron microscope views of the closed-cell glass foam with various types of the cell opening.

The effective fraction of open cells is estimated then by the equation:

$$\vartheta = \frac{N_{open} + (\frac{1}{2})N_{part}}{N_{open} + N_{part} + N_{pin} + N_{closed}} \qquad (4)$$

where N correspond to the number of walls of various classes.

In practice, it is difficult to make foam with only closed or only open cells. Open-cell foams contain mostly open cells (more than 90%), while the major number of cells in closed-cell foams is closed.

Relative foam density

The relative foam density ρ_f / ρ_s is a crucial parameter for the physical properties of foam. It shows the part of space which is occupied by the solid phase and, therefore, is very important for mechanical, thermal, electrical and many other characteristics of foams. Many empirical equations describing the mechanical properties of foams are connected to the relative foam density by the general formula:

$$\frac{\Phi_f}{\Phi_s} = C\left(\frac{\rho_f}{\rho_s}\right)^p \qquad \textbf{(5)}$$

where Φ_f and Φ_s are mechanical properties of foam and solid phase correspondingly, C and p are the coefficients obtained from the experiments [75, 76]. From Gibson and Ashby's model [75, 76], Goods et al. [59] gave a simplified relation of relative density with cell dimensions as in Eq. (6).

$$\frac{\rho^*}{\rho_s} \propto \frac{V^*}{V_s} \propto \left(\frac{t}{l}\right)^2 \qquad \textbf{(6)}$$

Also, from Eq. (2) for Φ=1 (open-cell foam), negligible gas pressure, small ρ_o, and high relative density, modulus was found to be varying as the square of the density; while at low relative densities, the modulus was linearly dependent on the density.

Cell size

Due to irregular cell structure and variation in size, it has been observed that during compression, extruded foam does not yield uniformly [94, 95]. Cell size is a critical parameter in identification of foam properties, though the base material may change the behavior completely. For example, cell size is not a governing parameter for Young's modulus [96], whereas increasing cell size makes closed-cell foam stiffer [93]. Foam tends to align as per the extrusion direction during compression [97]; and, on the other hand, microscopic inspection reveals a uniform cell distribution and orientation for all the examined material and this infers that mechanical behavior is independent of the direction of the loading [58].

Cell shape or geometrical anisotropy

Due to the production, when foams are extruded and they rise during foaming, the final foam structure is often anisotropic. Based on this production process, mostly three main directions can be determined in foam with different cell dimensions in these directions. Consequently, many foam properties are dependent on the direction. Moreover, mechanical characteristics of foam are better in the directions where foam cells have greater dimensions [98].

Cell walls thickness and distribution of solid between struts and faces

The solid material in foams can be considered to be distributed between 3 geometrical groups: walls, struts and vertices. The solid phase is assumed to concentrate in walls and struts for the closed-cell foams, and in struts for the open-cell foams. The presence of material in the vertices is assumed negligible and can be ignored [98].

Geometry of a foam cell and its constituents

To achieve realistic results in the prediction of the mechanical properties of foam, the structural elements of a foam should be studied thoroughly. This, as well as the properties of the solid material in a foam, is the crucial point in the modelling. An ideal geometry of a foam that has reached a thermodynamical equilibrium should comply with the following terms:

- ✓ A strut is an intersection of 3 walls (Plateau's law [99]).
- ✓ A knot-point is an intersection of 4 struts and an intersection of 6 walls (Plateau's law [51]).
- ✓ Struts are straight in the undeformed state.
- ✓ Several struts, belonging to the same cell wall and connected to each other, lay in one plane.
- ✓ As a result of the previous points, walls are flat in the undeformed state.
- ✓ During the production process of foam (growing), a dihedral angle (angle between faces) is equal to 120 ° .
- ✓ Struts intersect in a vertex under the bond angle equal to 109° 28'16".

These laws are based at the principles of the minimizing surface energy during the foam growth. An example of the strut cross-section in closed-cell polymethacrylimide (PMI) foam is given in following figure.

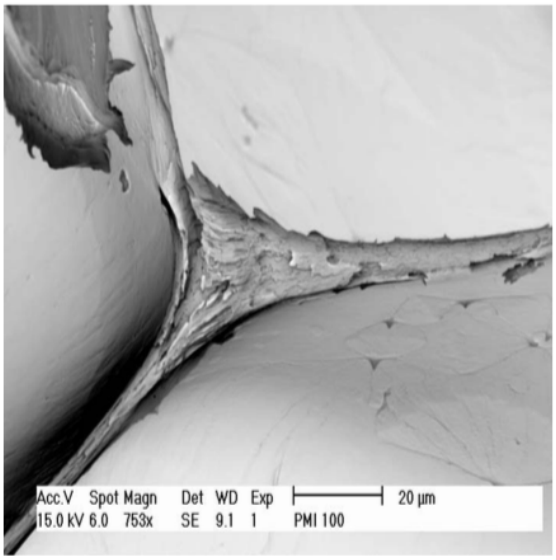

Figure 8: Strut cross-section in the form of Plateau-Gibbs border in PMI foam.

Tensile behaviour of polymeric foam

Ramsteiner et al. [100] report that the tensile modulus of isotropic foams can be described very well by the combination of stretching lamellae and bending of struts according to the well-known pioneering model by Gibson and Ashby.

In the following pictures the indicated parameters for the calculated lines are regarded as the percentage portions of struts/lamellae according to the model. For foams with open cells the fitting parameter φ=1 (portion 100/0) and for the closed cell structure φ=0 (0/100) were used to calculate the limiting lines.

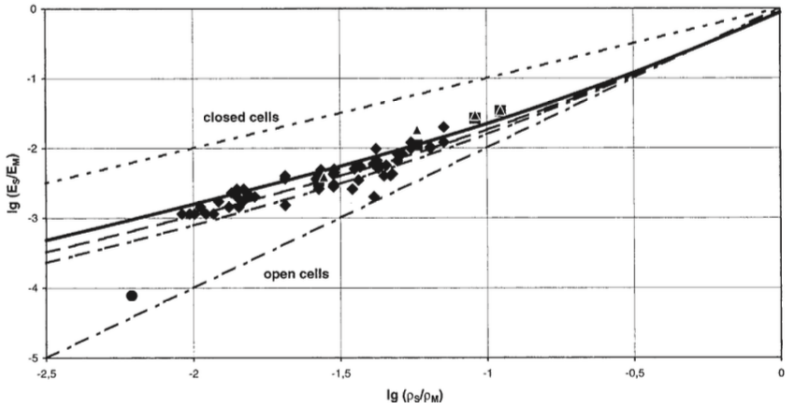

Figure 9: Tensile modulus of foams.

In Fig. 9 the solid line shows the density dependence of the modulus for the mixed situation with an effective strut portion of φ=0.85 and consequently a 0.15 portion of lamellae (85/15).

The modulus of the melamine foam with its open cells lies as expected near to the lower limit describing the open cell structure.

Cell adhesion on polymer substrates

Normally, cell adhesion to the substrate is necessary for a good polymer-cell interaction. Although the substrate does not need to present extracellular matrix-like characteristics for cell adhesion to occur, physicochemical similarity is often desired when the aim is to promote cell differentiation or a more effective interaction of a certain polymer at the implantation site [17-19,101]. Thus, polymers presenting physicochemical and/or mechanical properties as close as possible to those of the tissues into which they will be implanted are currently being developed. These properties include an adequate balance between hydrophilicity/hydrophobicity, electrical charge distribution, hardness, elasticity, and strength [102].

A relationship exists between hydrophilicity and cell adhesion. Among other parameters, more hydrophilic substrates tend to provide a better interaction with cells [103-105]. The relationship between cell adhesion and polar groups on the material surface has been demonstrated for polystyrene. Adhesion of cells was found to increase with increasing polarity of the substrate [106]. In a study investigating hepatic cells cultured on different substrates, cell adhesion increased proportionally to the surface energy of the growth membranes. Adhesion was even higher in the presence of serum proteins adsorbed to the substrates and the metabolic activity of hepatic cells increased on hydrophilic membranes [107]. Other studies demonstrated a relationship between wettability and cell adhesion.

Better adhesion, spreading and growth of cells were observed on surfaces with moderate hydrophilicity [108]. Maximum adhesion was found on substrates with a water contact angle of approximately 57º, irrespective of the type of cell used. Serum proteins also adhered better to substrates presenting moderate hydrophilicity [108].

Thus, cell adhesion is an extremely important factor for biomaterials research. Only after adhesion do the cells initiate the process of spreading, division and production of new extracellular matrix [102,103]. Cell spreading is a complex process that involves modifications in cell morphology as a consequence of alterations in the cytoskeleton, thus improving interaction with the substrate. In figure 10 are shown these modifications.

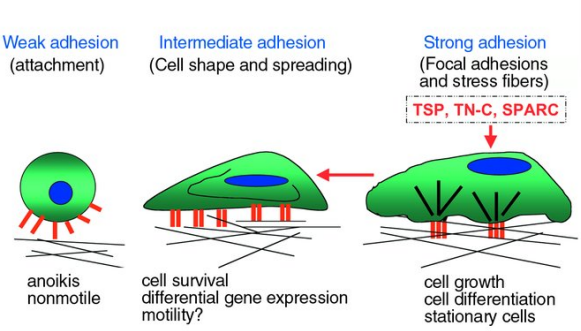

Figure 10: Cell adhesion: the cells start their interaction with the substrate. Note the onset of the phenomenon known as spreading, which is characterized by modifications in the cytoskeleton and, consequently, in cell morphology as a result of interactions with the growth surface, with the cell flattening on the growth surface.

Good integration of the biomaterial with cells or tissues also depends on the structure of the devices itself. Porous materials promote cell growth and induce the production of extracellular matrix components by the cells [105,109]. A uniform distribution and pore interconnections are important to facilitate the formation of tissues in the form of an organized network, with a wide range of applications in tissue reconstruction [18,110,111]. In vivo, porosity and pore interconnection are essential for the proliferation of vessels, facilitating tissue nutrition across the implant. In this respect, different types of scaffolds containing PLLA have been developed and tested as substrates for cell growth [18].

Many studies shown an initially slow cell adhesion to PLLA and PHBV scaffolds [105,109]. This finding does not necessarily indicate that the materials tested would not be useful for tissue engineering. Thus, the surface modifications introduced significantly increased cell adhesion and spreading. The surface properties of biomaterials can be altered in such a way as to make them more adequate for biomedical applications. The most commonly used techniques are chemical etching, gas plasma treatment and electron beam radiation [112]. the selection of scaffold is important to enable the cells to behave in the desired manner to generate tissues and organs of the desired shape and size.

Bioresorbable polymer as cell culture substrates

A wide variety of Bioresorbable polymer have been employed in biological systems, with the most widely used materials being based on -hydroxy acid-derived polyesters, such as poly(L-lactic acid) (PLLA), poly(D-lactic acid) (PDLA), poly(DL-lactic acid) (PDLLA), poly(glycolic acid) (PGA), and polycaprolactone (PCL) [21,22]. During degradation, the polymer is broken down into smaller units by simple hydrolysis and its degradation products are eliminated from the body by metabolic pathways, such as the citric acid cycle, or directly by renal excretion (see Figure 4) [113-114].

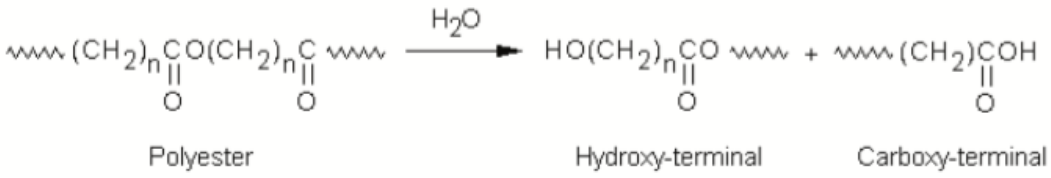

Figure 11: Degradation of poly(-hydroxy acids) by hydrolysis.

Although the degradation of bioresorbable polymers mainly occurs by simple hydrolysis, there are reports in the literature indicating that degradation of PGA and PLLA, at least in part, is also mediated by enzymes [114,115]. Figure 11 is a schematic presentation of the degradation of PLLA by hydrolysis [114]. The elimination routes of the degradation products of some polyesters are shown in Figure 12.

Other bioresorbable polymers used are polyhydroxyalcanoates, polyesters produced by microorganisms. These compounds find applications as raw materials of different devices in the areas of biomedicine and tissue engineering [116]. Polyhydroxyalcanoates include poly(3-hydroxybutyrate) (PHB), poly(3-hydroxybutyrate-co-3-hydroxyvalerate) copolymer (PHBV), poly(4-hydroxybutyrate) (P4HB), poly(3-hydroxybutyrate-co-3-hydroxyhexanoate) copolymer (PHBHHx), and poly(3-hydroxyoctanoate) (PHO). These compounds have been used for the development of sutures, devices to guide tissue repair, heart implants, orthopedic pins, stents, tubules for nerve regeneration, and membranes for skin regeneration [116]. The use of PLLA/PHBV blends has appeared as a new proposal in the literature. The biological evaluation of this compound is relevant for tissue engineering [117,118].

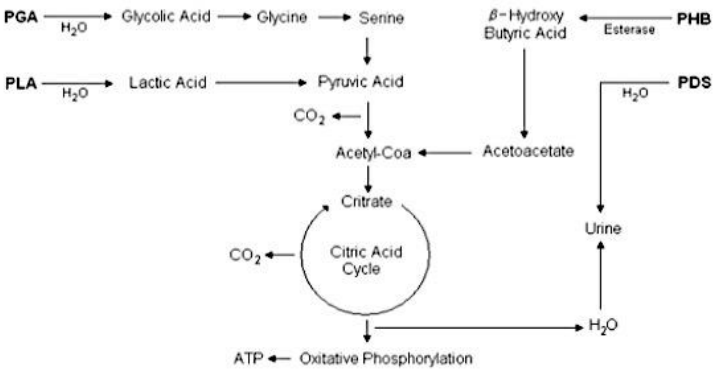

Figure 12: Routes of degradation and excretion of some polyesters: poly(p-dioxane) (PDS), poly(glycolic acid) (PGA), poly(lactic acid) (PLA), and poly(hydroxybutyrate) (PHB).

A well-designed three-dimensional scaffold is one of the fundamental tools to guide tissue formation in vitro and in vivo. Frontiers areas in medicine is changing rapidly from utilizing synthetic implants and tissue grafts to a tissue engineering approach that uses degradable porous material scaffolds integrated with biological cells or molecules to regenerate tissues.

Respiratory system

The main functions of the respiratory system involve carrying out gas exchange, bringing oxygen into the body and removing carbon dioxide waste by metabolism. The system includes the nose, pharynx, larynx, trachea, bronchi, and lungs and pleurae.

My attention is focused on trachea, human bronchial mucose and epithelial barrier because there is a need for better support for trachea and epithelial cell/ barrier for future application in tissue engineering.

Trachea

The trachea is a major airway of the lower respiratory system. The trachea is a cartilaginous and membranous tube extending from the lower part of the larynx to the upper border of the fifth thoracic vertebra, where it divides into the two bronchi, one for each lung. The trachea is an almost cylindrical structure that measures about 11 cm in length, with a diameter of about 2.5 cm [119]. The trachea is composed of rings of hyaline cartilage wrapped in elastic fibrous membrane; its interior is lined with a mucous membrane. The tracheal cartilages are stacked horizontally and separated by narrow intervals. They provide structural support that helps keep the airway open and are typically highly elastic until advanced age. The number of cartilages varies from 16 to 20; each forms an incomplete, crescent shaped ring around the frontal two thirds of the tube.

The mucosae of the trachea and main bronchi consist of a pseudo-stratified epithelium and lamina propria separated from the tunica by an elastic lamina; the outermost tunica adventitia is rich in collagen. In detail, the pseudo-stratified epithelium is composed by different types of cells, including muciparous goblet cells, serous cells, ciliated columnar cells, basal cells, and stem cells that are able to divide asymmetrically to give rise to cells capable of differentiating into the other cytotypes of the epithelial lining. While the bronchial diameter decreases, the structure of the respiratory tree changes: the epithelium becomes more and more cubic, with loss of cilia and scarce goblet cells, and the alveoli becoming flattened [120].

Epithelial Barriers—Why and How?

In multicellular organisms, cellular barriers (endothelia and epithelia) are essential for tissue compartmentalization and performance of specialized functions [121]. The effectiveness of epithelia as barriers to the external environment arises from the propensity of epithelial cells to elaborate a range of cell–cell adhesion complexes that link with the cytoskeleton to form a

robust sheet-like structure. This structure functions as a selective permeability barrier due to the properties of tight junctions, the apical most of the adhesive complexes.

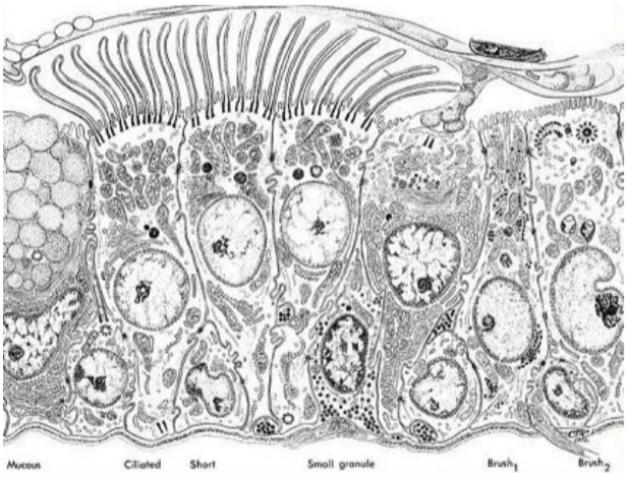

Figure 13: Illustration of normal human bronchial epithelium.

Tight junctions are formed by transmembrane and intracellular proteins that link to the actin cytoskeleton [122]. These junctions form around the whole perimeter of each cell, forming a continuous belt-like structure to control the barrier (or "gate") properties of the epithelium. Thus, tight junctions (see figure 14) regulate the paracellular passage of ions, water, and various macromolecules across epithelia. In addition, tight junctions prevent lateral diffusion and intermixing of molecules in the apical membrane with those in the lateral membrane.

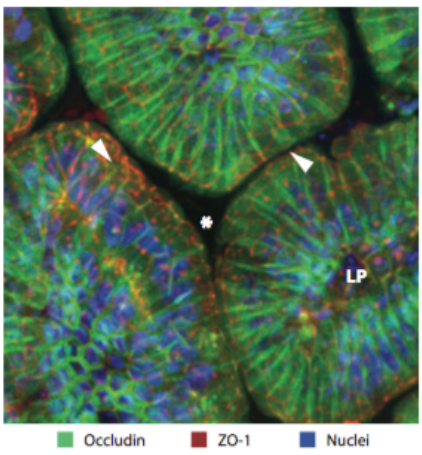

Figure 14: Tight junction proteins in villus enterocytes. Three-dimensional projection of jejunal villi from a transgenic mouse expressing enhanced green fluorescent protein–occludin and monomeric red fluorescent protein 1–zonula occludens 1 (ZO-1; arrowheads) under control of the villin promoter. Nuclei were stained blue. The gut lumen (asterisk) can be seen between the villi, and the lamina propria (LP) can be seen beneath the single layer of villus epithelial cells [123].

This so-called "fence" function maintains cell polarity, another key property for normal epithelial function. Located below the tight junctions are the adherens junctions, which also link to the actin cytoskeleton [124, 125], and the desmosomes, which link to the intermediate filaments [126]. These two types of junctions do not directly seal the space between epithelial

cells, but they are critical for providing the adhesive force to ensure the integrity of the cell layer. Adherens junctions are the first junctions to form and are essential for the formation of the other junctions [124]; they are also key regulators of epithelial cell proliferation and differentiation [127]. Hemidesmosomes [128] facilitate attachment of the intermediate filaments of the epithelial sheet to the basement membrane, a thin sheet of self- assembled extracellular matrix (ECM) proteins comprising laminin and collagen IV networks stabilized by nidogen/perlecan bridges [129]. The basement membrane plays an important role in maintaining epithelial structure, polarization, and compartmentalization.

Bronchial Epithelial Barrier Homeostasis

The pseudostratified epithelium of the conducting airways is exposed to a wide range of environmental materials present in inhaled air, including noxious gases and anthropogenic and natural particulates, including pathogens [130]. The epithelial layer is composed of a variety of cell types, including columnar ciliated and secretory cells that line the airways surface and contribute to its function as a barrier to the inhaled environment. These cells overlie smaller basal cells, which exhibit properties of progenitor cells, not only showing capacity for self-renewal and clonal expansion but also giving rise to basal, ciliated, and secretory lineages, during both steady state and epithelial repair conditions after damage [131]. In conjunction with submucosal glands, the secretory goblet cells produce mucus, a fluid containing hydrated gel-forming mucins and a range of host defense and cytoprotective molecules, including antimicrobial molecules, antiproteases, and antioxidants [130] that act as a “chemical” barrier. The properties of the mucus are dictated in large part by the oligomeric secreted mucins MUC5AC and MUC5B [132], multifunctional glycoproteins that provide the structural framework of the mucous barrier. The mucus traps and inactivates inhaled agents and facilitates their clearance via the mucociliary escalator. It is a testament to the effectiveness of the chemical and physical barriers of the bronchial epithelium that most environmental challenges are largely overcome without the need to develop an inflammatory response. This is well illustrated in recent studies of the importance of Muc5b for defense of airways and for maintaining immune homeostasis in mouse lungs [133]. Thus, Muc5b deficiency caused accumulation of materials in upper and lower airways and led to chronic infection by multiple bacterial species, including Staphylococcus aureus, and to inflammation that failed to resolve normally.

The epithelium also acts a site for cells of the immune system, supporting their role in immune surveillance. For example, tight junction proteins interact directly with dendritic cells

to allow them to sample the airway lumen without disruption of the epithelial barrier [134, 135], as occurs in the gastrointestinal tract [136]. Under homeostatic conditions, epithelial cells have a repressive effect on immune cells.

In recent years, there has been a significant appreciation of the key role of the airway epithelium as a component of the innate immune system. Airway epithelial cells are actively involved in immune surveillance, expressing a range of sensors including RNA helicases, nucleotide binding and oligomerization domain–like receptors, and Toll-like receptors [137–138] that allow detection of pathogen and/or damage-associated molecular patterns (DAMPs and PAMPs, respectively).

Thus, with appropriate stimulation, the bronchial epithelium can contribute to innate immunity by the secretion of immunostimulatory and modulatory mediators including cytokines, chemokines, growth factors, and lipid mediators that contribute to the recruitment and activation of effector cells and antigen-presenting cells [130, 139]. Critical to function of this immunological barrier are the tight junctions that determine apical–basolateral polarity and vectorial cytokine release, allowing gradients of chemoattractants to be produced to orchestrate immune cell movement [140]. As the initial cell of contact with the environment, the bronchial epithelium is pivotal in immune surveillance and appropriate activation of effector cells and antigen- presenting cells.

Thus, the bronchial epithelium plays a central role in controlling tissue homeostasis, and it has been hypothesized that abnormalities in airway epithelial barrier can contribute to disease pathologies, including bronchial asthma [141], which is the focus of this review, as well as chronic obstructive pulmonary disease.

Dysregulation of the Epithelial Barrier in Asthma

A number of lines of evidence support the concept that the bronchial epithelial barrier in asthma is structurally and functionally altered. It is not clear whether these phenotypic differences are due to fundamental genetic abnormalities, whether they are adaptive responses to environmental stresses - or, indeed, if they are a combination of genetic and environmental interactions. During an asthma attack, the lining of the bronchial tubes swell, causing the airways to narrow, thus reducing the flow of air into and out of the lungs (see figure 15). Recurrent asthma symptoms frequently cause sleeplessness, daytime fatigue, reduced activity levels and school and work absenteeism. Luckily, asthma has a relatively low fatality rate compared to other chronic diseases.

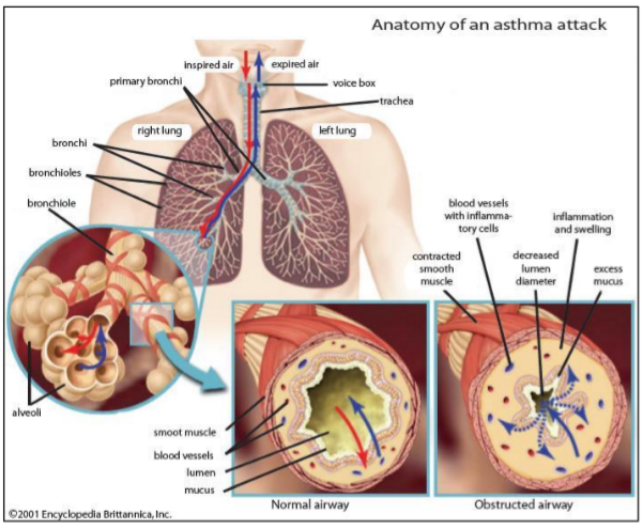

Figure 15: Anatomy of an asthma attack.

Furthermore, in small airways, mucus hypersecretion may lead to mucus plugging, which over time can lead to severe airflow obstruction. Epithelial fragility [142] and epithelial shedding [143] have been recognized for many years, although this has been a controversial area [144]. The physical barrier of the bronchial epithelium in asthma is disrupted, with evidence of loss of tight junction proteins [145, 146], a reduction in adherens junction proteins [146], and a reduction in desmosome length [147]. Consistent with the abnormalities in vivo, functional studies using epithelial cultures from donors with asthma or normal donors indicate that there is increased permeability and sensitivity to environmental challenges in asthma [145] and increased susceptibility to oxidant stress [148]. Studies using epithelial cells from pediatric donors have also shown evidence of an increased inflammatory response after mechanical wounding, exposure to particulate matter, or respiratory syncytial virus [149]. The increase in epithelial permeability in asthma has led to proposals that restoration of the barrier may offer new therapeutic approaches. Tight junctions are highly regulated by phosphorylation and by their association with the cytoskeleton. Serine and threonine phosphorylation of occludin is abundant in epithelia with intact junctions [150], whereas tyrosine phosphorylation of occludin is associated with increased permeability [151]. A number of studies have identified agents that have the potential to cause disruption of epithelial tight junctions in asthma. Cytokines such as IL-13 and TNF-a can cause disruption of the epithelial barrier in in vitro models [152, 153], whereas inhalation exposure to ovalbumin in sensitized mice or rats results in epithelial tight junction disruption [154, 155], consistent with inflammatory mediators causing barrier disruption.

References

[1] F. Causa, P.A. Netti, L. Ambrosio, G. Ciapetti, N. Baldini, S. Pagani, D. Martini, A. Giunti, Poly- ε-caprolactone/hydroxyapatite composites for bone regeneration: in vitro characterization and human osteoblast response. J. Biomed. Mater. Res. Part A (2006) 76A(1): 151–162.

[2] R.P. Lanza, R. Jackson, A. Sullivan, J. Ringeling, C. McGrath, W. Kuhtreiber, W.L. Chick, Xenotransplantation of cells using biodegradable microcapsules. Transplantation (1999) 67:1105–1111.

[3] M. Risbud, Tissue engineering: implications in the treatment of organ and tissue defects. Biogerontolgy (2001) 2(2):117-125.

[4] A.G. Mikos, L.V. McIntire, J.M. Anderson, J.E. Babensee, Host response to tissue engineered devices, Advanced Drug Delivery Reviews (1998) 33(1-2):111-139.

[5] B.N. Brown, J.E. Valentin, A.M. Stewart-Akers, G.P. McCabe, S.F. Badylak, Macrophage phenotype and remodeling outcomes in response to biologic scaffolds with and without a cellular component, Biomaterials (2009) 30(8):1482-91.

[6] F.G. Lyons, A.A. Al-Munajjed, S.M. Kieran, M.E. Toner, C.M. Murphy, G.P. Duffy, F.J. O'Brien, The healing of bony defects by cell-free collagen-based scaffolds compared to stem cell-seeded tissue engineered constructs, Biomaterials (2010) 31(35):9232-43.

[7] D.W. Hutmacher, Scaffolds in tissue engineering bone and cartilage, Biomaterials (2000) 21(24):2529-43.

[8] E.A. Phelps, A.J. Garcia, Update on therapeutic vascularization strategies, Regen Med (2009) 4(1):65-80.

[9] H.C. Ko, B.K. Milthorpe, C.D. McFarland, Engineering thick tissues--the vascularisation problem, Eur Cell Mater (2007) 14:1-18.

[10] I.V. Yannas, E. Lee, D.P. Orgill, E.M. Skrabut, G.F. Murphy, Synthesis and characterization of a model extracellular matrix that induces partial regeneration of adult mammalian skin, Proc Natl Acad Sci U S A (1989) 86(3):933-7.

[11] F.J. O'Brien, B.A. Harley, I.V. Yannas, L.J. Gibson, The effect of pore size on cell adhesion in collagen-GAG scaffolds, Biomaterials (2005) 26(4):433-41.

[12] C.M. Murphy, M.G. Haugh, F.J. O'Brien, The effect of mean pore size on cell attachment, proliferation and migration in collagen-glycosaminoglycan scaffolds for bone tissue engineering, Biomaterials (2010) 31(3):461-6.

[13] C.M. Murphy, F.J. O'Brien, Understanding the effect of mean pore size on cell activity in collagen-glycosaminoglycan scaffolds, Cell Adh Migr (2010) 4, 377.

[14] S. Partap, Scaffolds & Surfaces. In: Basic Engineering for Medics and Biologists, An ESEM Primer on Engineering for Medicine, Lee, T.C. and Niederer, P. (Eds.) IOS Press, Nieuwe Hemweg, (2010) 152, 187.

[15] S.J. Hollister, Scaffold engineering: a bridge to where?, Biofabrication (2009) 1, 012001.

[16] L. L. Hench, Biomaterials: a forecast for the future, Biomaterials (1998) 19: 1419-1423.

[17] J. A. Hubbell, Biomaterials in tissue engineering, Biotechnology (1995) 13: 565-576.

[18] E. S. Place, N. D. Evans, M. M. Stevens, Complexity in biomaterials for tissue engineering, Nature Materials (2009) 8: 457-470.

[19] B. Alberts, A. Johnson, J. Lewis, M. Raff, K. Roberts, P. Walter, Molecular Biology of the Cell, 5th ed., (2008) Garland Science, New York.

[20] A.R. Santos Jr., M.L.F. Wada, Polímeros biorreabsorvíveis como arcabouços para cultura de células e engenharia tecidual, Polímeros: Ciência e Tecnologia, (2007) 17: 308-317.

[21] P. Törmälä, T. Pohjonen, P. Rokkanen, Bioabsorbable polymers: materials technology and surgical applications, Proc. Instn. Mech. Eng. Part H - J. Eng.Med (1998) 212: 101-111.

[22] M. Vert, M.S. Li, G. Spenlehauer, P. Guerin, Bioresorbability and biocompatibility of aliphatic polyesters, J. Mater. Sci. Mater. Med., 3: 432-446.

[23] S.H. Barbanti, C.A.C. Zavaglia, E.A.R. Duek, Polímeros bioreabsorvíveis na engenharia de tecidos. Polímeros: Ciência e Tecnologia (2005) 15: 13-21.

[24] A.G. Mikos, L. Lu, J.S. Temenoff, J.K. Temmser, Synthetic Bioresorbable polymer scaffolds. In: An introduction to material in medicine, Ratner B D, Hoffman A S, Schoen F J, Lemons J E, (Ed.). pp 743, Elsevier Academic Press. USA (2004).

[25] A.G. Mikos, G. Sarakinos, S.M. Leite, J.P. Vacanti, R. Langer. Laminated three-dimensional biodegradable foams for use in tissue engineering, Biomaterials (1993a) 14, 323-330.

[26] A.G. Mikos, Y. Bao, L.G. Cima, D.E. Ingber, J.P. Vacanti, R. Langer, Preparation of Poly (glycolic acid) bonded fiber structures for cell attachment and transplantation. Journal of Biomedical Materials Research (1993b) 27, 183-189.

[27] A.G. Mikos, G. Sarakinos, J.P. Vacanti, R.S. Langar, L.G. Cima, Biocompatible polymer membranes and methods of preparation of three dimensional membrane structures, U.S. patent 5 (1996) 514, 378.

[28] P.X. Ma, R. Langer, Fabrication of biodegradable polymer foams for cell transplantation and tissue engineering, In Tissue Engineering Methods and Protocols, Morgan, J., and Yarmush, M. (eds.) Humana Press (1999) NJ, 47.

[29] L. Lu, S. Peter, M. Lyman, H. Lai, S. Leite, J. Tamada, S. Uyama, J. Vacanti, R. Langer, A. Mikos, In vitro and in vivo degradation of porous poly (DL-lactic-co- glycolic acid) foams, Biomaterials (2000) 21, 1595-1605.

[30] P. Plikk, S. Målberg, A.C. Albertsson, Design of resorbable porous tubular co-polyester scaffolds for use in nerve regeneration, Biomacromolecules (2009) 10(5), 1259-64.

[31] E. Sachlos, J.T. Czernuszka, Making tissue engineering scaffolds work, Review on the application of solid free from fabrication technology to the production of tissue engineering scaffolds. European cells and materials (2003) 5, 29-40.

[32] B.B. Mandal, S.C. Kundu, Cell proliferation and migration in silk fibroin 3D scaffolds, Biomaterials (2009a) 30, 2956-2965.

[33] B.B. Mandal, S.C. Kundu, Osteogenic and adipogenic differentiation of rat bone marrow cells on non-mulberry and mulberry silk gland fibroin 3D scaffolds, Biomaterials (2009b) 30, 5019–5030.

[34] H. Schoof, J. Apel, I. Heschel, G. Rau, Control of pore structure and size in freeze-dried collagen sponges, J. Biomed Mater Res (2001) 58, 352–7.

[35] E.D. Boland, P.G. Espy, G.L. Bowlin, Tissue engineering scaffolds. In Encyclopaedia of Biomaterials and biomedical engineering (2004) Wenk G. E.; Bowlin, G. L. (Edi). pp 1633-1635. Richmong, Verginia , USA.
[36] H. Strathmann, Production of microporous media by phase inversion processes, ACS Symp. Ser., 269 (1985) 165.
[37] H. Strathmann and K. Koch, The formation mechanism of phase inversion membranes, Desalination, 21 (1977) 241.
[38] J.G. Wijmans and C.A. Smolders, Preparation of asymmetric membranes by the phase inversion process, in H.K. Londsdale and M.H. Pinho (Eds.), Synthetic Membranes: Science, Engineering and Applications, Reidel, Dordrecht, The Netherlands, 1986, pp. 39-56.
[39] L. Zeman and T. Fraser, Formation of air-cast cellulose acetate membranes. Part I. Study of macrovoid formation, J. Membrane Sci., 84 (1993) 93.
[40] L. Zeman and T. Fraser, Formation of air-cast cellulose acetate membranes. Part II. Kinetics of demixing and mi- crovoid growth, J. Membrane Sci., 87 (1994) 267.
[41] H. Tompa, Polymer Solutions, Butterworths, London, 1956.
[42] F.W. Altena and C.A. Smolders, Calculation of liquid-liquid phase separation in a ternary system of a polymer in a mixture of a solvent and a nonsolvent, Mromolecules, 15 (1982) 1491.
[43] L. Yilmaz and A.J. McHugh, Analysis of nonsolvent-solvent- polymer phase diagrams and their relevance to membrane formation modelling, J. Appl. Polym. Sci., 31 (1986) 997.
[44] K. Binder, in Materials Science and Technology, A Comprehensive Treatment Vol. 5. Phase Transformations in Materials, P. Haasen, Ed., VCH Publishers, New York, 1991, p. 405.
[45] D.R. Lloyd, K.E. Kinzer, and H. S. Tseng, Microporus membrane formation via thermally induced fase separation, J. Membr (1990) Sci., 52, 239.
[46] S.S. Kim and D.R. Lloyd, Microporous membrane formation via thermally-induced phase separation. III. Effect of thermodynamic interactions on the structure of isotactic polypropylene membranes, J. Membr. Sci. (1991) 64, 13.
[47] D. R. Lloyd, S. S. Kim, and K. E. Kinzer, Microporous membrane formation via thermally- induced phase separation. III. Effect of thermodynamic interactions on the structure of isotactic polypropylene membranes, J. Membr. Sci. (1991) 64, 1.
[48] J.H. Aubert, Isotactic polystyrene phase diagrams and physical gelation, Macromolecules (1988) 21, 3468.
[49] R.C. Domszy, R. Alamo, C.O. Edwards, and L. Mandelkern, Thermoreversible gelation and crystallization of homopolymers and copolymers, Macromolecules (1986) 19, 310.
[50] L. Mandelkern, C. O. Edwards, R. C. Domszy, and M. W. Davidson, in Polymer Science and Technology Vol 30: Microdomains in Polymer Solutions, P. Dubin, Ed., Plenum Press, New York/London, 1985, p. 121.
[51] P. van de Witte, H. Esselbrugge, P. J. Dijkstra, J. W. A. van den Berg, and J. Feijen, Phase transitions during membrane formation of polylactides. I. A morphological study of membranes obtained from the system polylactide-chloroform-methanol, J. Membr. Sci., (1996) 113, 223.

[52] P. van de Witte, P. J. Dijkstra, J. W. A. van den Berg, and J. Feijen, Membrane formation of polylactides, Polym. Prepr. (1994) 35, 842.
[53] A. M. W. Bulte, B. Folkers, M. H. V. Mulder, and C.A. Smolders, Membranes of semicrystalline aliphatic polyamide nylon 4,6: Formation by diffusion-induced phase separation, J. Appl. Polym. Sci. (1993) 50, 13.
[54] L. Marsavina, E. Linul, Fracture toughness of poly- urethane foams, Experiments versus micromechanical models. (2010) In : Proc 18th European Conference on Fracture, Germany
[55] S.T. Lee, C.B. Park, N.S. Ramesh, Polymeric foams: science and technology (2006) vol. 3, CRC Press, Florida.
[56] L.J. Gibson, M.F. Ashby, Cellular solids: structures and properties 2nd edn. Cambridge University Press, (1997) Cambridge.
[57] C.C. Chou, Y. Zhao, L. Chai, J. Co, G.G. Lim, T.L, Lin Development of foam models as applications to vehicle interior, SAE Technical (1995) Paper 952733.
[58] M. Avalle, G. Belingardi, R. Montanini, Characterization of polymeric structural foams under compressive impact loading by means of energy-absorption diagram, Int J Impact Eng (2001) 25:455–472.
[59] S.H. Goods, C.L. Neuschwanger, C.C. Henderson, D.M. Skala, Mechanical properties of CRETE, a polyurethane foam, J Appl Polym Sci (1998) 68(7):1045–1055.
[60] H.X. Zhu, J.F. Knott, N.J. Mills, Analysis of the elastic properties of open-cell foams with tetrakaidecahedral cells, J Mechs Phys Solids (1997) 45(3):319–343.
[61] W.E. Warren, A.M. Kraynik, Linear elastic behavior of a low-density Kelvin foam with open cells, J Appl Mech (1997) 64(4):787–794.
[62] M.A. Fortes, J.J. Fernandes, I. Serralheiro, M.E. Rosa, Experimental determination of hydrostatic compression versus volume changes curves for cellular solids, J Test Eval (1989) 17:67–71
[63] M.C. Shaw, T. Sata, The plastic behavior of cellular materials, Int J Mech Sci (1966) 8(7):469–478
[64] F. Saint-Michel, L. Chazeau, J.Y. Cavaille, E. Chabert, Mechanical properties of high density polyurethane foams: I. Effect of the density, Composites Sci Technol (2006) 66(15):2700–2708.
[65] F. Saint-Michel, L. Chazeau, J.Y. Cavaille, Mechanical properties of high density polyurethane foams: II effect of the filler size Composites Sci Technol (2006) 66(15):2709–2718.
[66] L. Marsavina, T. Sadowski, D.M. Constantinesc, R. Negru, Polyurethane foams behaviour. Experiments versus modeling Key Eng Mat (2009) 399:123–130.
[67] L. Marsavina, T. Sadowski, D.M. Constantinescu, R. Negru, Failure of polyurethane foams under different loading conditions Key Eng Mat (2008) 385:205–208.
[68] L. Marsavina, T. Sadowski, Dynamic fracture toughness of polyurethane foam Polym Test (2008) 27(8):941–944.
[69] L. Marsavina, T. Sadowski, M. Knec, R. Negru, Non-linear behaviour of foams under static and impact three point bending, Int J Non-Linear Mech (2010) 45(10):969–975.
[70] A. Goto, K. Yamaguchi, H. Hamada, Influence of geometric shape of void on mechanical properties of polyurethane foam, (2003) Proc ANTEC: 3575–3578.

[71] K. Yamaguchi, A. Goto, H. Hamada, Compressive properties of urethane foam, Symp 8th Japan Int (2003) SAMPE: 689–692.
[72] Q.M. Li, R.A.W. Mines, R.S. Birch, The crush behaviour of Rohacell-51WF structural foam. Int J Solids Struct (2000) 37(43):6321–6341.
[73] F. Ramsteiner, N. Fell, S. Forster, Testing the deformation behaviour of polymer foams. Polym Test (2001) 20(6):661–670.
[74] N.J. Mills and A.M.H. Hwang, The multiple impact per- formance of high density polyethylene foam, Cell Polym (1989) 259–276.
[75] L.J. Gibson, M.F. Ashby, The mechanics of three dimensional cellular materials, Proc R Soc Lond (1982) A382:43–59.
[76] L.J. Gibson, M.F. Ashby, Cell solids. Pergamon Press, (1988) Oxford.
[77] M.R. Patel, I. Finni, Structural features and mechanical properties of rigid cellular plastics, J Mat (1970) 5(4):909–932.
[78] S. Timeshenko, D.H. Young, Elements of strength of materials, 4th edn. (1962) East West Press, New Delhi.
[79] A.N. Gent, A.G. Thomas, The deformation of foamed elastic materials, J Appl Polym Sci (1959) 1(1):107–113.
[80] J.M. Lederman, The prediction of the tensile properties of flexible foams, J Appl Polym Sci (1971) 15(3):693–703.
[81] R. Chan, M. Nakamura, Mechanical properties of plastic foams the dependence of yield stress and modulus on the structural variables of closed-cell and open-cell foams, J Cell (1969) Plast 5(2):112–118.
[82] P. Barma, M.B. Rhodes, R. Salovey, Mechanical properties of particulate-filled polyurethane foams, J Appl Phys (1978) 49(10): 4985–4991.
[83] G. Menges, F. Knipschild, Estimation of mechanical properties for rigid polyurethane foams, Polym Eng Sci (1975) 15(8):623–627.
[84] W.L. Ko, Deformations of foamed elastomers, J Cell Plasts (1965) 1(1):45–50.
[85] Z.H. Tu, V.P.W. Shim, C.T. Lim, Plastic deformation modes in rigid polyurethane foam under static loading, Int J Solids Structs (2001) 38(50):9267–9279.
[86] R.E. Skochdopole, L.C. Rubens, Physical property modifications of low-density polyethylene foams, J Cell Plasts (1965) 1(1):91–96.
[87] A. Goto, K. Yamashita, C. Nonomura, K. Yamaguchi, Modeling of cell structure in polyurethane foam, J Cell Plast (2004) 40(6):481–488.
[88] M.D. Montminy, A.R. Tannenbaum, C.W. Macosko, New algorithms for 3-D imaging and analysis of open-celled foams, J Cell Plast (2001) 37(6):501–515.
[89] K.M. Lewis, Kijak, K.B. Reuter, J.B. Szabat, An image analysis method for cell-size and cell-size distribution measurement in rigid foams, J Cell Plasts (1996) 32(3):235–259.
[90] A.K. Bledzki, J. Gassan, Kurek, Influence of the void fraction on the mechanical compression properties of foams, J Cell Plast (1996) 32(3):224–234.
[91] A.P. Roberts, E.J. Garboczi, Elastic properties of model random three-dimensional open-cell solids, J Mech Phys Solids (2002) 50(1):33–55.
[92] A.A. Berlin and F.A. Shutov, Chemistry and Processing of Foamed Polymers, (1980) Moscow.

[93] K. Yasunaga, R.A. Neff, X.D. Zhang, C.W. Macosko, Study of cell opening in flexible polyurethane foam, J Cell Plast (1996) 32(5):427–448.
[94] J.L. Throne, R.C. Progelhof, Closed cell foam behavior under dynamic loading-I stress-strain bchavior of low density foams, J Cell Plasts (1984) 20(6):437–442.
[95] J.L. Throne, R.C. Progelhof, Closed-cell foam behavior under dynamic loading-II loading dynamics of low-density foams, J Cell Plasts (1985) 21(1):43–50.
[96] J.S. Morgan, J.L. Wood, R.C. Bradt, Cell size effects on the strength of foamed glass, Mat Sci Eng (1981) 47(1):37–42.
[97] C.J. Benning, Plastic foams: structure properties, and applications, vol 2nd. (1969) Wiley-Interscience, New York.
[98] V. Shulmeister, Modelling of the mechanical properties of low-density foams, PhD Dissertation, (1998) Delft University of Technology.
[99] J.A.F. Plateau, Statique expe´rimentale et the´orique des liquides soumis aux seules forces mole´culaires, vol 2. (1873) Gauthier- Villars, Paris.
[100]F. Ramsteiner, N. Fell, S. Forster, Testing the deformation behaviour of polymer foams, Polymer Testing 20 (2001) 661–670.
[101] R. Langer, J.P. Vacanti, Tissue engineering. Science (1993) 260: 920-926.
[102] J.E. Davies, B. Causton, Y. Bovell, The migration of osteoblasts over substrata of discrete surface charge, Biomaterials (1986) 7: 231-233.
[103] J-L. Dewez, J. Lhoest, E. Detrait, V. Berger, C.C. Dupont-Gillain, L. Vincent, Y. Schneider, P. Bertrand, P.G. Rouxhet, Adhesion of mammalian cells to polymer surfaces: from physical chemistry of surfaces to selective adhesion of defined patterns, Biomaterials (1998) 19: 1441-1445.
[104] J.A. Neff, K.D. Caldwell, P.A. Tesco, A novel method for surface modification to promote cell attachment to hydrophobic substrates J. Biomed. Mater. Res. (1998) 40: 511-519.
[105] A.R. Santos Jr, S.H. Barbanti, E.A.R. Duek, H. Dolder, R.S. Wada, M.L.F. Wada, Growth and differentiation of Vero cells on poly(L-lactic acid) membranes of different pore diameters. Artif. Organs (2001) 25: 7-13.
[106] K. Birdi, Cell adhesion on solids and the role of surface forces, J. Theor. Biol. (1981) 93:1-5.
[107] L. De Bartolo, S. Morelli, A. Bader, E. Drioli, Evaluation of cell behaviour related to physico-chemical properties of polmeric membranes to be used in bioartifical organs, Biomaterials (2002) 23: 2485-2497.
[108] J.H. Lee, G. Khang, J.W. Lee, H.B. Lee, Interaction of different types of cells of polymer surfaces with wettability gradient. J. Colloid Interface Sci. (1998) 205: 323-330.
[109] A.R. Santos Jr, B.M.P. Ferreira, E.A.R. Duek, H. Dolder, R.S. Wada, M.L.F. Wada, Differentiation pattern of Vero Cells Cultured on Poly(L-Lactic Acid)/Poly(Hydroxybutyrate-co-Hydroxyvalerate) Blends. Artif. Organs (2004) 28: 381-89.
[110] H.L. Wald, G. Sarakinos, M.D. Lyman, A.G. Mikos, J.P. Vacanti, R. Langer, Cell seeding in porous transplantation devices, Biomaterials (1993) 14: 270-278.
[111] A. van Sliedregt, J.A. Van Loon, C. Van Der Brink, K. De Groot, C.A. Van Blitterswijk, Evaluation of polylactice monomers in a in vitro biocompatibility assay, Biomaterials (1994) 15: 251-256.

[112] I. Keen, O. Broota, L. Rintoul, P. Fredericks, M. Trau, L. Grondahl, Introducing amine functionalities on a poly(3-hydroxybutirate-co-3-hydroxivalerate) surface: compring the use of ammonia plasma treatment and ethylenediamine aminolysis, Biomacromolecules (2006) 7: 427-434.

[113] J.O. Hollinger, G.C. Battistone, Biodegradable bone repair materials: synthetic polymers and ceramics. Clin. Orthop. Rel. Res. (1986) 207: 290-305.

[114] S.H. Barbanti, C.A.C. Zavaglia, E.A.R. Duek, Porous and dense poly(L-lactic acid) membranes: in vitro degradation, Acta Microscopica (2002) 11: 85-89.

[115] S.M. Li, H. Garreau, M. Vert, Structure property relationship in the case of the degradation of massive poly(-hydroxy acids) in aqueous media, Part 1: poly (DLlactic acid). J. Mater Sci. Mater. Res. (1990) 1: 123-130.

[116] G.Q. Chen, Q. Wu, The application of polyhydroxyalkanoates as tissue engineering Materials, Biomaterials (2005) 26: 6565-6578.

[117] B.M.P. Ferreira, C.A.C. Zavaglia, E.A.R. Duek, Films of poly(L-lactic acid)/poly(hydroxybutyrate-co-hydroxyvalerate) blends: in vitro degradation. Mater. Res. (2001) 4: 34-42.

[118] B.M.P. Ferreira, C.A.C. Zavaglia, E.A.R. Duek, Films of PLLA/PHBV: thermal, morphological and mechanical characterization. J. Applied. Polymer Sci. (2002) 86: 2898-2906.

[119] J.F. Murray, The normal lung, WB Sanders (1986) Philadelphia.

[120] D.B. Gail C.J.M. Lenfant , Cells of the lung: Biology ad clinical implications, Am Rev Respir Dis (1983) 127: 366-87.

[121] A.M. Marchiando W.V. Graham J.R. Turner, Epithelial barriers in homeostasis and disease, Annu Rev Pathol (2010) 5:119–144.

[122] S. Tsukita, M. Furuse, M. Itoh, Multifunctional strands in tight junctions, Nat Rev Mol Cell Biol (2001) 2:285–293.

[123] Garrod D, Chidgey M. Desmosome structure, composition and function, Biochim Biophys Acta (2008) 1778:572–587.

[124] A.I. Ivanov, N.G. Naydenov, Dynamics and regulation of epithelial adherens junctions: recent discoveries and controversies, Int Rev Cell Mol Biol (2013) 303:27–99.

[125] W.J. Nelson, Regulation of cell-cell adhesion by the cadherin-catenin complex, Biochem Soc Trans (2008) 36:149–155.

[126] D.Garrod, M. Chidgey, Desmosome structure, composition and function, Biochim Biophys Acta (2008) 1778:572–587.

[127] M.C. Nawijn, T.L. Hackett, D.S. Postma, A.J. van Oosterhout, I.H. Heijink, E-cadherin: gatekeeper of airway mucosa and allergic sensitization, Trends Immunol (2011) 32:248–255.

[128] M.G. Nievers, R.Q. Schaapveld, A. Sonnenberg, Biology and function of hemidesmosomes, Matrix Biol (1999) 18:5–17.

[129] A. Glentis, V. Gurchenkov, D.M. Vignjevic, Assembly, heterogeneity, and breaching of the basement membranes, Cell Adhes Migr (2014) 8:8.

[130] E.J. Swindle, J.E. Collins, D.E. Davies, Breakdown in epithelial barrier function in patients with asthma: identification of novel therapeutic approaches, J Allergy Clin Immunol (2009) 124:23–34.

[131] J.R. Rock, S.H. Randell, B.L. Hogan, Airway basal stem cells: a perspective on their roles in epithelial homeostasis and remodelling, Dis Model Mech (2010) 3:545–556.
[132] D.J. Thornton, K. Rousseau, M.A. McGuckin, Structure and function of the polymeric mucins in airways mucus, Annu Rev Physiol (2008) 70:459–486.
[133] M.G. Roy, A. Livraghi-Butrico, A.A. Fletcher, M.M. McElwee, S.E. Evans, R.M. Boerner, S.N. Alexander, L.K. Bellinghausen, A.S. Song, Y.M. Petrova YM, et al., Muc5b is required for airway defence, Nature (2014) 505:412–416.
[134] T.Z. Veres, S. Voedisch, E. Spies, T. Tschernig, A. Braun, Spatiotemporal and functional behavior of airway dendritic cells visualized by two-photon microscopy, Am J Pathol (2011) 179:603–609.
[135] F. Blank, M. Wehrli, A. Lehmann, O. Baum, P. Gehr, C. von Garnier, B.M. Rothen-Rutishauser, Macrophages and dendritic cells express tight junction proteins and exchange particles in an in vitro model of the human airway wall, Immunobiology (2011) 216:86–95.
[136] M. Rescigno, M. Urbano, B. Valzasina, M. Francolini, G. Rotta, R. Bonasio, F. Granucci, J.P. Kraehenbuhl, P. Ricciardi-Castagnoli, Dendritic cells express tight junction proteins and penetrate gut epithelial monolayers to sample bacteria, Nat Immunol (2001) 2:361–367.
[137] A.K. Mayer, M. Muehmer, J. Mages, K. Gueinzius, C. Hess, K. Heeg, R. Bals, R. Lang, A.H. Dalpke, Differential recognition of TLR-dependent microbial ligands in human bronchial epithelial cells, J Immunol (2007) 178:3134–3142.
[138] H.N Qiu, C.K. Wong, I.M. Chu, S. Hu, C.W. Lam, Muramyl dipeptide mediated activation of human bronchial epithelial cells interacting with basophils: a novel mechanism of airway inflammation, Clin Exp Immunol (2013) 172:81–94.
[139] M. Loxham, D.E. Davies, C. Blume, Epithelial function and dysfunction in asthma, Clin Exp Allergy (2014) DOI:10.1111/cea.12309.
[140] C. Blume, E.J. Swindle, P. Dennison, N.P. Jayasekera, S. Dudley, P. Monk, H. Behrendt, C.B. Schmidt-Weber, S.T. Holgate, P.H. Howarth, Barrier responses of human bronchial epithelial cells to grass pollen exposure, Eur Respir J (2013) 42:87–97.
[141] S.T. Holgate, Pathophysiology of asthma: what has our current understanding taught us about new therapeutic approaches?, J Allergy Clin Immunol (2011) 128:495–505.
[142] B. Naylor, The shedding of the mucosa of the bronchial tree in asthma, Thorax 1962 17:69–72.
[143] L.A. Laitinen, M. Heino, A. Laitinen, T. Kava, T. Haahtela, Damage of the airway epithelium and bronchial reactivity in patients with asthma, Am Rev Respir Dis (1985) 131:599–606.
[144] C. Ordoñez, R. Ferrando, D.M. Hyde, H.H. Wong, J.V. Fahy, Epithelial desquamation in asthma: artifact or pathology? Am J Respir Crit Care Med (2000) 162:2324–2329.
[145] C. Xiao, S.M. Puddicombe, S. Field, J. Haywood, V. Broughton-Head, I. Puxeddu, H.M. Haitchi, E. Vernon-Wilson, D. Sammut, N. Bedke, Defective epithelial barrier function in asthma, J Allergy Clin Immunol (2011) 128:549–556.e1–e12.
[146] W.I. de Boer, H.S. Sharma, S.M. Baelemans, H.C. Hoogsteden, B.N. Lambrecht, G.J. Braunstahl, Altered expression of epithelial junctional proteins in atopic asthma: possible role in inflammation, J Physiol Pharmacol (2008) 86:105–112.

[147] S. Shahana, E. Bj ¨ornsson, D. L ´udv´ıksd ´ottir, C. Janson, O. Nettelbladt, P. Venge, G.M. Roomans, Ultrastructure of bronchial biopsies from patients with allergic and non-allergic asthma, Respir Med (2005) 99:429–443.
[148] F. Bucchieri, S.M. Puddicombe, J.L. Lordan, A. Richter, D. Buchanan, S.J. Wilson, J. Ward, G. Zummo, P.H. Howarth, R. Djukanović, Asthmatic bronchial epithelium is more susceptible to oxidant-induced apoptosis, Am J Respir Cell Mol Biol (2002) 27:179–185.
[149] T.L. Hackett, G.K. Singhera, F. Shaheen, P. Hayden, G.R. Jackson, R.G. Hegele, S. Van Eeden, T.R. Bai, D.R. Dorscheid, D.A. Knight, Intrinsic phenotypic differences of asthmatic epithelium and its inflammatory responses to respiratory syncytial virus and air pollution, Am J Respir Cell Mol Biol (2011) 45:1090–1100.
[150] A. Sakakibara, M. Furuse, M. Saitou, Y. Ando-Akatsuka, S. Tsukita, Possible involvement of phosphorylation of occludin in tight junction formation, J Cell Biol (1997) 137:1393–1401.
[151] J.M. Staddon, K. Herrenknecht, C. Smales, L.L. Rubin, Evidence that tyrosine phosphorylation may increase tight junction permeability, J Cell Sci (1995) 108:609–619.
[152] M. Ahdieh, T. Vandenbos, A. Youakim, Lung epithelial barrier function and wound healing are decreased by IL-4 and IL-13 and enhanced by IFN-gamma, Am J Physiol Cell Physiol (2001) 281:C2029–C2038.
[153] M.A. Hardyman, E. Wilkinson, E. Martin, N.P. Jayasekera, C. Blume, E.J. Swindle, N. Gozzard, S.T. Holgate, P.H. Howarth, D.E. Davies, TNF-a-mediated bronchial barrier disruption and regulation by src-family kinase activation, J Allergy Clin Immunol (2013) 132:665–675.e8.
[154] S.M. Evans, D.I. Blyth, T. Wong, S. Sanjar, M.R. West, Decreased distribution of lung epithelial junction proteins after intratracheal antigen or lipopolysaccharide challenge: correlation with neutrophil influx and levels of BALF sE-cadherin, Am J Respir Cell Mol Biol (2002) 27:446–454.
[155] I. Tillie-Leblond, P. Gosset, R. Le Berre, A. Janin, T. Prang `ere, A.B. Tonnel, B.P. Guery, Keratinocyte growth factor improves alterations of lung permeability and bronchial epithelium in allergic rats, Eur Respir J (2007) 30:31–39.

Thesis Aim

The aim of this project is to pursue a human bronchial model by adapting a combination of tissue engineering and microfluidics technology.

First of all, the project aims at the development of a highly porous scaffold with a high degree of interconnection to support tissue growth. Scaffolds will be made with biocompatible and biodegradable polymers, based on PLLA (poly-L-lactide). They were obtained via various techniques, the most promising and flexible way of which is the phase separation route, as it allows a good control of micro and macrostructure. In this project the DIPS method will be utilized for the design and production of two types of scaffolds: thin film and tubular [1].

The present proposal concerns the investigation about the use of the scaffold to implant of human bronchial cells and human bronchial mucosa tissue by section biopsies. PLLA thin film scaffolds were used as membrane for cell outgrowth utilizing a model describe in literature. In other PLLA tubular scaffolds were used to mimic the natural environment of epithelial cells. TEM (transmission electron microscopy) and SEM (scanning electron microscopy) analysis were used to investigate human bronchial mucosa and cells outgrowth [2].

With SEM analysis, it were possible to study the surface structure typical of the model in vitro, while, with TEM analysis, it will be possible to understand the feature structure by regenerated tissues. The SEM and TEM techniques are very important because they compare the vitro model with the adult human tissue.

Secondly, the research project aims at the development of a microfluidics system and its integration with the biodegradable scaffold. Microfluidics devices are developed with micro fabrication techniques such as photolithography and replica molding. In this case, soft photolithography can be suitable adapted for the development of a microfluidics platform. The microfluidics platforms are usually made of elastomeric material such as PDMS (polydimethylsiloxane). The PDMS is biocompatible, permeable to gases, cheap and translucid. Microfluidics platforms provide the opportunity to control heat and mass transfer, integration cell and tissue growth analysis and parallel high-throughput experimentation [4].

The microfluidics platform will represent the ideal set-up to create an accurately controlled microenvironment in which tissues derived from section biopsies will be cultured on PLLA scaffolds, while nutrients supplied via medium diffusion on the one side, and exposed to air on the other. Through this platform, it will be possible the control of the microenvironment and various interactions between cell and extracellular matrix present in vivo [3].

This platform provides the opportunity to study multicellular systems with great resolution and allow localized control of the experimental conditions into the system. Therefore the "assembly" scaffold + biopsy can be regarded as a suitable in vitro model to investigate the physiological response of two typologies of tissues (bronchial mucosa and rectal colon) to external stimuli, and the etiology of diseases such as emphysema and asthma and rectal colon tissue diseases.

The milestones of the research proposal can be summarized as follows:

- development of a scaffold in PLLA (Thin Film and Tubular scaffold) to design and develop a 3D outgrowth model of the human bronchial mucosa and colon rectal tissue, starting from biopsies acquired during bronchoscopic procedures and rectal surgery, respectively;
- characterisation, structural and ultra-structural, of the morphological features of these obtained outgrowth, through of electron microscopy analysis (SEM and TEM), to verify the degree of similarity of the 3D bronchial and rectal colon outgrowth with the normal human bronchial mucosa and rectal colon tissue respectively;
- development of a new scaffold-tissue device to be integrated into the microfluidic platform;
- set-up of innovative human bronchial mucosa 3D models to undertake functional studies in order to evaluate the responses of the outgrowths to environmental stresses, such as those occurring during exposure to cigarette smoke and its oxidant components to study the pathogenesis as emphysema and asthma;
- set-up of novel rectal colon 3D models to undertake functional studies in order to investigate the possibility of autotransplantation based on the in-vitro outgrowths.

References

[1] V. La Carrubba, F. Carfì Pavia, V. Brucato, S. Piccarolo, G. Ghersi. PLLA biodegradable scaffolds for angiogenesis via Diffusion Induced Phase Separation (DIPS). Int J Mater Form (2008) Suppl 1:623–626, Springer/Esaform.

[2] F. Bucchieri, A. Fucarino, A. Marino Gammazza, A. Pitruzzella, V. Marcianò, C. Paderni, V. De Caro, M. G. Siragusa, L. Lo Muzio, S. T Holgate, D. E Davies, F. Farina, G. Zummo, Y. Kudo, I. L. Giannola and G. Campisi. Medium-term Culture of Normal Human Oral Mucosa: A Novel Three-dimensional Model to Study the Effectiveness of Drugs Administrati. Current Pharmaceutical Design, 2012, 18, 000-000.

[3] A. A. Banaeiyan, D. Ahmadpour, C. B. Adiels. Design and fabrication of high-throughput application-specific microfluidic devices for studying single-cell responses to extracellular perturbations. SPIE 8765, Bio-MEMS and Medical Microdevices, 87650K (May 28, 2013).

[4] T. M. Squires, S. R. Quake. Microfluidics: Fluid physics at the nanoliter scale. Reviews of modern physics, volume 77, july 2005.

Chapter 2

PLLA Membranes preparation via DIPS

The production of polymeric membranes via Diffusion Induced Phase Separation (DIPS) has been widely studied and applied for a number of model systems. The main steps of membrane formation through DIPS protocol are: (i) casting of a polymer solution on a support and (ii) immersion into a coagulation bath, usually composed by a non-solvent. The mutual exchange of solvent and non-solvent will modify the casted solution composition, inducing phase separation when the equilibrium curve is crossed (see Figure 16). The liquid-liquid phase separation is responsible for the formation of a porous membrane, and it can occur via nucleation and growth and/or spinodal decomposition mechanisms.

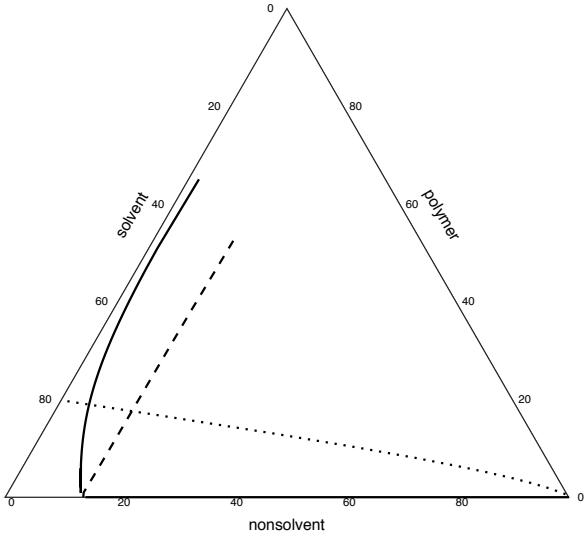

Figure 16: Schematic of DIPS process. Bold line is binodal curve, dashed line is spinodal curve, dotted line represents a reasonable composiiton path.

As DIPS technique allows the preparation of a porous membrane with a rather simple procedure, it has converged a great and increasing interest during last forty years, as witnessed by numerous scientific publications focused on this topic [1]. Researchers tried to modulate every possible processing parameter, such as casting and coagulation bath composition, temperature and system components. The net effect of all parameters is the modification of outward/inward flux of solvent/non-solvent, which influences concentration distributions inside the casted film. Local composition, in its turn, determines the demixing mechanism and the amounts of separated phases, on the basis of its location in phase diagram.

As a general rule, the immersion in a coagulation bath composed only by non-solvent will produce a porous membrane, but with a dense skin: this was related to a rapid increase of polymer concentration at the interface, owing to a fast outward solvent diffusion, which induces crystallization. This fact has been underlined by the mass transfer modeling, providing an estimate of concentration profiles inside the polymeric film [2, 3, 4].

As regards to the polymer employed in this study (poly-L-lactide, PLLA), Van de Witte et al. [5,6] studied the influence of solid-liquid demixing, liquid-liquid demixing and vitrification on PLLA membrane morphology obtained via immersion precipitation. Chloroform and methanol were used as solvent and non-solvent, respectively. In a different study, the same research group applied the relations between phase diagram and membrane morphology for the ternary PLLA-chloroform-methanol system to PLLA-dioxane-methanol, PLLA-dioxane-water and other ternary systems [7]. Further experimental studies regarding the formation of PLLA membranes by immersion precipitation have been reported in literature [8, 9, 10, 11], where the effect of different solvents and non-solvents, casting and coagulation bath concentration, and temperature, were investigated to control the resulting membrane morphology. By varying those processing parameters, a vast latitude of membrane morphologies, in terms of pore size and distribution, shape and interconnection can be produced.

Undoubtedly, these studies present a satisfactory picture of main features involved in DIPS process. However, some points, related to the external surface morphology and the influence of drying step, need to be further investigated and clarified. As a matter of fact, membranes prepared via DIPS ordinarily show a completely closed and nonporous external surface, owing to a local polymer concentration increase [12]. This fact reduces sensibly the overall membrane permeability, thus affecting the choice of potential applications. A number of solutions to this limitation were investigated, e.g. employing a coagulation bath composed of both non-solvent and solvent [13,14] or multiple coagulation baths [15,16,17], adopting a sacrificial layer approach [18,19] or wetting both surfaces with a modified spinneret [20]. In this chapter, the use of a binary coagulation bath and/or multiple coagulation baths were explored, showing the influences of composition and immersion time on resulting surface microstructure. Moreover, the experimental campaign presented in this thesis is aimed to demonstrate the influence of desiccation step, i.e. of solvent removal, on the morphology of external surface. In typical DIPS practice, the membrane is washed or dried immediately after the immersion step: however, researchers often neglect the effects of this last operation on the membrane microstructure. As a matter of fact, during solvent removal the system composition

will vary: thus, an influence on membrane morphology can be reasonably expected. For example, by washing the membrane with a non-solvent, a further mass transfer will occur, with a related composition modification. On the other hand, if the membrane is exposed to a gaseous phase to promote drying, the presence of non-solvent vapor in desiccation environment will influence the driving force for mass transfer, i.e. its direction and rate. Therefore, the solvent removal rate can be modulated by tuning the partial pressure of nonsolvent in desiccation environment. A further option provided by this phenomenology is the induction of phase separation by diffusion of nonsolvent vapor into the liquid phase [21]. Following this latter rationale, polyethersulfone [22] and poly(vinylidene fluoride) [23] membranes with a porous external surface were produced, by exposing the casted solution to a vapor phase containing nonsolvent (Vapor Induced Phase Separation, VIPS).

To sum up, the objective of this section is the understanding of the effects of double immersion and desiccation conditions on the morphology of membrane surfaces, in order to take advantage of these features to prepare skinless membranes to use in tissue engineering.

Experimental

Materials

The polymer examined was the PLLA RESOMER® L 209 S, purchased from Boehringer-Ingelheim (inherent viscosity 3 dl/g). The solvents employed were deionized water and 1-4 dioxane (Sigma-Aldrich, used without further purifications).

Membrane preparation

The membrane preparation protocol can be subdivided into three steps:

1. dip-coating
2. immersion into one (or more) coagulation bath(s)
3. desiccation

The dip-coating consists in a slow pulling-out of a glass slide (15x50 mm, thickness 2 mm) immersed in a PLLA-dioxane solution (see Figure 17). In this way, the slab surface gets coated with a layer of polymer solution. The as-obtained layer thickness depends on pull-out velocity, solution concentration and temperature, as widely shown in literature 24. In this work, these parameters were taken constant in all experiments: the pull-out velocity was 3 cm/min, the polymer solution concentration was 8 wt% PLLA and the temperature was set to 30 °C.

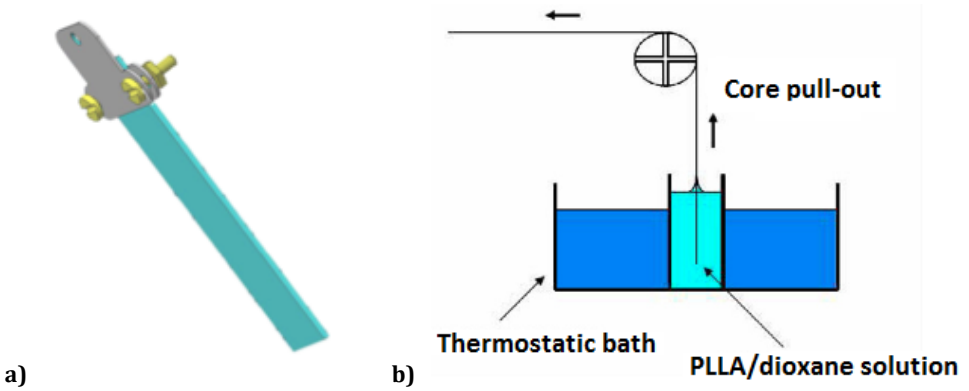

Figure 17: a) Glass slide; b) Schematic of dip-coating process.

The typical DIPS operation is accomplished via pool immersion of the coated slab into a coagulation bath, for a certain time interval. During this step, the diffusion of solvents from and to the casted solution changes its composition, inducing liquid-liquid phase separation and/or polymer crystallization. A schematic of this stage is presented in Figure 18, showing a calculated phase diagram of PLLA-dioxane-water.

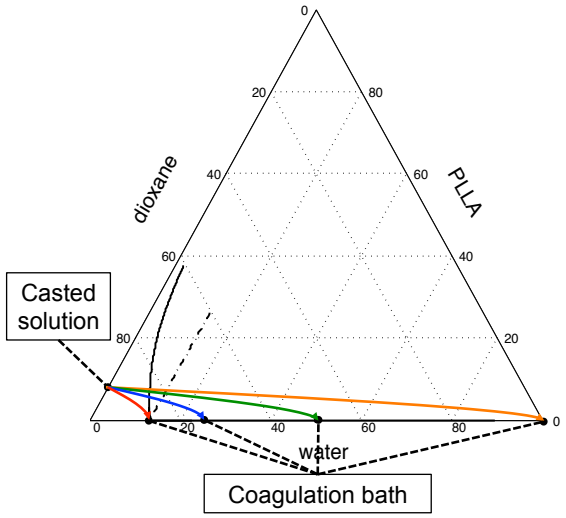

Figure 18: Phase diagram of PLLA-dioxane-water system calculated via Sanchez-Lacombe model, with reasonable composition paths encountered in DIPS experiments performed.

The model adopted was based on Sanchez-Lacombe with specific interactions [25,26] with the interaction parameters slightly modified to achieve a better fit on cloud point data (details on measurement and results are reported in [27,28]). In this thesis, membranes were prepared via immersion into one or two (subsequent) coagulation bath(s) (see Figure 19a), in order to investigate the influence of bath concentration and immersion time on the resulting microstructure.

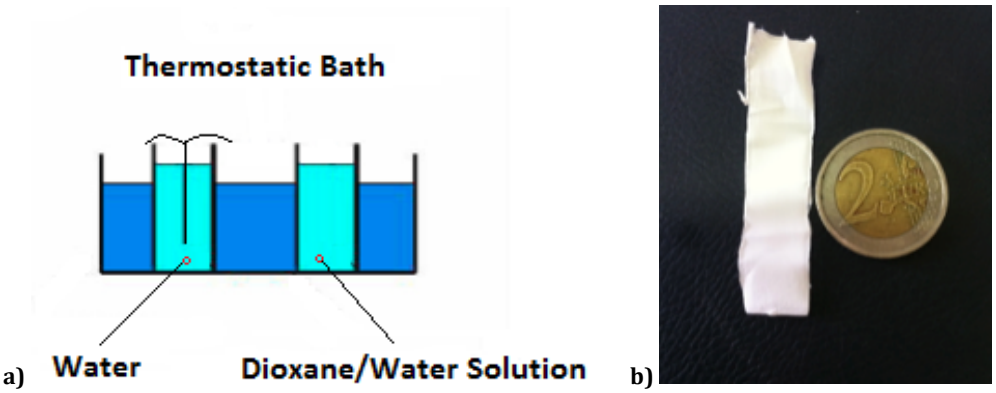

Figure 19: a) Schematic of DIPS baths; b) PLLA membrane.

The investigated compositions of first coagulation bath were 87/13, 75/25 and 50/50 (dioxane/water wt/wt). The (optional) second coagulation bath was constituted of water. The baths temperatures were maintained at 30 °C. As showed in Figure 15, by modulating the water concentration in coagulation bath, the composition path will accordingly vary, entering the miscibility gap at different points and times, thus influencing phase separation.

After the DIPS process, the as-obtained samples (see figure 19b) were desiccated in an environment with controlled humidity for 24 h. Two kinds of desiccating environments were tested: dry (nitrogen atmosphere) and humid (around 70% relative humidity) ambient.

SEM analysis

In order to analyse the effect of bath composition and immersion time on the resulting microstructure, both inner and outer surfaces of the as-produced samples were observed via Scanning Electron Microscopy (SEM), utilizing a Philips SEM quanta FEI, at 10 kV. Before the measurements, samples were gold coated to make them conductive.

DSC analysis

The crystallinity of PLLA membranes was investigated through Differential Scanning Calorimetry (DSC), employing a DSC131 EVO (Setaram). Membrane samples were heated at 10 °C/min in the range 50-200 °C.

Results and discussion

Direct drying and immersion in a water bath

When desiccating the casted binary solution in a dry environment, without performing a DIPS step, a dense membrane is obtained, with both closed internal and external surfaces (see (Figure 20a). This result can be ascribed to the evaporation of dioxane, which does not

induces any phase separation, except to polymer crystallization, thus not producing any porosity. On the other hand, if the solution is desiccated in a wet environment, the resulting external surface gets porous (see Figure 20b), owing to the water diffusion into the casted polymeric film which induces phase separation. However, in both cases, the internal surface remains closed: this suggests that, in humid environment, water penetration does not involve the whole film thickness.

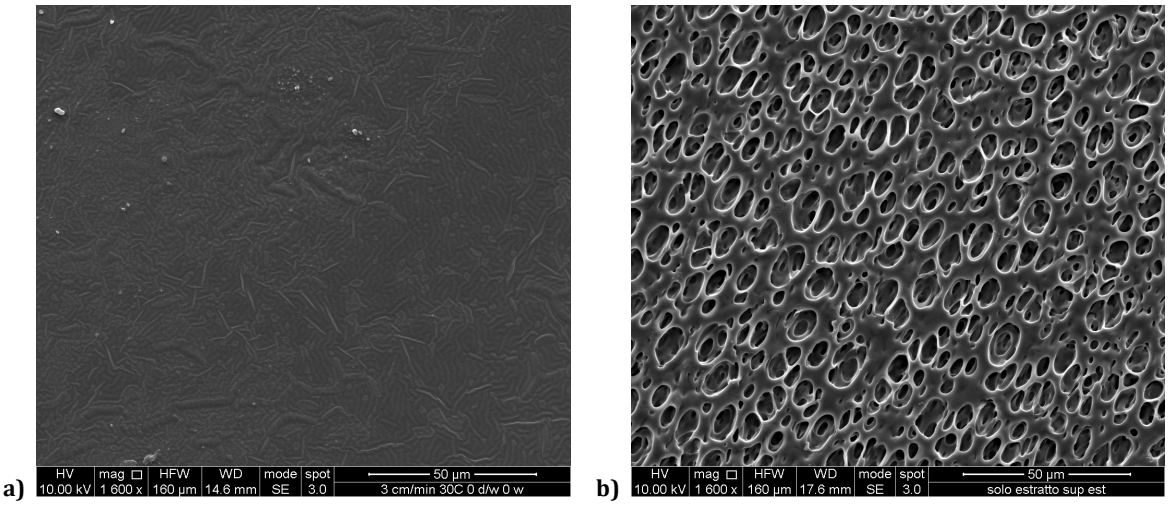

Figure 20: Morphology of membrane external surfaces obtained without immersion in a coagulation bath, i.e., direct desiccation. (a) Dry. (b) Humid.

Conversely, immersion in a water bath gives out a porous membrane, as the non-solvent diffusion induces phase separation in the whole casted solution. However, the external surface does not exhibit any pore: this fact is related to the rapid polymer crystallization at the interface with the coagulation bath, induced by the fast outer diffusion of dioxane that locally increases polymer concentration, as reported in several works [2,3,4].

These results suggest that to obtain a porous membrane without a dense skin, a different protocol must be adopted. In the following sections, membranes prepared with a binary coagulation bath are presented.

Single immersion: influence of coagulation bath composition and desiccation

When the binary polymer solution is immersed in a dioxane/water bath for 5 minutes, and then desiccated, the resulting morphology depends on both coagulation bath composition and desiccation environment (humid vs. dry ambient).

If desiccation is performed in a dry ambient, a closed external surface was obtained for both 87/13 and 75/25 coagulation baths (see Figure 21). The dioxane/water system shows a minimum azeotrope, for which the liquid phase enriches of dioxane if its concentration is higher than 83 wt% [29]. As the system focused in this investigation has a third component,

which is non-volatile, a variation in azeotropic concentration is expected. Although no vapor-liquid equilibrium data for this ternary system are available, the azeotropic concentration should be reasonably located close to two mixed bath compositions tested in this thesis work, i.e. 87/13 and 75/25. Therefore, non-ideal vapor-liquid equilibrium behavior can affect membranes prepared with the aforementioned baths.

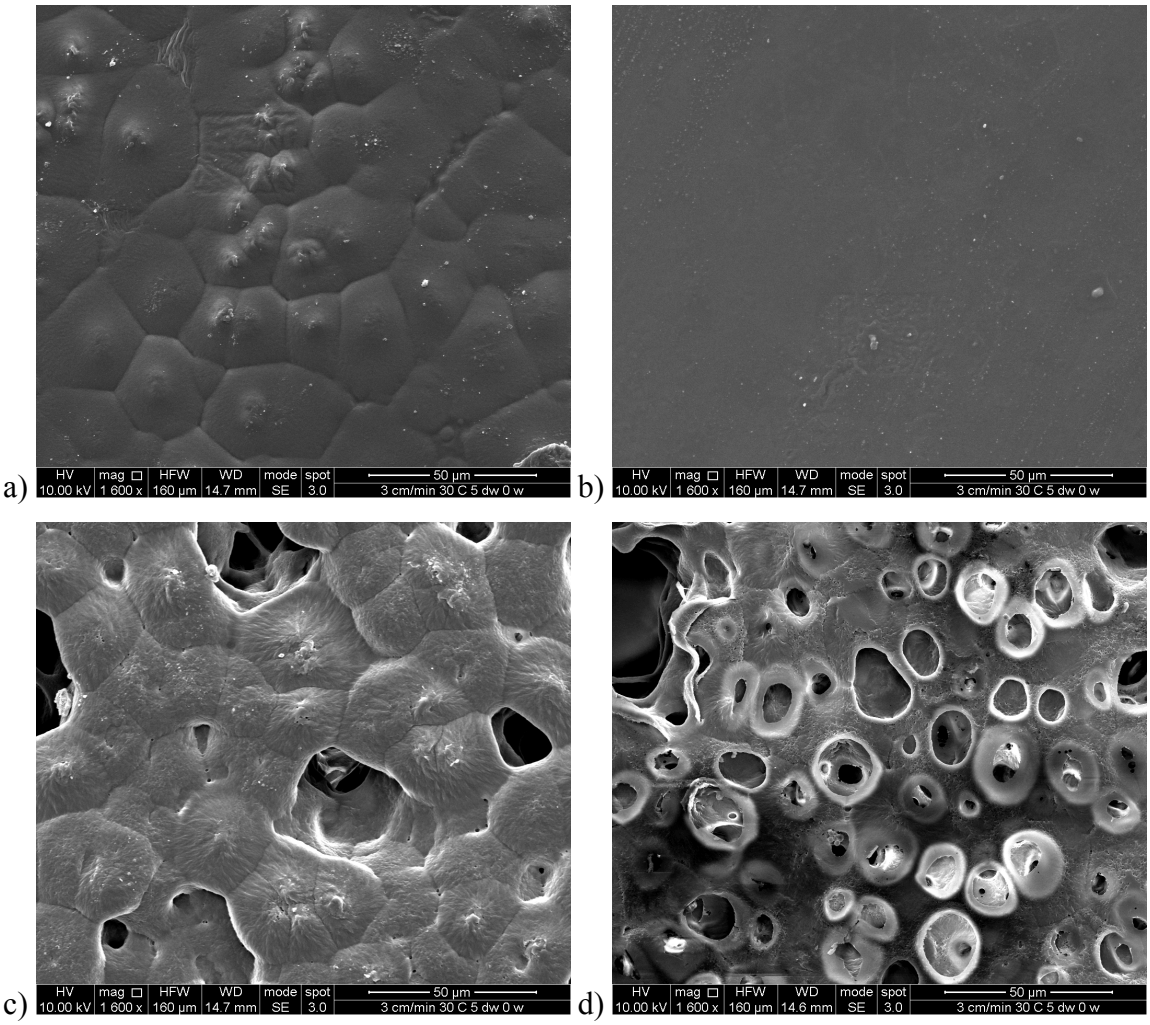

Figure 21: Morphology of membrane surfaces obtained with a single immersion in a dioxane/water bath for 5 min and desiccated in dry environment: a) external surface 87/13 d/w, b) internal surface 87/13 d/w, c) external surface 75/25 d/w, d) internal surface 75/25 d/w.

As a matter of fact, as the external surface may decrease its water content by evaporation, an increased dioxane concentration could be able to re-establish a single-phase condition, thus giving out a crystalline morphology of polymer after solvent evaporation. This fact is more noticeable in membranes prepared with the 87/13 bath: in this case, both inner and outer surfaces result closed and crystalline. On the other hand, with the 75/25 bath, the internal surface resulted open, whereas the external one is crystalline. Even if voids are noticeable on the external surface, they are not the result of a liquid-liquid phase separation: it is more likely the occurrence of a local fracture due to shrinkage induced by crystallization. As for the

internal surface, the pore morphology suggests a separation mechanism by nucleation and growth, thus prompting that water has reached the support in a sufficient amount to cross the binodal curve, but not the spinodal one, owing to the relative short immersion time.

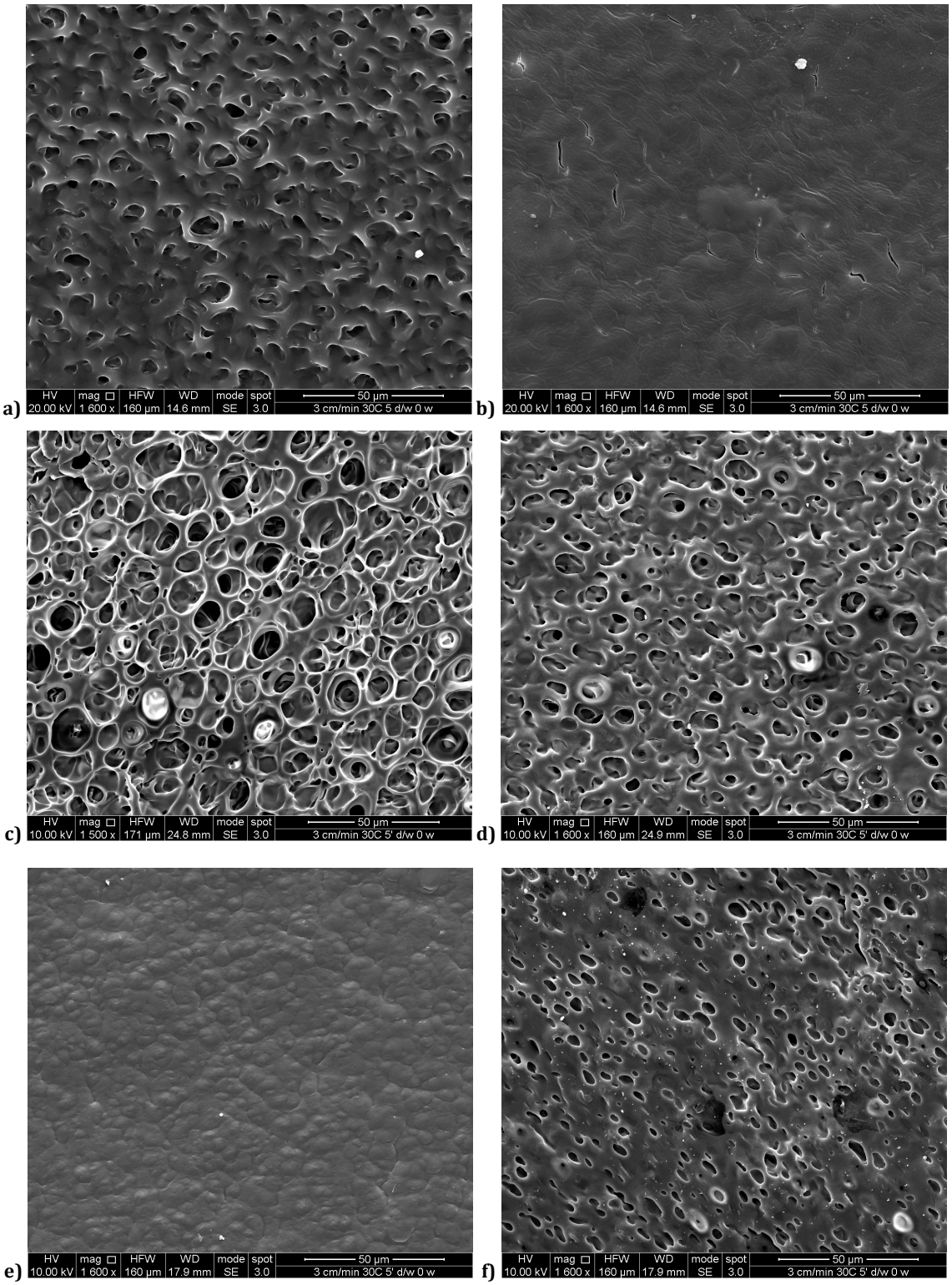

Figure 22: Morphology of membrane surfaces obtained with a single immersion in a dioxane/water bath for 5 min and desiccated in humid environment: a) external surface 87/13 d/w, b) internal surface 87/13 d/w, c) external surface 75/25 d/w, d) internal surface 75/25 d/w, e) external surface 50/50 d/w, d) internal surface 50/50 d/w.

If samples are desiccated in a humid ambient, external surfaces will be more likely porous (see Figure 22). As a matter of fact, membranes obtained with the 75/25 bath are porous on both surfaces.

On the other hand, membranes prepared with the 87/13 bath show a open porosity on the external surface, whereas the inner one is closed. A third case is offered by the 50/50 bath, which showed no pores on the outer surface, whereas the inner one has few and small pores. The morphology obtained in the latter case is comparable with that recorded when using a coagulation bath constituted of pure water. As a matter of fact, when a polymer-solvent solution is immersed in a non-solvent bath, the solvent is able to diffuse rapidly from casted film to the bath, increasing the polymer concentration at the interface, and then inducing the crystallization on that surface. Obtaining similar results with a 50/50 bath could mean that this condition is characterized by a relatively low content of solvent, which does not sufficiently reduces the driving force to outward dioxane flux. On the other hand, higher dioxane concentrations will reduce the outer diffusion of solvent from membrane, thus inhibiting the surface crystallization and giving out an open-pore morphology on the external surface. However, the internal surface of 87/13 sample appears closed, as few non-solvent can reach that section and then inducing liquid-liquid demixing. As showed in previous section, the humid/dry environment has a direct effect on the external surface, whereas the internal one is determined by the coagulation bath. Therefore, the resulting morphology of internal surface does not depend on the desiccation environment, but only on the coagulation bath concentration. A midway situation is represented by the 75/25 bath: in this case, the water concentration is high enough to reach the inner surface and induce demixing, and low enough to avoid a rapid crystallization of the polymer at the outer surface.

Influence of the second immersion step

As seen previously, with the immersion in a water bath, the inner surface can experience liquid-liquid demixing, and then shows an open-pore morphology. On the other hand, the outer surface results closed, owing to the polymer crystallization induced by an increase in its concentration. As a matter of fact, when immersing a binary solution in a non-solvent bath, a rapid outflow of solvent will increase the polymer concentration at the surface. Simulated values are around 20-30% [4]. In order to limit the solvent outflow (and contemporarily controlling the non-solvent inflow), a double immersion into two different coagulation baths was investigated. The first one is a dioxane/water mixture (with the same concentrations explored previously), whereas the second one is constituted of pure water. The net effect of

the first immersion step is an enrichment in water of the proto-membrane, without loosing a consistent amount of dioxane, as its outflow is reduced, owing to a small driving force. The second immersion will enhance mass transfer, promoting solvent/non-solvent exchange between casted film and coagulation bath. However, the water contained in the casted film, due to the first immersion, will reduce the driving force to non-solvent inflow with respect to the direct immersion of casted film in a water bath, thus providing an intermediate condition between binary and pure water coagulation baths. A summary of as-obtained membrane surfaces morphology is reported in Table 1.

Table 1: Membranes Surfaces (Internal/External, C, Closed, O, Open) Obtained by Varying Coagulation Bath Concentration (Rows) and Immersion Times (Columns, Reported in Minutes).

	Dry			**Humid**		
d/w	5'+0	5'+5'	10'+5'	5'+0'	5'+5'	10'+5'
87/13	C/C	O/O	O/O	C/O	O/O	O/O
75/25	O/C	O/C	O/C	O/O	O/O	O/O
50/50	-	-	-	O/C	O/C	O/C

The first number refers to immersion time in the d/w bath, the second number refers to immersion time in pure water.

If samples are desiccated in a dry environment, different morphologies are noticed, on the basis of coagulation bath composition. For example, 75/25 bath produces an essentially closed external surface, with few and very small pores (see Figure 23). Increasing the first immersion time, the surface becomes completely closed. These results are in line with those showed previously, as the first immersion step is responsible for the formation of a dense skin layer on the external surface; moreover, the internal surface appears porous, as the morphology of this face is not determined by the desiccation condition. On the other hand, when using a 87/13 bath, the external surface results open. The second immersion in water gave out a non-solvent intake that allowed the cross of azeotropic concentration: therefore, as liquid phase will lose more dioxane than water by evaporation, the return to a single phase system is avoided. As a further effect of this increased inward water flux, internal surface become porous, with a shape recalling nucleation and growth kinetics.

When drying in a humid environment, membranes obtained with both 87/13 and 75/25 coagulation baths showed an open external surface, with the internal one showing also an open structure (see Figure 24). This fact suggests that a slower water removal extends the time for phase separation, thus giving out pore sizes higher than those obtained by desiccation

in dry environment. Moreover, as the desiccation process takes place in a longer time interval, a mass diffusion within the polymer film, which locally modifies concentrations with respect to those established after the immersion, may occur.

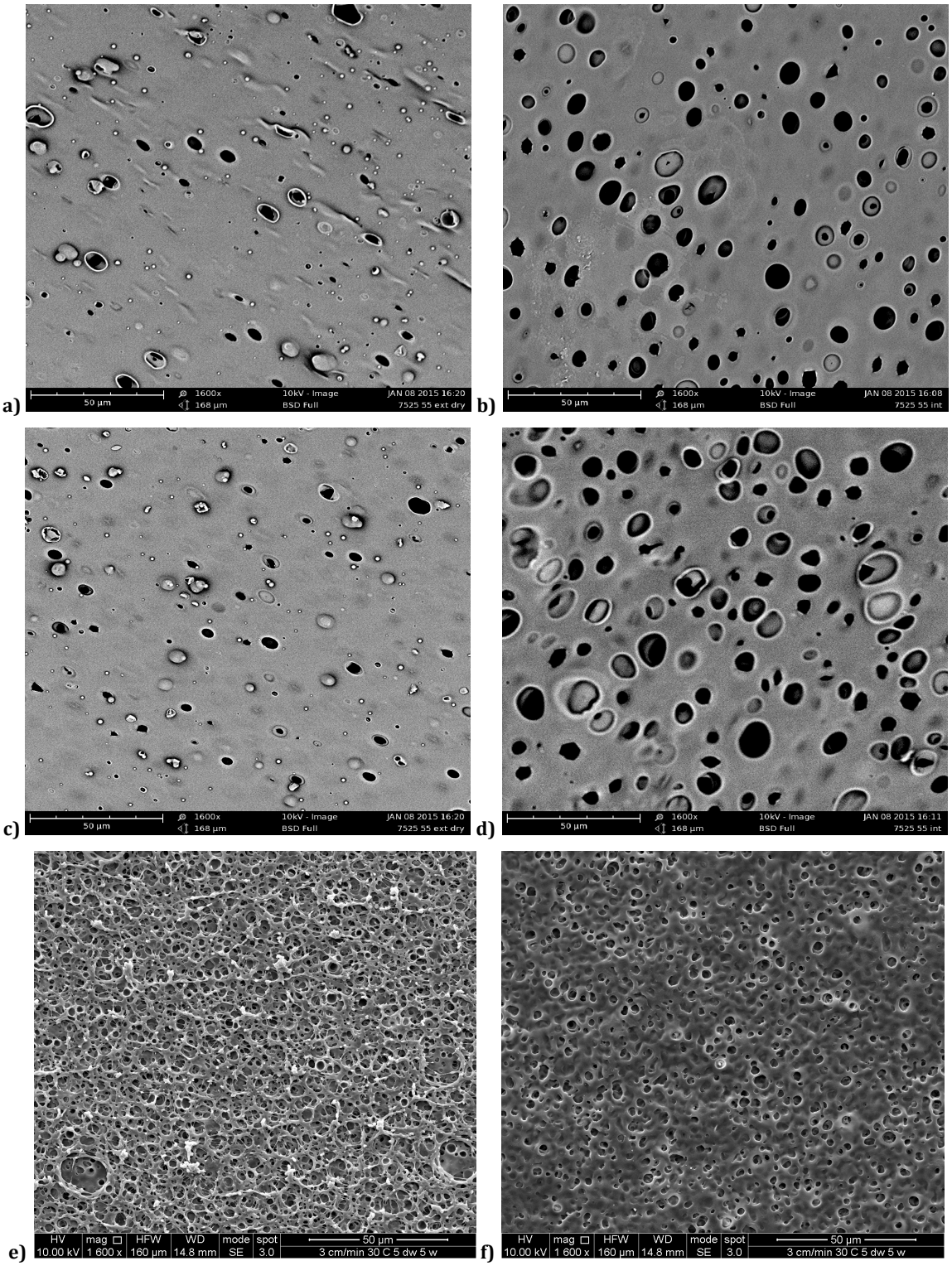

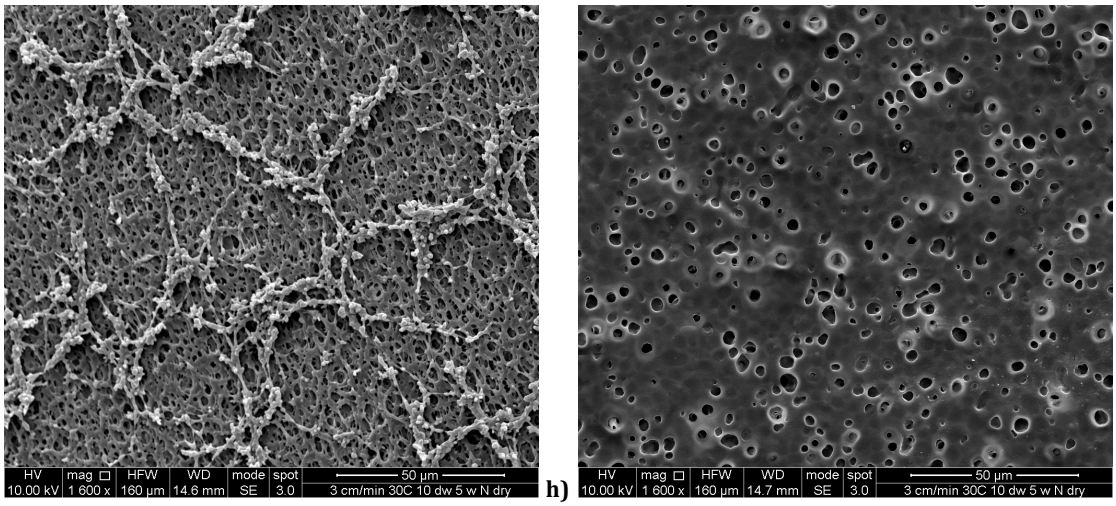

Figure 23: Morphology of membrane surfaces obtained with a double immersion, first in a dioxane/water bath, then in pure water, and desiccated in dry environment: a) external surface 75/25 d/w 5'+5', b) internal surface 75/25 d/w 5'+5', c) external surface 75/25 d/w 10'+5', d) internal surface 75/25 d/w 10'+5', e) external surface 87/13 d/w 5'+5', f) internal surface 87/13 d/w 5'+5', g) external surface 87/13 d/w 10'+5', h) internal surface 87/13 d/w 10'+5'.

However, the morphology of external surfaces depends on the first coagulation bath composition. At higher dioxane concentration, the outer surface exhibits a higher porosity and pore size than the inner one. On the other hand, when lowering the dioxane content in coagulation bath, the external surface appears similar to the internal one, with circular pores and similar porosity value.

Increasing the immersion time in the dioxane/water bath does not influence appreciably the membrane morphology. This could be due to the relatively small variation in sample composition during the first immersion step. As a matter of fact, the sample should absorb a small amount of water.

These results show that even a short immersion time (5 minutes) in water produces a significant modification of membrane morphology. Therefore, the common used washing step after DIPS, consisting in a long lasting immersion in a water bath, will strongly influence the final membrane morphology. This fact suggests that, in immersion precipitation, the membrane post-treatment step for solvents removal should be taken into account when discussing the relations between processing parameters and resulting morphologies.

When reducing the dioxane/water ratio in the coagulation bath to 50/50, results were similar to those obtained with a single immersion. External surface remains closed, whereas the internal one is porous, with a pore size higher than that obtained with a single immersion. This result is in line with those obtained with a single immersion: as discussed in the previous section, the water concentration in the coagulation bath is high enough to give out result similar to a pure water bath, thus a second immersion step does not introduce any substantial difference in concentrations and morphologies.

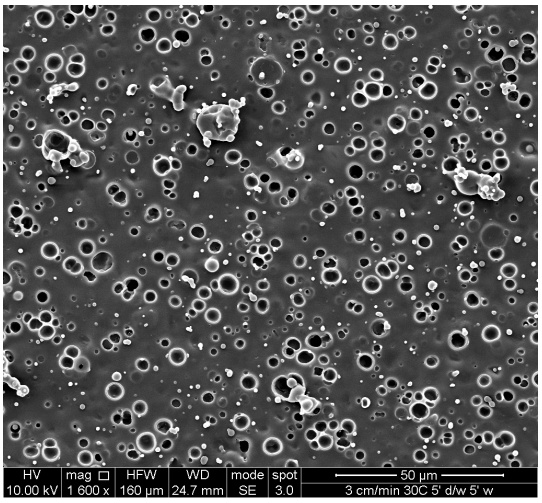
HV
10.00 kV
mag
1 600 x
HFW
160 µm
WD
24.7 mm
mode
SE
spot
3.0
50 µm
3 cm/min 30C 5' d/w 5' w

a)

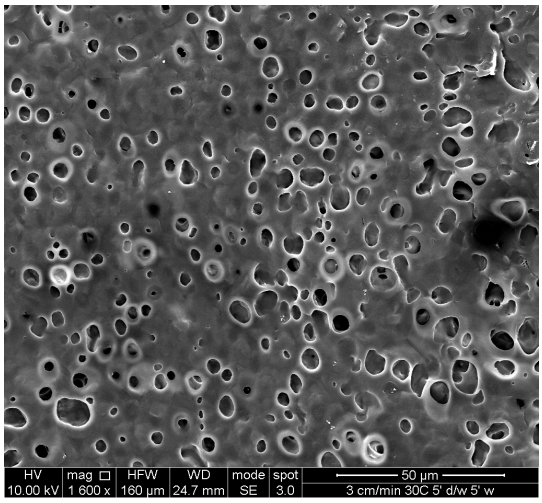
HV
10.00 kV
mag
1 600 x
HFW
160 µm
WD
24.7 mm
mode
SE
spot
3.0
50 µm
3 cm/min 30C 5' d/w 5' w

b)

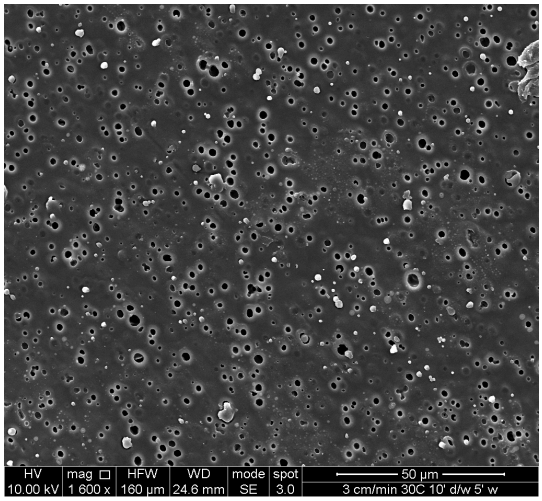
HV
10.00 kV
mag
1 600 x
HFW
160 µm
WD
24.6 mm
mode
SE
spot
3.0
50 µm
3 cm/min 30C 10' d/w 5' w

c)

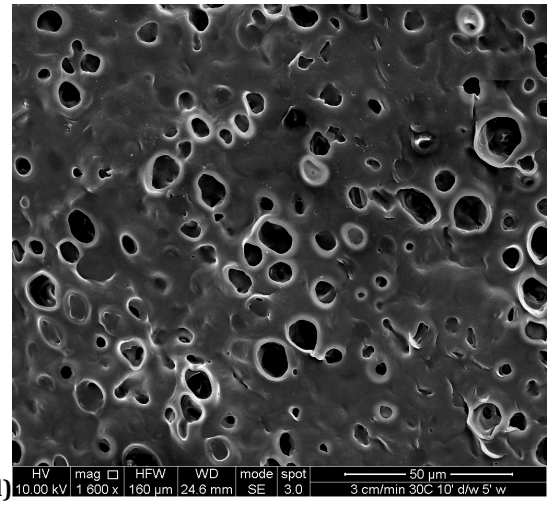
HV
10.00 kV
mag
1 600 x
HFW
160 µm
WD
24.6 mm
mode
SE
spot
3.0
50 µm
3 cm/min 30C 10' d/w 5' w

d)

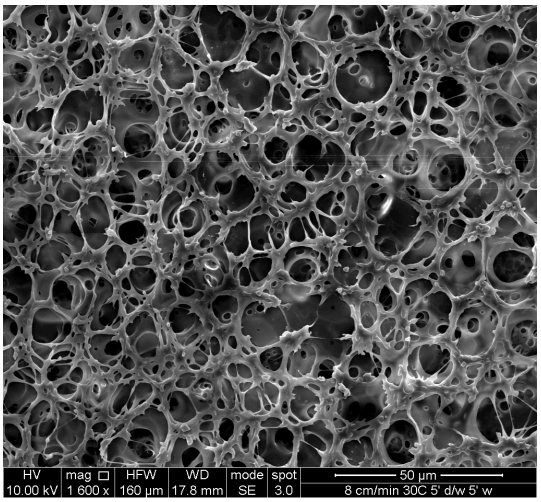
HV
10.00 kV
mag
1 600 x
HFW
160 µm
WD
17.8 mm
mode
SE
spot
3.0
50 µm
8 cm/min 30C 5' d/w 5' w

e)

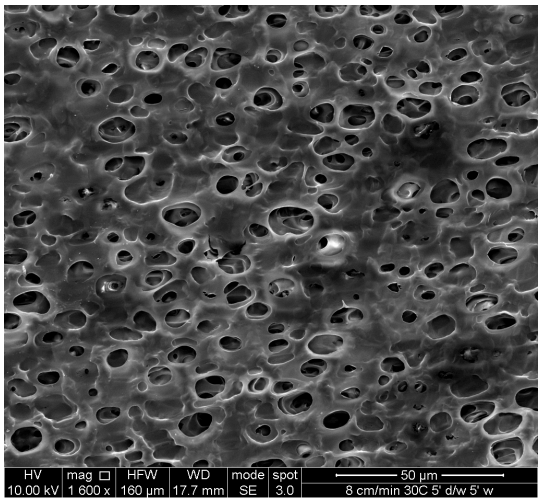
HV
10.00 kV
mag
1 600 x
HFW
160 µm
WD
17.7 mm
mode
SE
spot
3.0
50 µm
8 cm/min 30C 5' d/w 5' w

f)

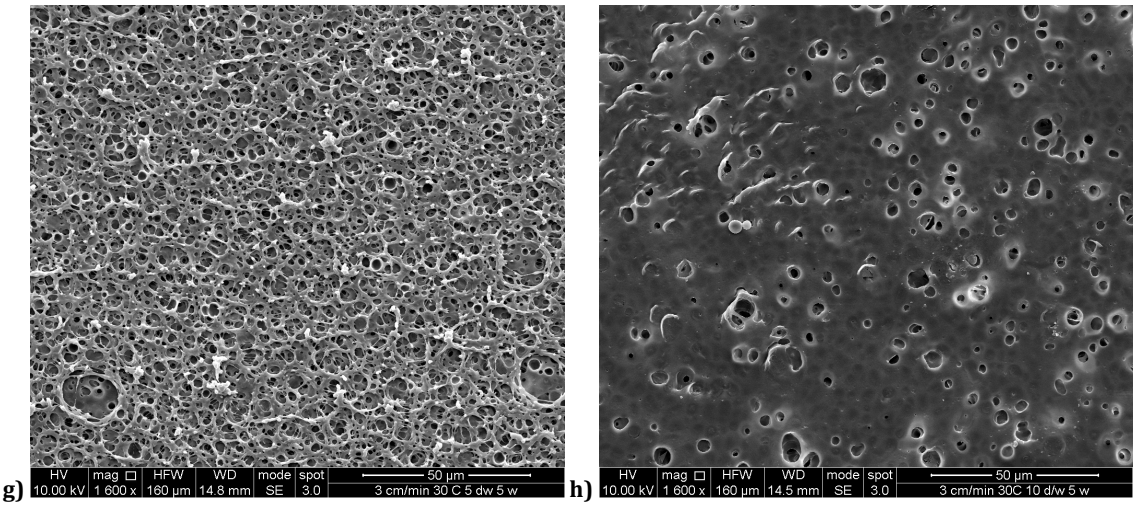

Figure 24: Morphology of membrane surfaces obtained with a double immersion, first in a dioxane/water bath, then in pure water, and desiccated in humid environment: a) external surface 75/25 d/w 5'+5', b) internal surface 75/25 d/w 5'+5', c) external surface 75/25 d/w 10'+5', d) internal surface 75/25 d/w 10'+5', e) external surface 87/13 d/w 5'+5', f) internal surface 87/13 d/w 5'+5', g) external surface 87/13 d/w 10'+5', h) internal surface 87/13 d/w 10'+5'.

DSC analysis

A further characterization of membranes was performed via DSC measurements. The heating curves of membranes prepared with a 87/13 coagulation bath (single and double immersion) and desiccated in dry environment are depicted in Figure 25.

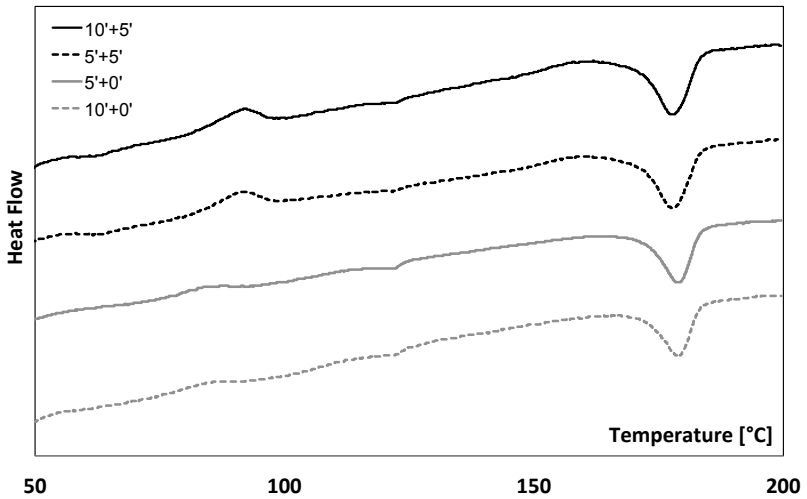

Figure 25: DSC heating curves of membranes prepared at various immersion times (reported in minutes) in 87/13 coagulation bath and desiccated in a dry environment.

The heat flow data were normalized with the total sample weight: thus, the area of melting peaks is related to the melting enthalpy of the crystalline fraction. The melting peak is about 178°C for all investigated samples. The small endothermic peaks located around 120°C are ascribable to water desorption, therefore are not related to physical properties of membranes. A summary of collected data (melting and cold crystallization enthalpy) is reported in Table 2.

Table 2: Enthalpy of Melting (ΔHm) and Cold Crystallization (ΔHcc) Measured via DSC.

d/w	Humidity	t_{DW} (min)	t_W (min)	ΔH_m (J/g)	ΔH_{CC} (J/g)
87/13	L	5	0	32.25	3.98
87/13	L	10	0	31.50	5.22
87/13	L	5	5	40.65	11.80
87/13	L	10	5	40.58	11.87
87/13	H	5	0	34.40	3.01
87/13	H	10	0	37.79	8.84
87/13	H	5	5	41.60	14.14
87/13	H	10	5	41.46	18.89
75/25	L	5	0	45.99	0.00
75/25	L	10	0	47.01	0.00
75/25	L	5	5	35.67	2.73
75/25	L	10	5	44.48	12.87
75/25	H	5	0	32.14	0.00
75/25	H	10	0	40.33	0.00
75/25	H	5	5	34.49	3.85
75/25	H	10	5	40.26	5.80

The melting enthalpy (ΔHm) does not vary significantly by changing the experimental conditions, falling in the 30-50 J/g range. For d/w ratio 87/13, for both the humidity conditions tested, the immersion time in d/w bath does not influence sensibly ΔHm, whereas it was increased at high humidity. An opposite trend was recorded for 75/25 samples, where high humidity gave out membranes with a lower ΔHm, and the immersion time in d/w bath positively influenced the melting enthalpy.

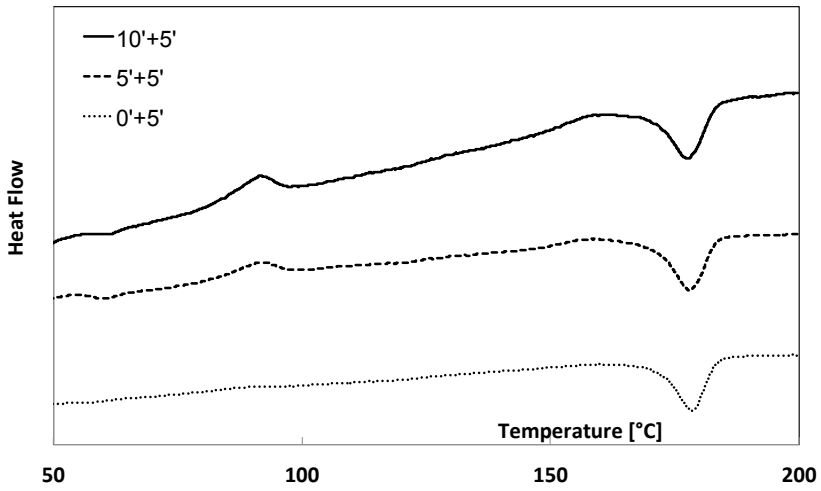

Figure 26: DSC heating curves of membranes prepared at various immersion times (reported in minutes) in 87/13 coagulation bath and desiccated in a humid environment.

A remarkable difference may be noticed when looking at cold crystallization. As a matter of fact, membranes prepared with 87/13 coagulation bath showed the cold crystallization phenomenon in all explored cases (see the exothermic peaks at around 80-90 °C in Figures 25 and 26), but it gets more evident in samples obtained via double immersion; conversely, membranes prepared via single immersion in pure water do not show cold crystallization. Moreover, the desiccation environment did not influence sensibly this behavior. Similar results were obtained with 75/25 and 50/50 coagulation baths: however, in those cases, the cold crystallization was detected only in samples prepared via double immersion. Membranes prepared via double immersion are then characterized by an amorphous phase with a higher mobility, i.e., they are more prone to crystallize from the amorphous state, than those prepared with a single step. This is probably due to the practically instantaneous demixing induced by the immersion in water, which rapidly generates a polymer rich phase; owing to the dioxane diffusion to water bath, the polymeric phase looses mobility and the crystallization process is slowed down. As already pointed out by other authors, phase separation onset is almost instantaneous for samples pre-immersed in a mixed solvent, whereas a direct immersion in a pure non-solvent bath will delay the demixing process [13].

Conclusion

The effects of coagulation bath composition and desiccation environment on surface morphology of membranes prepared via DIPS were explored and discussed. The composition of coagulation bath determines the morphology of internal surface, corresponding with the casted solution in contact with the support, whereas desiccation environment affects the

external surface, i.e., the zone directly exposed to the coagulation bath. When adopting a desiccation in humid environment, external surface was more likely open. This fact can be related to the slower water removal, which extends the time available for the growth of phase-separated domains. Otherwise, when desiccating in a dry environment, the external membrane surface is more likely closed, as a faster water removal could re-establish a single-phase condition, thus favoring polymer crystallization.

The double bath technique promotes the formation of an open external membrane surface. As a matter of fact, the immersion in a pure non-solvent will produce a dense skin, owing to the polymer concentration increase at the interface between casted solution and coagulation bath. Skinless membranes were produced with a double immersion, first in a dioxane/water bath, and then in a pure water bath. The compositions of first baths were 87/13 and 75/25 dioxane/water wt/wt.

A final consideration regards the role of membrane post-treatment after the immersion stage. Results showed that controlling the desiccation conditions, i.e., non-solvent partial pressure, could modify membrane morphology. This evidence provides a way to control surface morphology, and underlines the importance of post-treatment stages on final membrane properties. Therefore, to fully understand the mechanisms involved in membrane production via phase separation and to achieve better control on membrane morphologies, all steps after immersion must be taken into account.

References

[1] G. Guillen, Y. Pan, M. Li, E. Hoek, Preparation and Characterization of Membranes Formed by Nonsolvent Induced Phase Separation: A Review, Ind. Eng. Chem. Res. (2011) 50, 3798.

[2] A.J. Reuvers, J.W.A. van den Berg, C.A. Smolders, Formation of membranes by means of immersion precipitation: Part I. A model to describe mass transfer during immersion precipitation J. Mem. Sci. (1987) 34, 45.

[3] Reuvers, A. J.; Smolders, C. A. J. Mem. Sci. 1987, 34, 67.

[4] L.P. Cheng, Mechanism of microporous membrane formation by precipitation of semicrystalline polymers; Columbia University: PhD thesis (1993).

[5] P. van de Witte, P.J. Dijkstra, J.W.A. van den Berg, J. Feijen, Phase separation processes in polymer solutions in relation to membrane formation, J. of Mem. Sci. (1996) 117, 1.

[6] P. van de Witte, H. Esselbrugge, P. Dijkstra, J.W.A. van den Berg, J. Feijen, Phase transitions during membrane formation of polylactides. I. A morphological study of membranes obtained from the system polylactide-chloroform-methanol, J. Mem. Sci. (1996) 113, 223.

[7] P. van de Witte, H. Esselbrugge, P. Dijkstra, J.W.A. van den Berg, J. Feijen, A morphological study of membranes obtained from the systems polylactide-dioxane-methanol, polylactide-dioxane-water and polylactide-N-methyl pyrrolidone-water, J. Polym. Sci. B Polym. Phys. (1996) 34, 2569.

[8] R.A. Zoppi, S. Contant, E.A.R. Duek, F.R. Marques, M.L.F. Wada, S.P. Nunes, Porous poly(L-lactide) films obtained by immersion precipitation process: morphology, phase separation and culture of VERO cells, Polymer (1999) 40, 3275.

[9] A. Moriya, T. Maruyama, Y. Ohmukai, T. Sotani, H. Matsuyama, Preparation of poly (lactic acid) hollow fiber membranes via phase separation methods, J. Mem. Sci. (2009) 342, 307.

[10] H. Sawalha, K. Schroen, R. Boom, Mechanical Properties and Porosity of Polylactidefor Biomedical Applications, J. Appl. Polym. Sci. (2007) 104, 959.

[11] Q. Xing, X. Dong, R. Li, H. Yang, C. Han, D. Wang, Morphology and performance control of PLLA-based porous membranes by phase separation, Polymer (2013) 54, 5965.

[12] A.M.W. Bulte, M.H.V. Mulder, C.A. Smolders, H. Strathmann, Diffusion induced phase separation with crystallizable nylons. II. Relation to final membrane morphology, J. Mem. Sci. (1996) 121, 37.

[13] J.G. Wijmans, J.P.B. Baaij, C.A. Smolders, The mechanism of formation of microporous or skinned membranes produced by immersion precipitation, J. Mem. Sci. (1983) 14, 263.

[14] C.A. Smolders, A.J. Reuvers, R.M. Boom, I.M. Wienk, Microstructures in phase-inversion membranes, J. Mem. Sci. (1992) 73, 259.

[15] Q. Yang, T.S. Chung, Y.E. Santoso, Tailoring pore size and pore size distribution of kidney dialysis hollow fiber membranes via dual-bath coagulation approach, J. Mem. Sci. (2007) 290, 153.

[16] R. Thomas, E. Guillen- Burrieza, H.A. Arafat, Pore structure control of PVDF membranes using a 2-stage coagulation bath phase inversion process for application in membrane distillation (MD), J. Mem. Sci. (2014) 452, 470.

[17] J.A. van't Hof, A.J. Reuvers, R.M. Boom, H.H.M. Rolevink, C.A. Smolders, Preparation of asymmetric gas separation membranes with high selectivity by a dual-bath coagulation method, J. Mem. Sci. (1992) 70, 17.
[18] X. Li, Y. Ji, T. He, M. Wessling, Does more solvent in bore liquid create more open inner surface in hollow fiber membranes?, J. Mem. Sci. (2008) 320, 1.
[19] X. Li, Y. Ji, Y. Yin, Y. Zhang, Y. Wang, T, He, Origin of delamination/adhesion in polyetherimide/polysulfone co-cast membranes, J. Mem. Sci. (2010) 352, 173.
[20] T. He, M.H.V. Mulder, M. Wessling, Preparation of porous hollow fiber membranes with a triple-orifice spinneret, J. Appl. Polym. Sci. (2003) 87, 2151.
[21] H. Matsuyama, M. Teramoto, R. Nakatani, T. Maki, Membrane formation via phase separation induced by penetration of nonsolvent from vapor phase. I. Phase diagram and mass transfer process, J. Appl. Polym. Sci. (1999) 74, 159.
[22] J.F. Li, Z.L. Xu, H. Yang, Microporous polyethersulfone membranes prepared under the combined precipitation conditions with non-solvent additives, Polym. Adv. Tech. (2008) 19, 251.
[23] H. Matsuyama, M. Teramoto, R. Nakatani, T.J. Maki, Membrane formation via phase separation induced by penetration of non-solvent from vapor phase II: membrane morphology, Appl. Polym. Sci. (1999) 74, 171.
[24] F. Carfì Pavia, V. La Carrubba, G. Ghersi, V. Brucato, Poly-left-lactic acid tubular scaffolds via diffusion induced phase separation: Control of morphology, Polym. Eng. Sci. (2013) 53, 431.
[25] I.C. Sanchez, A.C. Balazs, Generalization of the lattice-fluid model for specific interactions, Macromolecules (1989) 22, 2325.
[26] G.A. Mannella, V. La Carrubba, V. Brucato, I.C. Sanchez, Lattice fluid model generalized for specific interactions: An application to ternary polymer solutions, Fl. Pha. Equi. (2011) 312, 60.
[27] G.A. Mannella, V. La Carrubba, V. Brucato, Measurement of cloud point temperature in polymer solutions, Rev. Sci. Instr. (2013) 84, 075118.
[28] G.A. Mannella, F. Carfì Pavia, G. Conoscenti, V. La Carrubba, V. Brucato, Evidence of mechanisms occurring in thermally induced phase separation of polymeric systems, J. Polym. Sci. B Polym. Phys. (2014) 52, 979.
[29] C.H. Schneider, C.C. Lynch, Binary vapor-liquid diagram for the system 1,4-dioxane/water, J. Am. Chem. Soc. (1943) 65, 1063.

Chapter 3

Evaluation of mechanical and morphologic features of PLLA membranes as supports for perfusion cells culture systems

A well designed tissue engineering scaffold should provide initial support to the seeded cells, localise the cells in the appropriate spaces, and provide physical and biological cues for adhesion, migration, proliferation, differentiation and eventually formation of model tissues and organs [1, 2, 3]. Biodegradable polymeric scaffolds have been harnessed as temporal structural supports to regenerate various tissues such as bone, cartilage, nerve, ligament, skin and liver. An open porous geometry with interconnected channels is a prerequisite for high density cell growth as well as for a sustained mass transport of nutrients, oxygen, and metabolic waste; as a matter of fact, a high cell density and efficient mass transport contribute to cell viability, proliferation, and ultimate rehabilitation into functional tissues [4, 5, 6]. A wide range of biodegradable scaffolds with diverse morphologies have been fabricated by conventional methods such as solid porogen leaching, gas foaming, emulsion/freeze drying, expansion in supercritical fluid and phase separation techniques [7, 8, 9].

More specifically, the production of polymeric scaffolds and membranes via DIPS has been widely studied and applied for a number of model systems. Various researchers investigated systematically the structure, porosity and crystallization behaviour of poly (L-lactic acid), blend of poly (L-lactic acid)/poly-Urethane and poly (L-lactic acid)/poly-Caprolactone Triol membranes, prepared from ethanol/dioxane and ethanol/water coagulation baths via phase separation [10, 11, 12, 13], finding interesting correlations between phase behaviour, kinetics of demixing and the resulting membrane morphology. Other authors showed that mechanical properties of foams are mainly controlled by the gas pressure, material properties, manufacturing methods, and cell geometry. With this respect, the geometrical features influencing the mechanical properties were determined: number of open cells, relative foam density, cell size and cell shape [14, 15].

In the aforementioned context, the aim of the present section is analysed the PLLA membrane obtained in previous section, to be used as supports for perfusion cell culture systems, by using dioxane content and immersion time in the first coagulation bath as tuning parameters to control mechanical and surface morphological features. The surface morphology in terms of average

pore size and surface porosity obtained was examined by imageJ software [9, 16, 17]. Relative densities of PLLA membrane were measured by independent weight and volume measurement. Furthermore, mechanical properties were evaluated by measuring storage, loss modulus and loss angle via dynamic mechanical analysis [18, 19]. The dependence of the glass transition temperature, storage modulus and relative density upon dioxane content and immersion time was examined. The role of the interconnection degree on the membrane's mechanical properties was highlighted by using the Gibson and Ashby model [20]. Finally, to show the applicability of the membranes in cell culture experiments, cell adhesion assays on different membrane surface were also performed by using a standard count method [12]. Whit respect to the scientific literature on this topic, the present results show the versatility of the proposed technology in fine-tuning the final morphology and mechanical performance of the membranes obtained.

Experimental

Morphology characterization

The pore number and pore size distribution of the membranes were determined by analysing SEM pictures via the ImageJ software. The pore size of each sample was averaged by accounting for at least 100 pores. The average pore size, D, was calculated through the following equation:

$$D = \frac{\sum_{i=1}^{n} d_i}{n} \quad \textbf{(7)}$$

where n is the number of pores with the pore size of d_i. The surface porosity, $\boldsymbol{\theta}$ (surface of pores over total surface of PLLA membrane), was determined by the following equation:

$$\theta = \frac{\sum_{i=1}^{n_T} \pi \frac{(d_i)^2}{4}}{S_T} \quad \textbf{(8)}$$

where n_T is the total number of pores in the SEM micrograph and S_T is the area of the micrograph.

Relative density measurements

The relative density, ρ_f/ρ_s, of the membrane, where ρ_f and ρ_s are the density of the membrane and of the compact polymer respectively, was evaluated to determinate the influence of the overall porosity and of the membrane texture (in terms of combination of various layers of different thickness) on the resulting mechanical properties. The membrane density ρ_f was measured by weighing a sample and dividing the mass by the volume. Round samples were cut with a precision tool to a diameter of 5.9 mm, while the thickness was measured by a thickness

gauge. The membrane density of each sample was averaged on at least 10 different samples.

Dynamic mechanical analysis

Dynamic mechanical analysis (DMA) was used to investigate the mechanical behaviour of PLLA membrane obtained by using coagulation baths with different dioxane/water ratios and immersion times. Metravib DMA 25 was utilized to determine the stress/strain behaviour as a function of temperature. Samples of 30 x 7.5 mm and thickness in the range 80 ÷ 100 μm were subjected to a static deformation with an amplitude of 100 μm and to a sinusoidal deformation with an amplitude of 20 μm at a constant frequency of 1.00 Hz, in the temperature range 37 - 80 °C with a heating rate of 5 $°C \cdot min^{-1}$ by using tensile mode. In addition, a standard tensile test was performed to determine the modulus of elasticity, tensile strength and strain at break at the temperatures of 30°C and 80°C, respectively, and at a force rate of 0.01 N/s.

Cell Adhesion assays

16HBE (Human Bronchial Epithelium) cells were used to test the cellular adhesion on PLLA membranes, obtained by using 87/13 and 75/25 (dioxane/water wt/wt) coagulation baths. Samples were stuck by 770 Loctite primer and 406 Loctite glue to a Transwell of 6.5 mm. Five samples of each membrane surface were tested, whereas BD Transwell with a commercial PET membrane was used as a control. A 100-μL liquid volume containing 2×10^5 cells/mL was seeded onto membranes and cultured in DMEM containing 10% (v/v) fetal bovine serum and 1% (v/v) penicillin/streptomycin. Cells adhesion was assessed after 2 h and after 24 h with and without a treatment consisting in submerging the sample in culture medium for 1 h at room temperature. Hence, after 2 and 24h, the cultures were washed twice in phosphate-buffered saline (PBS), and then the adherent cells were collected by treating with 0.05% trypsin. Cells were counted in a Burker Chamber and the ratio of adherent cells with respect to the seeded cells was calculated. Each test was performed five times and data averaged. Cell adhesion assays were analysed statistically to evaluate the influence of the surface morphology and mechanical properties on the cell adhesion process.

Results and Discussion

Morphological analysis

In this section SEM images of both internal (glass facing) and external (coagulation solution facing) surface morphologies of all PLLA membranes are shown in Fig. 24, reporting surface type (internal or external), immersion time in minutes (first and second coagulation bath,

respectively) and composition of the first coagulation bath. The membranes analysed in this section show open pores on both the internal (glass) and external (solution) surfaces, which are most appropriate as support for perfusion cells culture systems. It can be clearly observed that at higher dioxane concentration (87/13 dioxane/water w/w), the external surface is fully covered by pores while the internal one show sparse pores (Fig. 24e – h). On the other hand, when a lower dioxane content (75/25 dioxane/water) in the first coagulation bath was used, the external surface exhibits morphology similar to the internal one, with sparse pores and a relatively lower surface porosity (Fig. 24a – d) [17].

Increasing the immersion time in the dioxane/water bath from 5 to 10 minutes does not appreciably influence the membrane morphology in terms of both the pore size and the surface porosity of the internal (glass) surface (Fig. 24a and c), while both the pore size and the surface porosity of the external (solution) surface decrease (Fig. 24b and d).

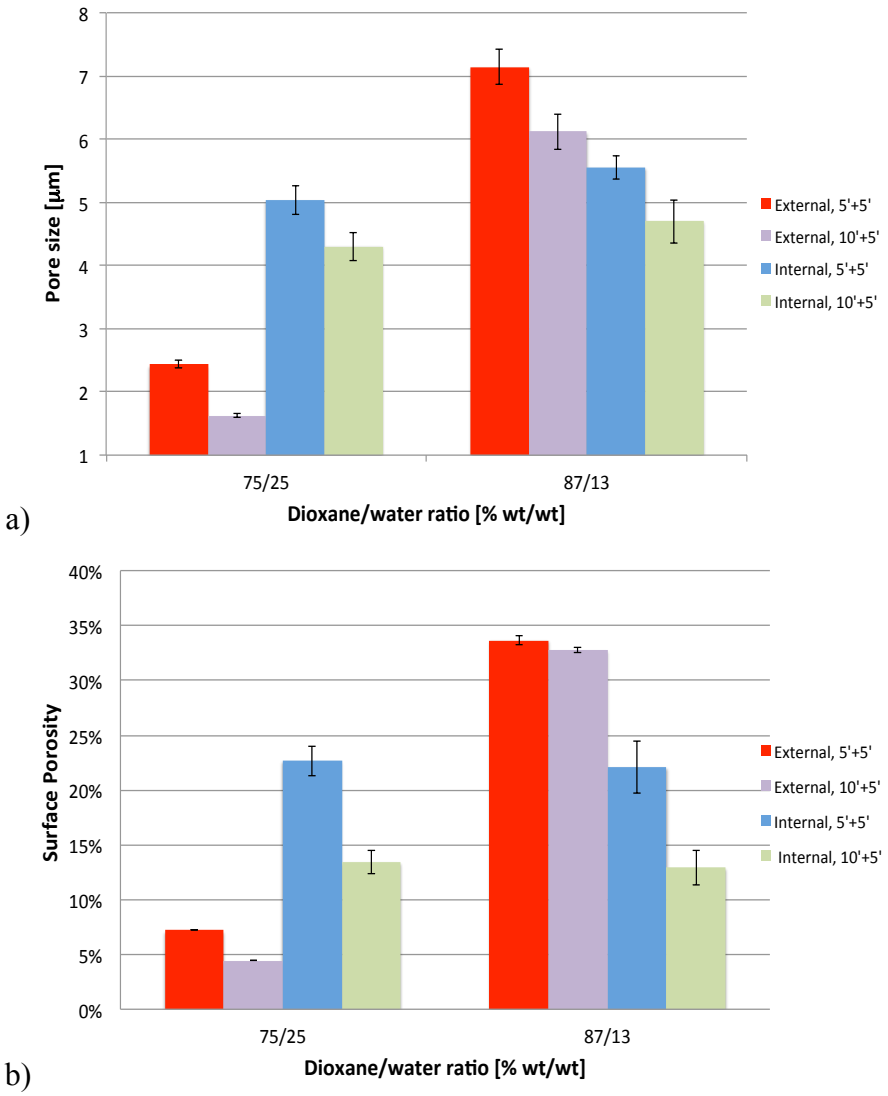

Figure 27: Pore size and surface porosity vs. dioxane/water ratio in the first coagulation bath.

All things considered, the morphology of external surface depends essentially on the composition of the first coagulation bath. Fig. 27 summarizes the surface characteristics of PLLA membranes (e.g. the average pore size and surface porosity) obtained at different water contents in the first coagulation bath. Each bar is identified by surface type (internal vs. external) and soaking time (first and second coagulation bath, respectively).

It can be observed that the external surface porosity of PLLA membranes decreases from 33% to 5% by increasing from 13% to 25% w/w the amount of water into the first coagulation bath. Conversely, the internal surface porosity remains almost constant at the values of 23% and 13%, by increasing from 5 to 10 minutes the immersion time.

Relative foam density

The relative foam density ρ_f / ρ_s is a crucial parameter as it influences mechanical, thermal and many other characteristics of foams. The obtained values were averaged over the volume of the sample, since the structure is not homogeneous and the density of the surface layers may be 3 to 10 times greater than the average value, due to the protocol adopted in the forming process [20]. Fig. 28a shows that the average density of PLLA membranes decreases by changing from 13% to 25% w/w the water content into the first coagulation bath. Furthermore, by increasing the soaking time from 5 to 10 minutes in the dioxane/water bath, foam's average density decreases of about 10% for 75/25 dioxane/water ratio and of about 35% for 87/13 dioxane/water ratio coagulation baths, respectively.

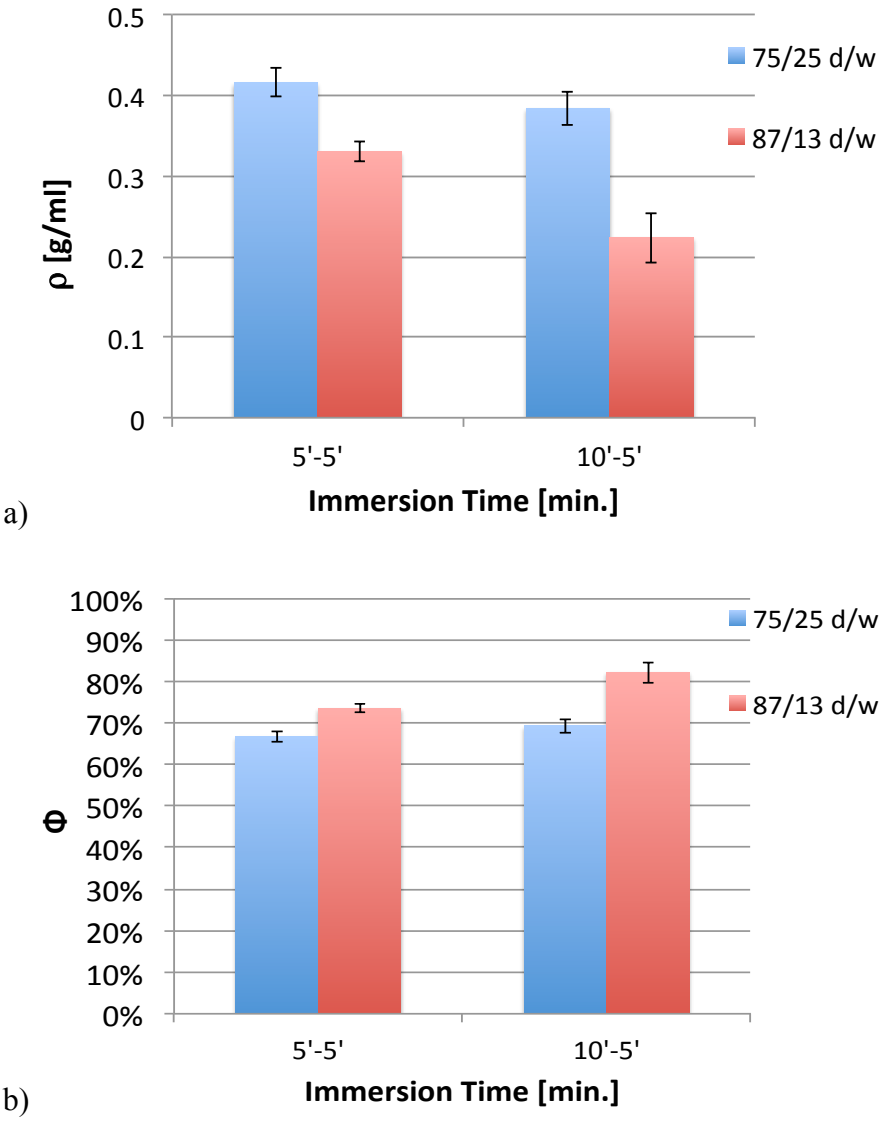

Figura 28: Relative foam density and volume porosity (void fraction) vs. immersion time in the dioxane/water coagulation bath.

Volume porosity (void fraction) is a similar parameter often reported [21]. It represents the ratio between the voids volume and the overall volume. Fig. 28b reports the trend of volume porosity (void fraction) as a function of immersion time, which is obviously opposite to that of foam's density. It can be easily noticed that volume porosity was higher than surface porosity and that the immersion time, in the dioxane/water bath from 5 to 10 minutes, appreciably influence the surface porosity (Figure 27b) whereas volume porosity is almost unaffected (Figure 28b). Therefore, according to our protocol, it is possible to control surface porosity while keeping about constant the volume porosity.

Mechanical behaviour of PLLA membrane

Dynamic mechanical thermal analysis

The main goal of DMA is to relate macroscopic properties, such as mechanical properties, to the molecular relaxations associated with conformational changes and microscopic deformations generated by molecular rearrangement [21, 22]. Figure 29 shows loss tangent and storage modulus vs temperature, for all the membranes analysed along this work, illustrating the variation of glass transition temperature (T_g) and stiffness with temperature. The peaks of tan δ curve (Fig. 29a) indicate that Tg decreases with both the dioxane content in the first coagulation bath and the immersion time in the dioxane/water bath. The Tg values obtained in this work by DMA are in line with those obtained by DSC in a previous work [9]. It should be recalled that, as Tg is a second-order transition, in DSC traces is detected by an ideally step change in the baseline (arising from a change in heat capacity). In the case of foamed materials a broad transition is however obtained and is difficult to detect the step change. The dynamic mechanical analysis, instead, detects a significant drop in the E' vs. T plot, thus allowing a more reliable evaluation of Tg.

However, it may be noticed that the tan δ peak height show higher values (from 0.34 to 0.43) the increasing both the dioxane content in the first coagulation bath and the immersion time. Lee et al. [22] pointed out that the peak height is associated to the molecular chain motion. Therefore, a PLLA membrane with higher tan δ peak exhibits a molecular chain motion less hindered.

Therefore, as observed in Fig. 29a, chain motion of PLLA membranes decreases when passing from 13% to 25% w/w of water content into the first coagulation bath. On the other hand, by increasing the immersion time from 5 to 10 minutes chain motion is promoted for 75/25 w/w, and it remains about constant for 87/13 w/w coagulation bath. PLLA foam structures with larger relative foam density (or smaller void fraction) may hinder the chain mobility, thus reducing tan δ peak height.

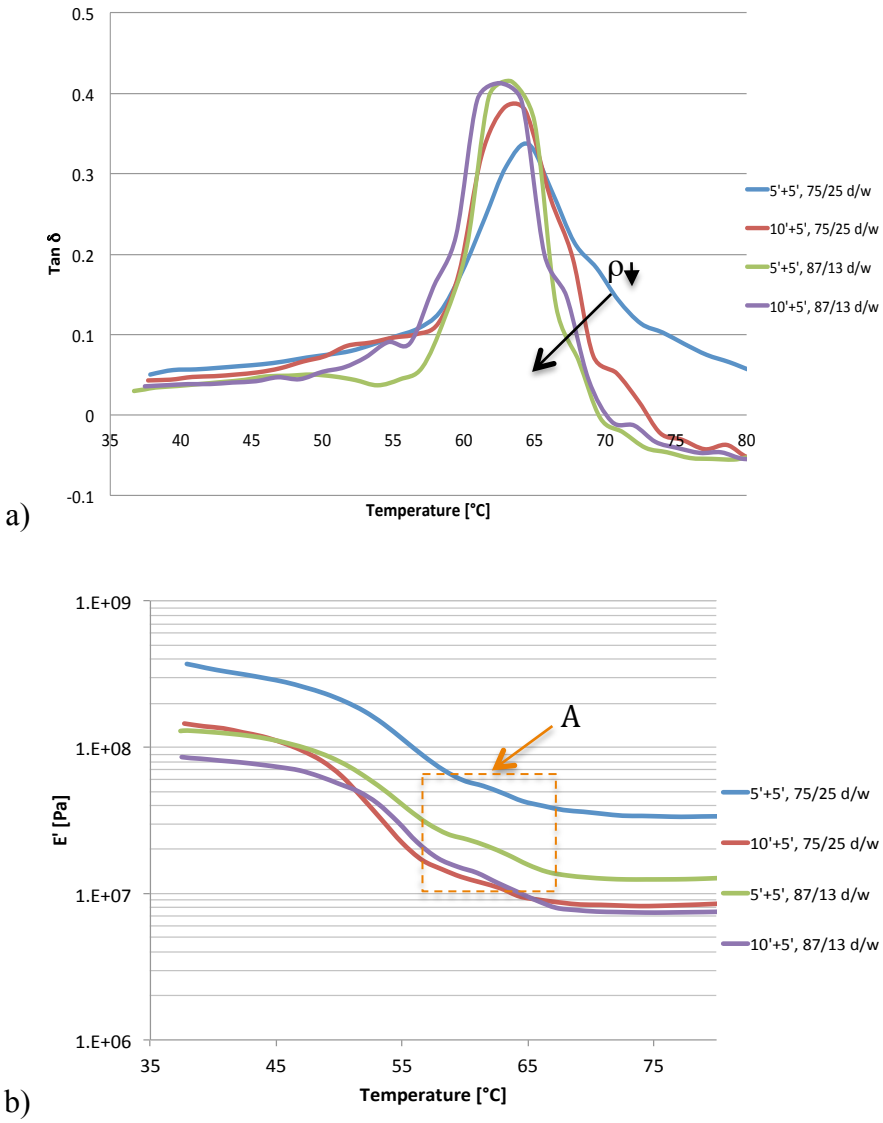

Figura 29: Tanδ(a) and E' (b) as a function of temperature for the membranes studied in this work. Each curve is identified by immersion time (first and second coagulation bath, respectively) and compositions of first coagulation bath (dioxane/water wt/wt).

By looking at Fig. 29b, one can notice that the value found for storage modulus (E') of PLLA foams at the temperature of 40°C, is in the range 90 ÷ 300 MPa, in agreement with the value reported in literature [23, 24, 25]. The storage modulus of PLLA foams obtained with smaller dioxane contents is higher than the one with larger dioxane content, and it decreases with the immersion time. Thus, the mechanical behaviour of the PLLA membrane is clearly influenced by foam's density, porosity and surface morphology. A considerable drop of the storage modulus occurs in the range from 50 to 68 °C, as highlighted by the box A in figure 5b. The development of localised deformation is caused by a process taking place on the material's microscale. The microscopic behaviour is governed by the occurrence, growth and interaction of cracks and

voids, which finally lead to a complete fracture on the macroscale [26, 27]. The damage process of the foam takes place on multiple scales, determining changes of several physical and structural properties of the material, which may also lead to negative values of tan δ as already reported in literature [25, 28]. The occurrence of this circumstance, although of difficult interpretation from a physical viewpoint, can be attributed to softening and/or hardening damage phenomena taking place above glass transition. From the analysis of Fig. 29a one may notice that the lower the relative PLLA membrane density (87/13 dioxane/water, see figure 28a), the faster the set-in of negative tan δ values.

Tensile behaviour of PLLA membranes

In order to understand more in detail the mechanical performance of PLLA membranes, the stress/strain behaviour was investigated via standard tensile test. Figure 30a and 30b show the stress–strain curves of PLLA membranes at the temperatures of 30 and 80 °C, respectively. By taking the slope of the linear portion of the curve, Young's modulus or modulus of elasticity (E) was determined (see Fig. 30c and 30d). It is easy to notice that at lower dioxane concentration (75/25), Young's modulus is larger than at higher dioxane concentration (83/13). On the other hand, when increasing the immersion time from 5 to 10 minutes in coagulation bath, Young's modulus moves towards smaller values. Furthermore, when temperature is brought to 80 °C (Fig. 30d), Young's modulus gets smaller and is affected by immersion time, while the bath concentration dependence remains unchanged with respect to the behaviour observed at 30 °C (Fig. 30c).

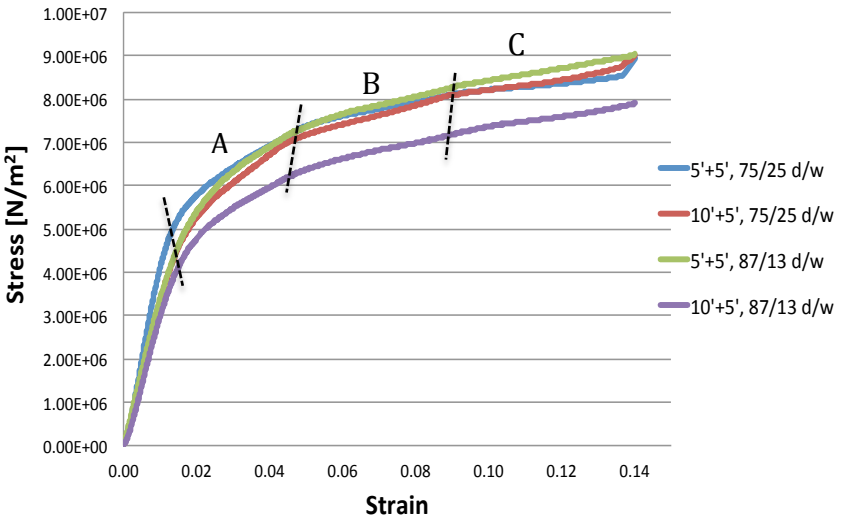

a)

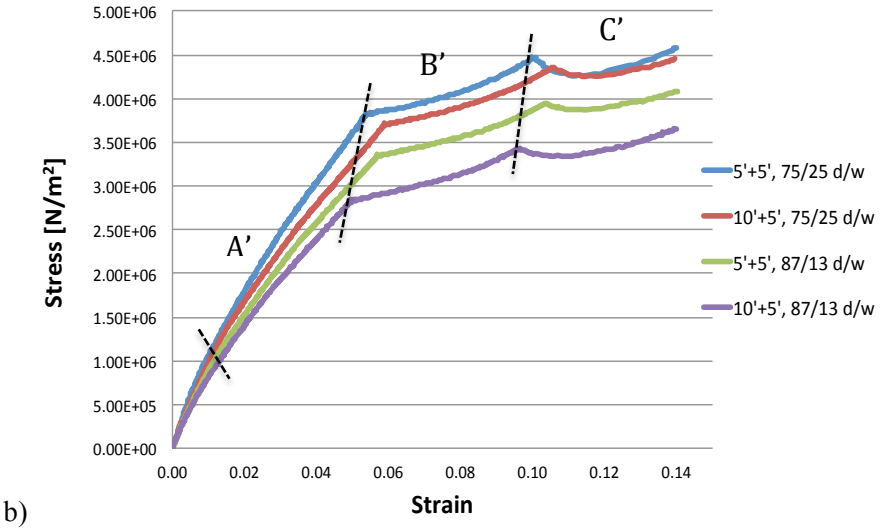

b)

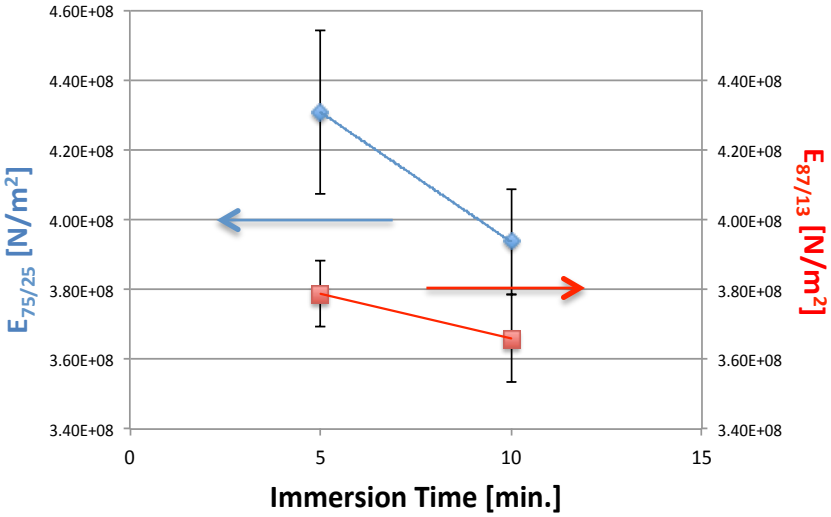

c)

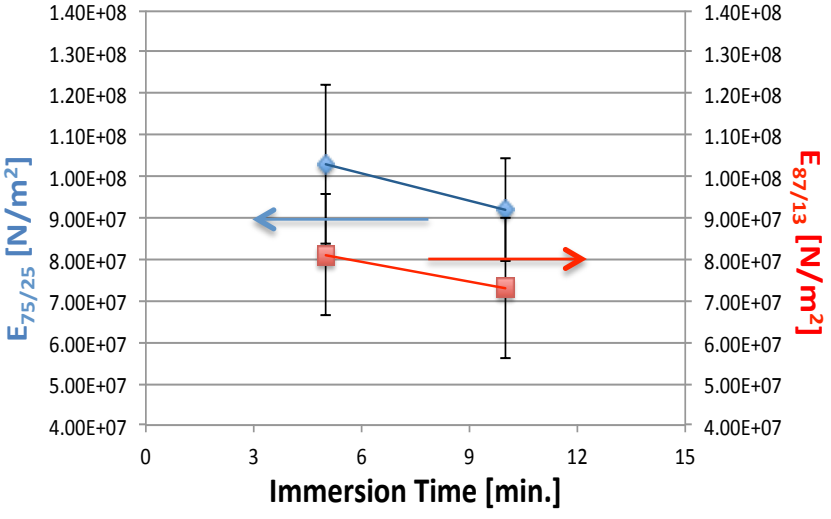

d)

Figura 30: a) Stress-Strain curves at 30 °C, b) Stress-Strain curves at 80°C, c) Young's modulus at 30 °C and d) Young's modulus at 80 °C.

By looking at Fig. 30a and 30b one can observe that all curves present a similar trend. Beyond the elastic range, there are three regimes of plastic deformation indicated with A, B and C at the temperature of 30°C and A', B' and C' at the temperature of 80°C, respectively. If one focuses on the linear elastic part of the curves (i.e. at low deformation), when plotting the calculated Young's modulus as a function of foam's density, the trend reported in Fig. 31 is obtained, with an increase of modulus with increasing density. It should be also noticed that the values of Young's modulus reported in fig. 30 c) and d) are in good agreement with DMA measurements reported in fig. 29 b. The relatively small differences among the Young's modulus values recorded at 30°C (below Tg) and 80°C (above Tg) can be explained by recalling the significant amount of crystallinity exhibited by PLLA when processed from solution.

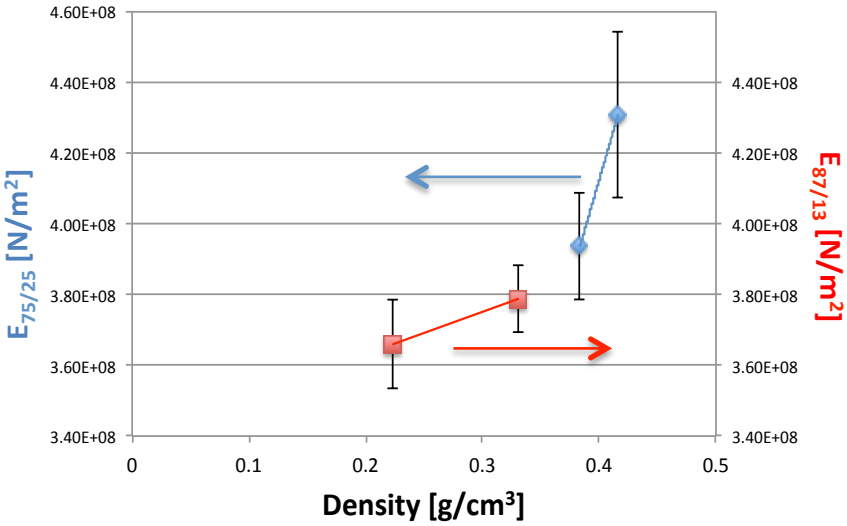

Figura 31: Young's Modulus vs. density at 30 °C.

As expected, when increasing volume porosity (i.e. reducing density) a reduction in the elastic modulus occurs, as it happens in homogeneous foams, where a density increase involves a rise of the plateau stress [29, 30]. In other words, a higher density obviously implies a larger relative amount of polymer, as either the cell number is more significant or the cell walls are thicker. Then, the reduction in density is reasonably caused by the presence of a high volume of pores, as reported in literature [31, 32,]. However, PLLA membranes studied in the present work, as they exhibit different surface textures, are definitely non-homogeneous; therefore, it seems plausible to associate the overall response of the three sections A - B - C and A' - B' - C' to a combination in parallel of layers of different average densities. Consequently, section, A - B - C and A' - B' - C' can represent several changes of regime, depending upon the contribution exerted by each layer combined in parallel with the others [33].

On the other hand, when temperature is increased from 30 to 80 °C, a considerable decrease of the elastic section is displayed (Fig. 30a and b) accompanied by a parallel reduction of elastic

deformation (from about 0.8% to 0.4%) and fracture toughness (decreasing of about 50%) [34]. All things considered, it seems logical to figure out that at of 80°C, i.e. above Tg, softening and/or hardening damage phenomena take place more rapidly than below Tg. Figure 32 shows a cross section of membrane obtained with a double immersion, first in a 87/13 dioxane/water bath, then in pure water, and desiccated in humid environment. It can be observed that the cross section, which has a thickness about of 130 μm, shows a complex morphology with denser outer layers at the edges and a less dense (more porous) core.

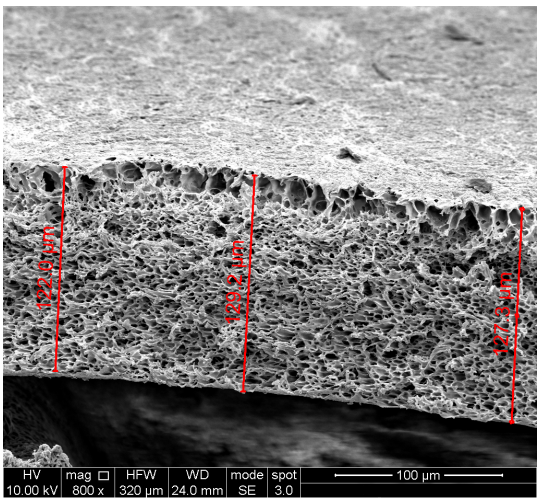

Figura 32: Cross section of a membrane obtained with a double immersion (first in a 87/13 dioxane/water bath then in pure water) and desiccated in humid environment.

In the light of a simplified modelling of the membrane morphology, with the aim of highlighting the dependence of mechanical properties (namely Young's modulus) upon the geometric features (material density, porosity and interconnection), the well known pioneering model by Gibson and Ashby [35] can be adopted, which describes the tensile modulus of isotropic foams by the combination of stretching lamellae and bending of struts. Although our foams are not strictly isotropic (as shown in fig. 32 and indirectly inferred from the mechanical behaviour reported in fig. 30 a) and b)) the model can provide useful information anyhow on membranes' mechanical behaviour averaged across thickness.

Young's Modulus follows a second order polynomial law dependence with respect to density of foam, according to following equation:

$$\frac{E_f}{E_m} = \psi^2 \left(\frac{\rho_f}{\rho_s}\right)^2 + (1-\psi)\left(\frac{\rho_f}{\rho_s}\right) \qquad \textbf{(9)}$$

where E is Young's modulus, ρ the density, and the indices *s* and *f* refer to the matrix phase and the foam, respectively. The fitting parameter ψ, in Gibson and Ashby's model corresponds to the portion of the material acting as struts. The data elaborated according to the model at 30 °C are

plotted in Fig. 33a. For foams with open cells a value ψ =1 for the fitting parameter was set, whereas for a closed cell structure ψ =0 was imposed, in order to calculate the limiting behaviour [36, 37, 38].

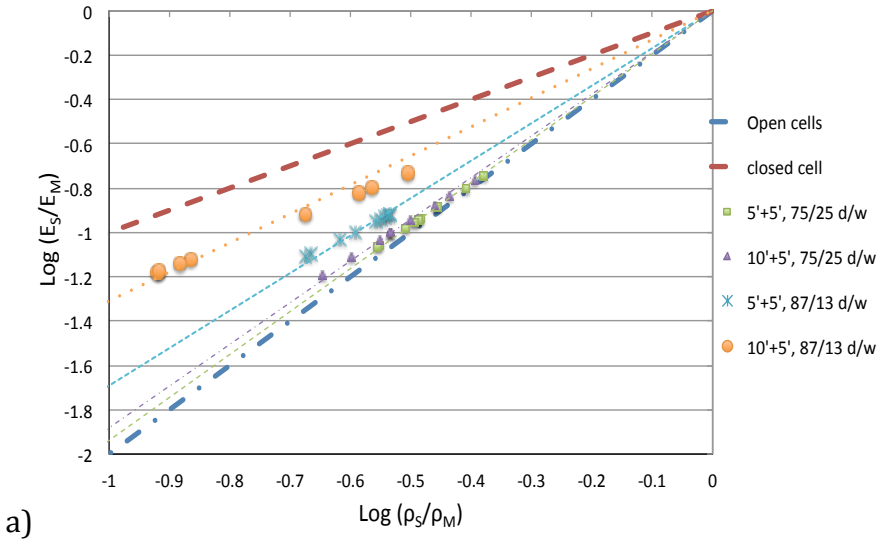

a)

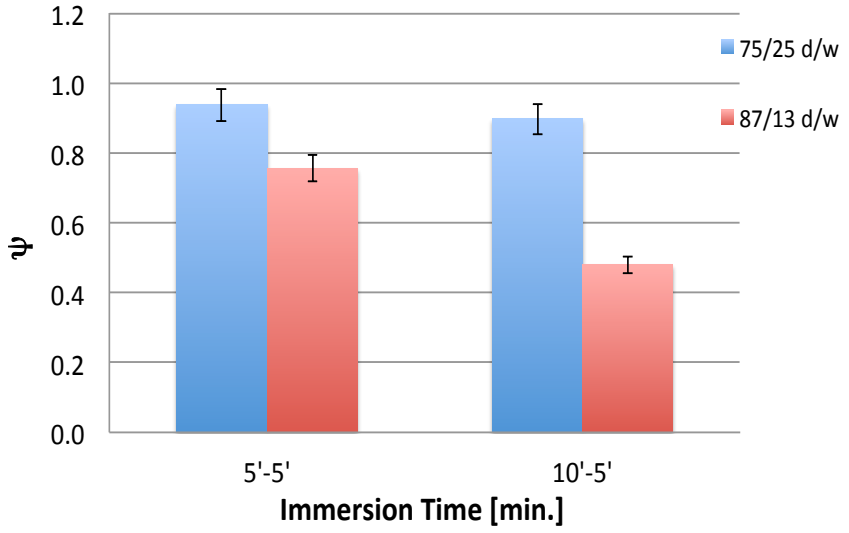

b)

Figura 33: Tensile modulus of PLLA membrane at the temperature of 30°C (a) and Fitting parameter (b).

The data points reported in Fig. 32a refer to all the PLLA membranes studied in this work. It is easy to observe that higher water contents (75/25 dioxane/water) in the DIPS process lead to the formation of PLLA membranes with more open cells, hence characterized by a higher interconnection degree. On the other hand, when increasing the immersion time from 5 to 10 minutes and dioxane content from 75% to 87% into the coagulation bath, the fitting parameter ψ moves toward smaller values (see fig. 33b) and the membrane tends to exhibit a closed cell behavior (see Fig. 33a).

An intermediate situation with an effective strut portion of ψ =0.48 (and a complementary 0.52 portion of lamellae) was obtained by using an immersion time of 10 minutes and a coagulation bath 87/13 wt/wt.

Cell Adhesion assays

16HBE (Human Bronchial Epithelium) cells were cultured in serum-containing medium. Serum contains large quantities of a variety of bioactive components such as the extracellular matrix (e.g. proteins, collagen) and cell-growth factors. These components take priority in adsorption by the membrane, and when these components are subsequently recognized by integrin and other receptors on the cell membrane, signals are transmitted to the cell interior [39]. Both internal and external surfaces were used as substrates, which were either non-treated or treated, for in vitro cell adhesion assays. The various surfaces, characterized by different morphological properties, exhibit different behaviors with regard to the level of cell adhesion. Figures 34a and b display the ratio of adhered cells to seeded cells after 2h and 24h respectively, for some of the membrane surfaces explored in this work. The external surfaces of the PLLA membranes obtained with coagulation bath 87/13 (dioxane/water) wt/wt were not tested due to their very high porosity and pore size, which make them not suitable to be used as scaffolds for this kind of cell culture.

By looking at fig. 34 one may notice that any PLLA membrane shows a less relevant cell adhesion with respect to the control membrane (a standard non-biodegradable PET membrane). The adhesion process was improved by a medium pre-treatment both at 2h and 24h [12, 40, 41], as the ratio of adherent cells to seeded cells after 24h resulted about doubled. Furthermore, it is clear that surface features play a crucial role in controlling the adhesion process, as surfaces with lower pore size and porosity (75/25 dioxane/water, 10' immersion time in the coagulation bath) exhibit a more significant cell adhesion. Moreover, a slow-down of the cell growth dynamics on PLLA membranes can be observed with respect to the control membrane, by comparing the data at 2 and 24 h.

These results confirm that surface characteristics directly and indirectly influence the way molecules present in the biological world act, and this might ultimately control new tissue formation, as cell proliferation and differentiation both depends on the quality of their early adhesion [42, 43]. Moreover, biocompatibility does not imply the necessary bioactivity for a good tissue regeneration [44], as the surface texture must be carefully designed to maximize the cell adhesion.

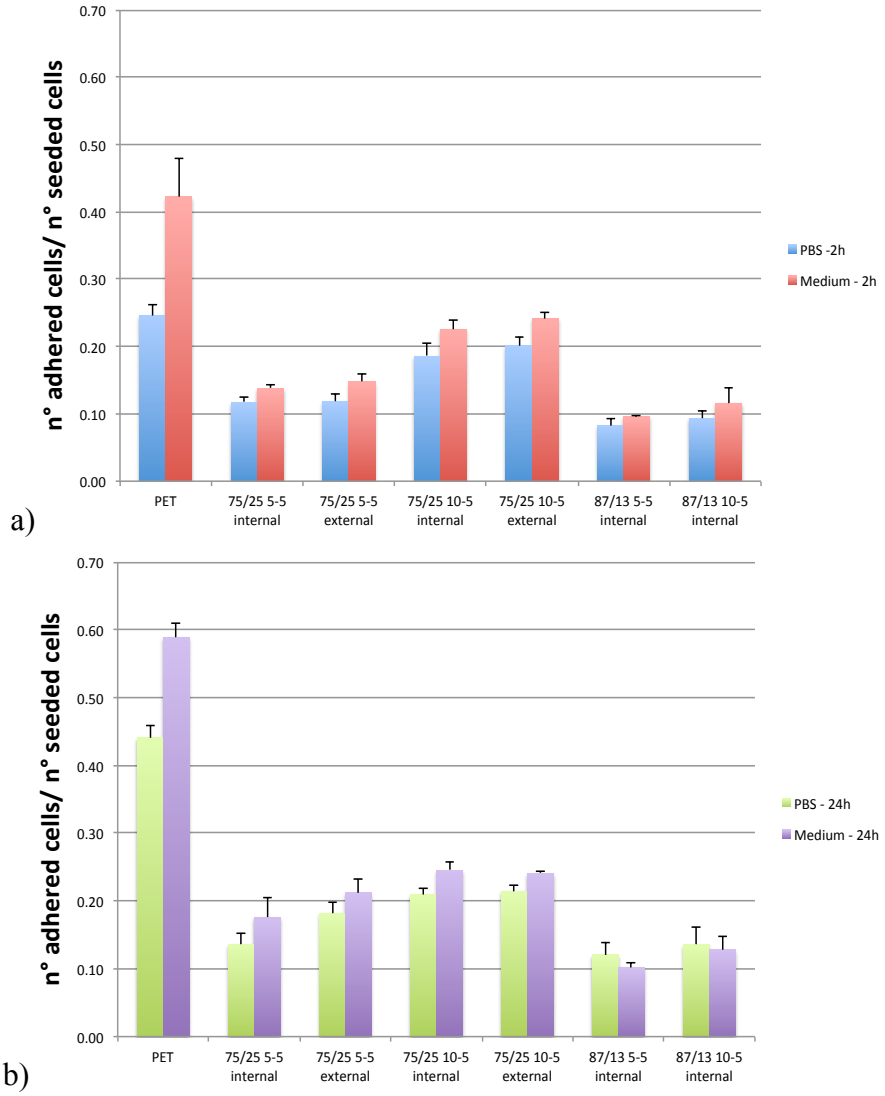

Figura 34: Ratio of adhered cells to seeded cells after a) 2 hours b) 24 hours.

To sum up, by playing with the process parameters (composition of the coagulation bath both and immersion time) it is possible to tune the surface morphology in order to achieve the desired combination of mechanical performance and cell adhesion beahviour.

Conclusion

Based on the results presented, it was observed that the water content in the first coagulation bath influences the mechanical and morphological properties of PLLA membranes prepared by diffusion induced phase separation and suitable for perfusion cell culture systems.

A thorough investigation of the effects of different immersion times on the mechanical performance was carried out. Gibson and Ashby's model was used to investigate the relationship

between Young's modulus and foam's density, a fitting parameter was evaluated and related to the observed behaviour.

Cell adhesion assays were performed on the best surface morphologies, to assess the use of PLLA membranes as supports for cell perfusion systems.

The results obtained not only provide new insights into the application foaming methods for producing bioabsorbable polymer membranes, but also provide indications on how to optimise the fabrication parameters to design a polymeric membrane exhibiting tailored morphology and mechanical properties. This might address new applications in tissue regeneration of bioabsorbable membranes. Further investigations, still in progress, are aimed at evaluating and modelling the damage process (stress-strain behaviour) of the membranes and at utilizing the PLLA membrane as supports for Human Bronchial Mucosa Cell 3D perfusion models [45, 46].

References

[1] R. Langer, J.P. Vacanti, Tissue engineering, Science 260 (1993) 920-926.

[2] Y. Kimura, Y. Tabata, Experimental tissue regeneration by DDS technology of bio-signalling molecules, J. Dermatol. Sci. 47 (2007) 189–199.

[3] I.O. Smith, X.H. Liu, L.A. Smith, P.X. Ma, Nanostructured polymer scaffolds for tissue engineering and regenerative medicine, Wiley Interdiscip. Rev. Nanomed. Nanobiotechnol. 1 (2009) 226–236.

[4] S.J. Hollister, Porous scaffold design for tissue engineering, Nat. Mater. 4 (2005) 518-524.

[5] J.J. Marler, J. Upton, R. Langer, J.P. Vacanti, Transplantation of cells in matrices for tissue regeneration, Adv Drug Delivery Rev. 33 (1998) 165-182.

[6] H.J. Sung, C. Meredith, C. Johnson, Z.S. Galis, The effect of scaffold degradation rate on three-dimensional cell growth and angiogenesis, Biomaterials 25 (2004) 5735-5742.

[7] V. Thomas, D.R. Dean, Y.K. Vohra, Nanostructured biomaterials for regenerative medicine, Curr. Nanosci. 2 (2006) 155-177.

[8] H.J. Chung, T.G. Park, Surface engineered and drug releasing pre-fabricated scaffolds for tissue engineering, Adv. Drug Delivery Rev. 59 (2007) 249-262.

[9] S. Montesanto, G.A. Mannella, F. Carfì Pavia, V. La Carrubba, V. Brucato, Coagulation bath composition and desiccation environments tuning parameters to prepare skinless membranes via diffusion induced phase separation. J. Appl. Polym. Sci. 132 (2015), DOI: 10.1002/app.42151.

[10] P. Van De Witte, H. Esselbrucce, P.J. Dijkstra, J.W.A. Van Den Berg and J. Feijen, Morphological Study of Membranes Obtained from the Systems Polylactide-Dioxane-Methanol, Polylactide-Dioxane-Water, and Polylactide-N-Methyl Pyrrolidone-Water, J. Polymer Sci.: Part B Polymer Physics 34 (1996) 2569-2578.

[11] M.S. Huang, J. Coudane, S. Li, M. Vert, Methylated and pegylated PLA–PCL–PLA block copolymers via the chemical modification of di-hydroxyl PCL combined with the ring opening polymerization of lactide, J. Polym. Sci. Polym. Chem. 43 (2005) 4196–4205.

[12] D.V. Mistura, A.D. Messias, E.A.R. Duek, M.A.T. Duarte, Development, characterization, and cellular adhesion of Poly(l-Lactic Acid)/Poly(Caprolactone Triol) membranes for potential application in bone tissue regeneration, Artif Organs 37 (2013) 978-984.

[13] H. Chen, M. Pyda, P. Cebe, Non-isothermal crystallization of PET/PLA blends, Thermochim. Acta 492 (2009) 61–66.

[14] V. Shulmeister, Modelling of the Mechanical Properties of Low-Density Foams, PhD Thesis, 1998.

[15] F. Ramsteiner, N. Fell, S. Forster, Testing the deformation behaviour of polymer foams, Polymer Testing, 20 (2001) 661–670.

[16] H.I. Kim, K. Ishihara, S. Lee, J.H. Seo, H.Y. Kim, D. Suh, M.U. Kim, T. Konno, M. Takai, J.S. Seo, Tissue response to poly(L-lactic acid)-based blend with phospholipid polymer for biodegradable cardiovascular stents, Biomaterials 32 (2011) 2241–2247.

[17] F. Carfì Pavia, V. La Carrubba, G. Ghersi, V. Brucato, Poly ‐ left ‐ lactic acid tubular scaffolds via diffusion induced phase separation: Control of morphology, Polym Eng Sci 53

(2013) 431-442.
[18] M. Shimbo, I. Higashitani, Y. Miyano, Mechanism of strength improvement of foamed plastics having fine cell, J. Cell. Plast. 43 (2007) 157–167.
[19] H.L. Zhu, X.X. Feng, H.P. Zhang, Y.H. Guo, J.Z. Zhang, J.Y. Chen, Structural characteristics and properties of silk fibroin/poly(lactic acid) blend films, J. Biomater. Sci. 20 (2009) 1259–1274.
[20] K. Sivertsen, Polymer foams, Polymer Physics, Spring, 2007.
[21] S.N. Cassu, M.I. Felisberti, Análise dinâmico-mecânica aplicada a polímeros e blendas poliméricas, Química Nova 28 (2005) 255–263.
[22] S.M. Lee, D. Cho, W.H. Park, S.G. Lee, Novel silk/poly(butylene succinate) biocomposites: the effect of short fibre content on their mechanical and thermal properties, Compos. Sci. Technol. 65 (2005) 647–654.
[23] S.S. Ray, K. Yamadab, M. Okamotoa, and K. Ueda, New polylactide-layered silicate nanocomposites. 2. Concurrent improvements of material properties, biodegradability and melt rheology, Polymer, 44 (2003) 857-866.
[24] Y. Li, C. Han, X. Zhang, K. Xu, J. Bian, L. Dong, Poly(L-lactide)/Poly(D-lactide)/Clay nanocomposites: Enhanced dispersion, crystallization, mechanical properties, and hydrolytic degradation, Polymer Engineering and science 2014, DOI: 10.1002/pen.23620.
[25] P. Douglas, A.B. Albadarin, A.H. Al-Muhtaseb, C. Mangwandia, G.M. Walker, Thermo-mechanical properties of poly ε-caprolactone/poly L-lactic acid blends: Addition of nalidixic acid and polyethylene glycol additives, Journal of the mechanical behaviour of biomedical materials 45 (2015) 154–165.
[26] A. Geringer, S. Diebels, A phase-field approach to damage modelling in open-cell foams, Technische Mechanik, 34 (2014) 3–11.
[27] R.H.J. Peerlings, L.H. Poh, M.G.D. Geers, An implicit gradient plasticity–damage theory for predicting size effects in hardening and softening, Engineering Fracture Mechanics 95 (2012) 2–12.
[28] Z.P. Bazant, F. Asce, T.B. Belytschko, M. Asce, T.P. Chang, S.M. Asce, Continuum theory for strain- softening, Journal of Engineering Mechanics, 110 (1986) 1666-1692.
[29] P. Viot, F. Beani, J-L. Lataillade, Polymeric foam behaviour under dynamic compressive loading, Journal of materials science 40 (2005) 5829–5837.
[30] Z. Hussain and N.S.A. Suffin, Microstructure and mechanical behaviour of aluminium foam produced by sintering dissolution process using NaCl space holder, Journal of Engineering Science 7 (2011) 37–49.
[31] P Cheanga, K.A Khorb, Effect of particulate morphology on the tensile behaviour of polymer–hydroxyapatite composites, Materials Science and Engineering: A 345 (2003) 47–54.
[32] L. Peronia, M. Scapina, M. Avallea, J. Weiseb, D. Lehmhusc, Dynamic mechanical behaviour of syntactic iron foams with glass microspheres, Materials Science and Engineering: A 552 (2012) 364–375.
[33] M. Finot, S. Suresh, Small and large deformation of thick and thin-film multi-layers: Effects of layer geometry, plasticity and compositional gradients, Journal of the Mechanics and Physics of Solids 44 (1996) 683–721.
[34] N.A. Fleck, R.A. Smith, Effect of density on tensile strength, fracture toughness, and fatigue crack propagation behaviour of sintered steel, Powder Metallurgy 3 (1982) 121-125.

[35] L.J. Gibson, M.F. Ashby, Cellular solids: structures and properties, 2nd edn. Cambridge University Press, Cambridge, (1997).
[36] F. Ramsteiner, N. Fell, S. Forster, Testing the deformation behaviour of polymer foams, Polymer testing 20 (2001) 661-670.
[37] C.C. Chou, Y. Zhao, L. Chai, J. Co, G.G. Lim, T.L. Lin, Development of foam models as applications to vehicle interior, SAE Technical Paper 1995, DOI: 10.4271/952733.
[38] V. Srivastava, R. Srivastava, On the polymeric foams: modelling and properties, J Mater Sci 49 (2014) 2681–2692.
[39] M. Yamaguchi, T. Shinbo, T. Kanamori, P. Wang, M. Niwa, H. Kawakami, S. Nagaoka, K. Hirakawa, M. Kamiya, Surface modification of poly(L-lactic acid) affects initial cell attachment, cell morphology, and cell growth, J Artif Organs 7 (2004) 187–193.
[40] A. Bagno, A. Piovan, M. Dettin, A. Chiarion, P. Brun, R. Gambaretto, G. Fontana, C. Di Bello, G. Palù, I. Castagliuolo, Human osteoblast-like cell adhesion on titanium substrates covalently functionalized with synthetic peptides, Bone 40 (2007) 693–699.
[41] A. Bagno, M. Genovese, A. Luchini, M. Dettin, M.T. Conconi, A.M. Menti, P.P. Parnigotto, C. Di Bello, Contact profilometry and correspondence analysis to correlate surface properties and cell adhesion in vitro of uncoated and coated Ti and Ti6Al4V disks, Biomaterials 25 (2004) 2437–2445.
[42] B.D. Boyan, T.W. Hummert, D.D. Dean, Z.D. Schwartz, Role of material surfaces in regulating bone and cartilage cell response, Biomaterials, 17 (1996) 137-46.
[43] A. Hunter, C.W. Archer, P.S. Walker, G.W. Blunn, Attachment and proliferation of osteoblasts and fibroblasts on biomaterials for orthopaedic use, Biomaterials, 16 (1995) 287-95.
[44] K. Anselme, Osteoblast adhesion on biomaterials, Biomaterials 21 (2000) 667-81.
[45] F. Bucchieri, A. Fucarino, A.M. Gammazza, A. Pitruzzella, V. Marcianò, C. Paderni, V. De Caro, M. Gabriella Siragusa, L. Lo Muzio, S.T. Holgate, D.E. Davies, F. Farina, G. Zummo, Y. Kudo, I.L. Giannola and G. Campisi, Medium-term Culture of Normal Human Oral Mucosa: A Novel Three-dimensional Model to Study the Effectiveness of Drugs Administration, Current Pharmaceutical Design 18 (2012) 000-000.
[46] F. Bucchieri, The influence of the environment on cell-cell communication in the epithelial–mesenchymal trophic unit, University of Southampton, Thesis for the degree of Doctor of Philosophy, March 2011.

Chapter 4

Polmunary epithelial barrier formation on biodegradable poly-L-lactic-acid (PLLA) membrane

Epithelial barriers are essential for the physiological functioning of tissues and organs allowing the creation and preservation of compartments with different environments. The respiratory epithelium of the lung is in direct contact with the atmosferic environment being the interface between blood and air. The respiratory system is characterized by epithelial barriers whose cellular composition changes along the proximal-to-distal respiratory areas to meet local specific functions. the lung epithelial barrier plays a fundamental role in tissue homeostasis and immunity preventing damage and contamination of the interstitial tissues [1-2]. Different models in vitro of the lung and intestinal epithelial barriers have been well characterized, however these tend to use non-biodegradable and/or poorly biocompatible scaffolds. Therefore, there is need of better supports for epithelial cells for future applications in tissue engineering. The development of functional and biocompatible scaffolds for tissue engineering is a major challenge in biomedical engineering. Poly-L-lactic acid (PLLA) membranes are widely used for this purpose because of their biodegradability, mechanical properties, and most importantly because of their degradation rate, which is comparable to the healing time in a wound healing situation [3].

Considering that living cells first come into contact with the surface of a biomaterial, the surface properties of the PLLA membrane are critical to establish an interface compatible with the cells [4]. PLLA membranes prepared via conventional Diffusion Induced Phase Separation (DIPS) show a non-porous or poorly porous external surface reducing overall membrane permeability and limiting potential applications of PLLA membranes [5]. Therefore the ability to modify and control the characteristics of PLLA membrane surfaces should improve membrane cytocompatibility and expand potential application in tissue engineering.

In this section we tested PLLA membranes with distinct morphologies and investigated epithelial barrier formation in the view of application in bioengineering studies. Effect of dexamethasone, which is required for epithelial barrier formation by these cells [6], and TNF-α were investigated via ELISA test, TEER measure and immunocytochemistry analysis.

Experimental

Materials and Methods

PLLA membrane

The PLLA membranes shown in figure 1a and 1b (apical and basolateral side, respectively), produced according to the protocol described in section 2 (87/13 d/w 5'+5' immersion time and humid drying), were used as support to realize epithelial barrier. This membrane was selected because internal surface shown regular porosity to support epithelial cells culture, while external surface look like at ExtraCellular Matrix (ECM) where it is possible realize fibroblasts cells cultures. Figure 1c and 1d show membranous component of ECM and a PLLA scaffold used to cell culture of endothelial cells [7, 8].

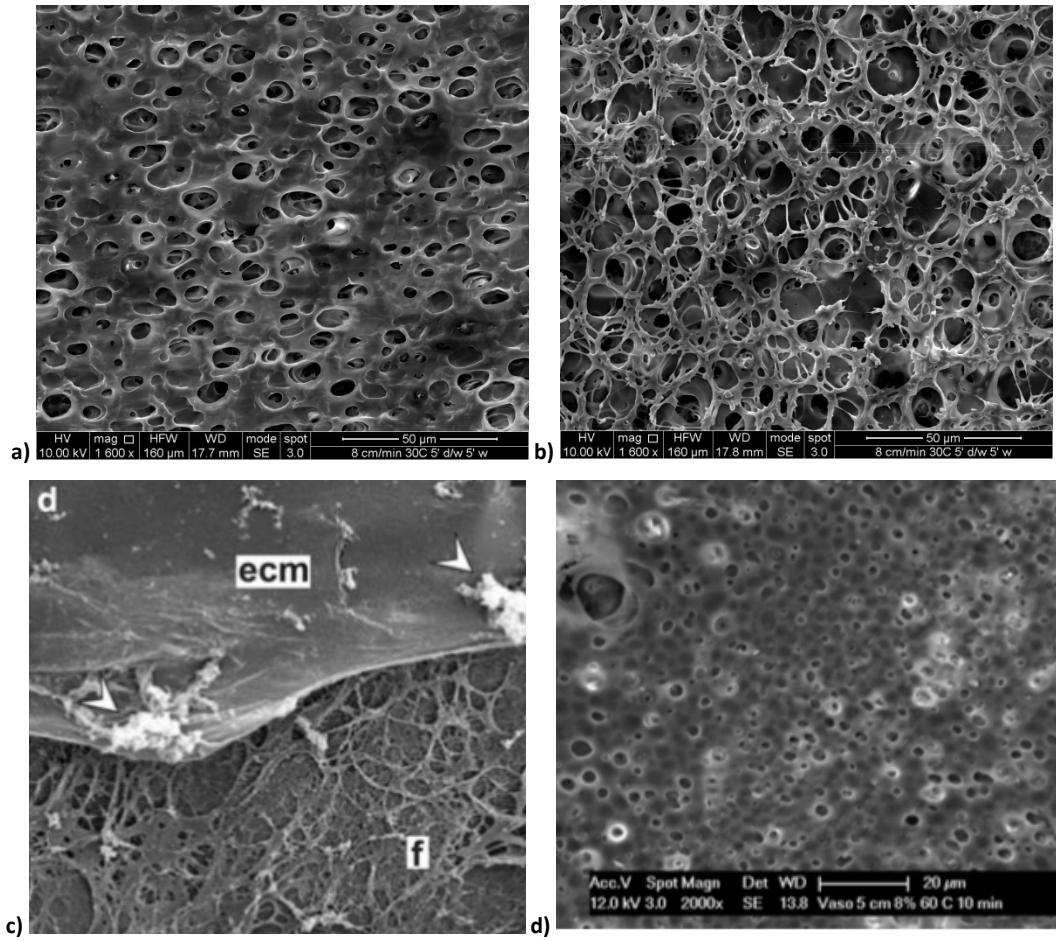

Figure 1: SEM pictures of: a) PLLA membrane apical side, b) PLLA membrane basolateral side, c) membranous component of ECM [7], d) PLLA scaffold used to cell culture of endothelial cells [8].

Cell Culture

NCl-H441 (American Type Culture Collection, HTB-174) cells were obtained from LGC Standards (Teddington, U.K.) and cultured at 37 °C in 5% CO_2 atmosphere in Gibco RPMI-1640 medium (life technologies, Paisley, UK) supplemented with 10% fetal bovine serum (FBS), 1% sodium pyruvate, 100 U/mL penicillin, and 100 µg/mL streptomycin (all from

Sigma-Aldrich, Dublin, Ireland). NCl-H441 cells (H441) were routinely cultured in 175 cm^2 growth area tissue culture flasks (Greiner BioOne, Frickenhausen, Germany) and passaged when approximately 80% confluence was reached.

Transwell culture on Polyethylene membrane

Submerged cellular cultures (SUB) were realized on Transwell Clear inserts (Polyethylene membrane (PE), 12 mm in diameter, pore size 0.4 µm; Corning, VWR, Dublin, Ireland), and apical and basolateral fluid volumes were 200 and 800 µL, respectively. After preliminary trials, the seeding density was established to be 150,000 cells/cm^2. Twenty-four hours post seeding, the medium was replaced with RPMI-1640 medium, which in addition contained dexamethasone (0, 10, 20, 30, 40, 50 and 200 nM, Sigma-Aldrich) and 1% insulin-transferrin-sodium selenite (ITS) supplement (Roche Diagnostics Limited, West Sussex, U.K.). The culture medium was exchanged every other day. NCl-H441 cells were obtained at passage number 10 and used until passage number 24 in this project.

Transwell culture on poly-L-lactic-acid membrane

The polyester membrane of Transwell Clear inserts, was removed, and they were used as support for PLLA membrane. Porous PLLA membranes were cut to a diameter close to the insert one and bonded to the support by biocompatible silicon rubber (SIMTEC silicone parts). After glue driyng, the sample holder (support and membrane) were sterilized by using ethanol 70 %v/v. Figure 2 is a schematic of the sample holder used for those experiments.

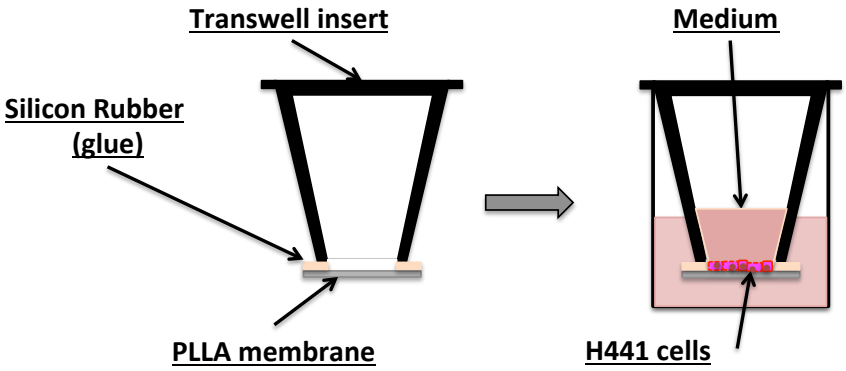

Figure 2: Schematic representation of PLLA membrane and transwell insert. H441 were cultured submerged on the top side of the PLLA membrane.

H&E staining

Haematoxylin and Eosin (H&E) were used to evaluate cell monolayer growth on PLLA membrane. H441 cells were cultured on PLLA transwells for 48h and then fixed with 4% formaldehyde before staining with Haematoxylin and Eosin stain (H&E) to asses the cell

adhesion on PLLA membrane. The samples were quickly dipped 5-6 times in the washing solution and then stained 2 minutes in Mayer's Hematoxylin solution. After, the samples were rinsed for 1 minute in the washing solution and stained 10 seconds in Eosin. Finally, the samples were washed with a series of increasing ethanol solutions (70 %, 96 %, 100 %).

Bioelectric Measurements

TEER values were measured daily with STX01 electrodes connected to a Millicell ERS-2 volt-ohm meter (Millipore, Carrigtwohill, Ireland). TEER values were corrected for the increasing background value induced by support and medium growing. Transepithelial electrical resistance (TEER) was measured daily after culturing H441 cells in the absence or presence of dexamethasone to asses the formation of a continuous electrical barrier.

Exposure to the Proinflammatory Cytokine TNF-α

Cultures were exposed to TNF-a (Sigma, 300 U/ml) on the apical surface on day 4 for further 24h. A volume of 1 ml TNF-a (300 U/ml) in 1 ml [10ng/ml] of culture medium with dexamethasone was added to the apical surface (upper Transwell, NCI H441). The corresponding opposite side of the culture was exposed to culture medium without TNF-a. After 24h the culture mediums (apical and basolateral side) were stored to be analysed by EILSA test, while the transwells were prepared to immunocytochemical staining.

Immunocytochemical staining

Transwell Clear inserts were used to grow cell monolayers for immunostaining. Cells were cultured for 5 days (SUB), after they were fixed with 4% paraformaldehyde solution for 10 min and then washed for 10 min in PBS, followed by permeabilization for 15 min with 0.1% (w/v) Triton X-100 in PBS (permeabilisation buffer). Permeabilization buffer was replaced with 1% BSA and 0.1% (w/v) Tween 20 in PBS (blocking buffer), followed by incubation for 30 min at room temperature. After blocking buffer was removed and replaced with 50 µL of a 1:100 (Occludin, Mouse Monoclonal Antibody-Alexa Fluor® 488) dilution of the relevant primary antibodies in the blocking buffer. The samples were incubated over night at 4 ºC in fridge. The specimens were again rinsed three times with permeabilization buffer and added of DAPI (1:1000 in PBS) which was used to counterstain cell nuclei. After 10 min of incubation at room temperature, the specimens were again rinsed three times with permeabilisation buffer. The samples were moved in a slide with cover slip without trapping air bibbles and dried before of the microscopic analysis. Images were obtained using a fluorescence microscope (Leica, CTR 7000, Milton Keynes, United Kingdom).

ELISA analysis

Elisa test (DuoSet ELISA, DY208-05) was performed after 5 day, on culture medium of apical and basolateral side, to evaluate the production of Human Interleukin 8 (IL8) in culture induced by TNF-a. General ELISA protocol was:

Plate preparation:

- Capture Antibody was diluted in PBS without carrier protein to the working concentration and conditioning at room temperature overnight the 96-well microplate;
- the solution was aspirated and washed with Wash Buffer;
- Block Buffer Solution (300 ml to each well) was used to block the preparation process. After, 96-well microplate were washed and used for the measurements;

Assay procedure:

- the samples (culture mediam stored in -20°C) or standard in reagent diluent (50 ml), were added to each well and incubated at room temperature for 1h;
- then they were washed with a Wash Buffer;
- Detection Antibody (100 ml to each well), diluted in reagent diluent, was added followed by incubation for 2h at room temperature;
- then they were washed with a Wash Buffer.
- working dilution of Streptavidin-HRP (100 ml) was added to each well followed by incubation for 20 minutes at room temperature
- then they were washed with a Wash Buffer.
- 100 ml of Substrate Solution was added to each well followed by incubation for 20 minutes at room temperature avoiding placing under direct light;
- Stop Solution (50 ml) was added to each well and samples were finished to the analysis.

Optical density of each well was determined using a microplate reader set to 450 nm. Optical density of each well was determined using a microplate reader set to 450 nm. The wavelength correction factor (optical density of the plate, reading at 570 nm) was subtracted to the values obtained.

H441 - MRC5 co-culture

Transwells® were coated with collagen I solution (30 µg/ml) for 30 min. at 37ºC. For contact co-cultures, inserts were inverted and seeded with 50,000 MRC5s in 50 µl fibroblast medium (figure 3). Cultures were then incubated for 2 h in a humidified atmosphere of 5% CO_2 at 37ºC to allow the MRC5s to adhere before adding H441 (150,000/well) to the apical

compartment of the Transwell®. Cultures were maintained in H441 complete medium (200 µl and 800 µl in the apical and basolateral compartments of the Transwell® respectively) in a humidified atmosphere of 5% CO_2 at 37ºC. Cultures were fed with fresh medium every day after seeding.

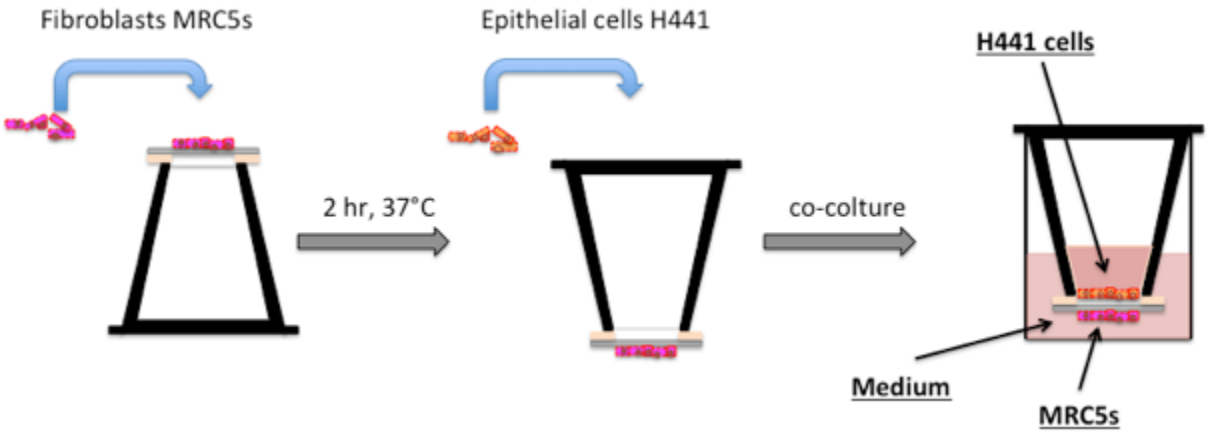

Figure 3: Schematic representation of PLLA membrane and transwell insert of co-culture H441 and MRC5s.

Immunocytochemistry of MRC5s was investigated using 1:2000 TRITC – Conjugated Phalloidin (Temecula California, MILLIPORE) dilution of the relevant primary antibodies in the blocking buffer.

Results and discussion

Evaluating of cellular monolayer on PLLA membranes

The cell growth on PLLA membrane was optimized the formation of cell monolayer was assessed by immunocytochemical and H&E staining.

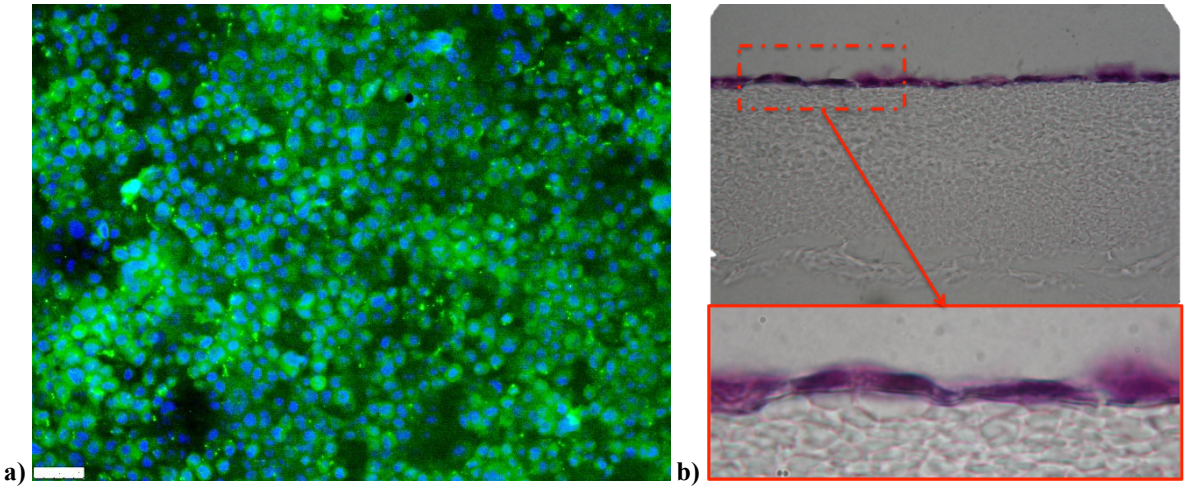

Figure 4: a) Fluorescence cell monolayer on PLLA transwell (Blue DAPI and fluorescence Green Dye-Cell tracker), b) H&E staining of an epithelial monolayer formed on a PLLA membrane after 48 h culture in a transwell culture insert.

The H441 epithelial cell were cultured on the upper surface of the PLLA membrane on transwells and after 48h they were able to form a confluent and well-organized cell monolayer (figure 4a and b).

In parallel to the previous experiment, the formation of function epithelial barrier was investigated by measuring the TEER generated by the formation of a well organized epithelial cell monolayer. TEER values of cultures in PLLA and PE membrane with and without 50 nM of dexamethasone are shown in figure 5.

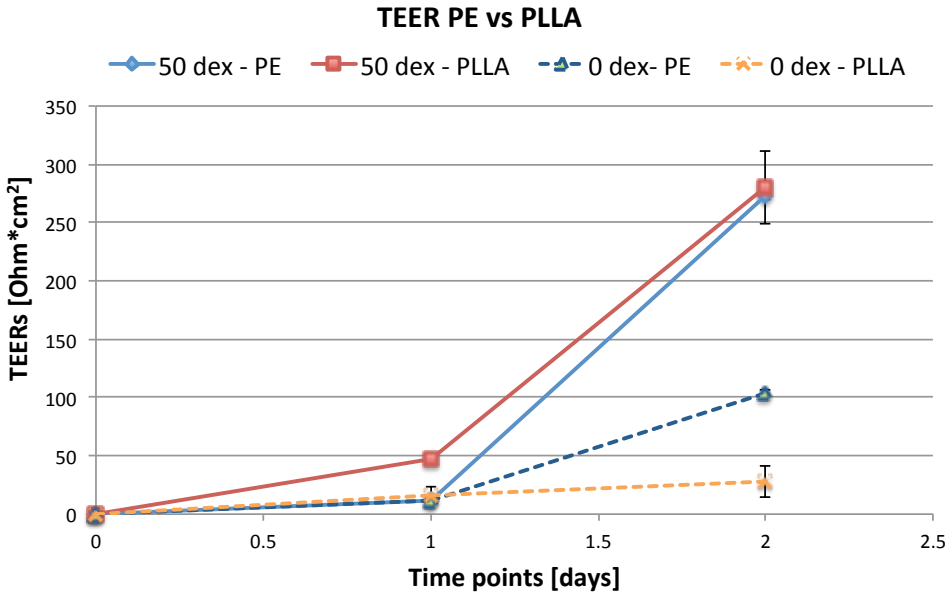

Figure 5: Time course of TEER of H441 epithelial cells cultured on poly-L-lactic-acid (PLLA) compared to Polyethylene (PE) membrane n=6.

TEER values of cultures in PLLA membrane resulted comparable to those of cultures in PE membrane confirming the need of dexamethasone for the proper formation of epithelial barrier as reported in literature [9, 10].

Effects of Dexamethasone on TEER comparing PLLA versus PE membrane

The time course evaluation of TEER in H441 transwell culture treated with different concentrations of Dexamethasone (0, 10, 20, 30, 40, 50 and 200 nM) show similar trend for PE and PLLA membrane (figure 6).

Despite dexamethasone is needed for the formation of a proper epithelial barrier, our results show a more marked difference in TEER measurements between the dexamethasone treatment at 10nM and the rest neither in PE membrane and PLLA membrane.

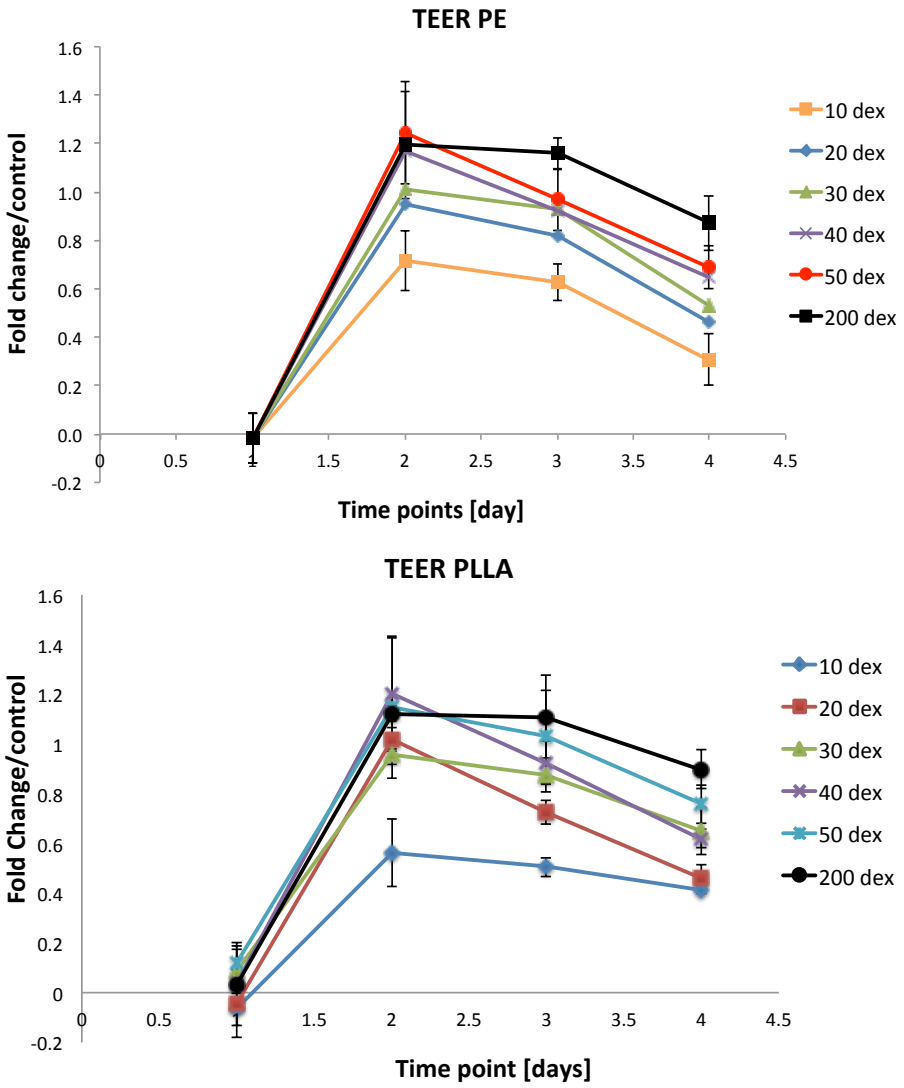

Figure 6: Time course H441 traswell culture on PE membrane and PLLA membrane. TEER values are expressed in fold change to the control (no dexamethasone), were measured in ohms*cm^2 and corrected for the background value contributed by the transwell membrane alone. Data are mean ± SD.

Formation of Tight-Junction between epithelial cells cultured on PLLA membrane

The cell-cell interaction and formation of specific cellular junction are critical for the establishment of a functional epithelial barrier. Between the different cellular junctions the tight-junctions are the molecular structure that seals the cell-cell interspace forming a functional epithelial barrier. The immunofluorescence for occludin in H441 transwell culture on PLLA shows a clear formation of tight-junction between the cells and confirm the need of dexamethasone in H441 culture for the formation of a proper epithelial barrier.

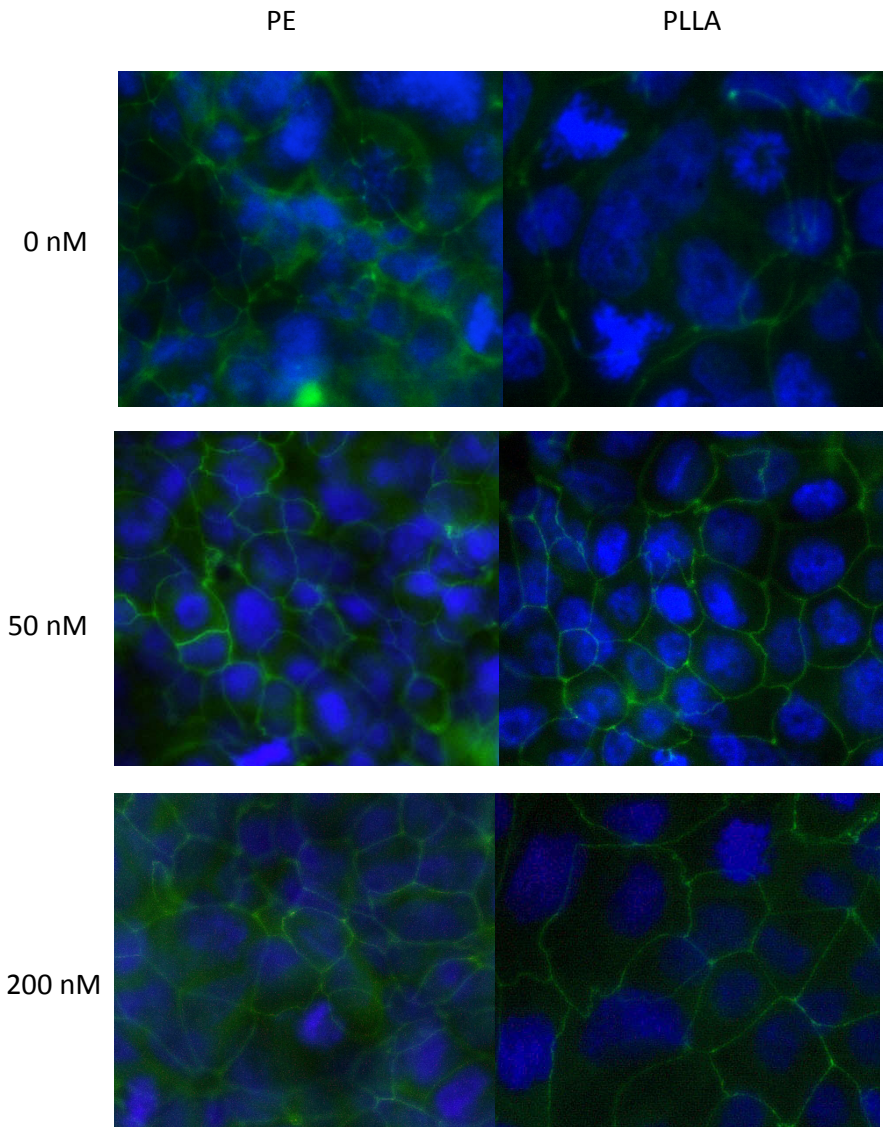

Figure 7: Immunofluorescence images showing tight junctions immunostained using an anti-occludin 488 Alexa Fluor conjugated antibody. Cells were cultured for 5 days on a PLLA membrane (RIGHT) or a PE membrane (LEFT) in transwells with and without dexamethasone treatment (50 and 200 nM).

In H441 cells cultured without dexamethasone, the occluding staining appeared poor and occasionally present at cell–cell contacts (figure 7). In accord with previous results, immunofluorescence of occluding in H441 cultured in PLLA membrane show comparable results to PE membrane.

Epithelial barrier on PLLA membrane response to the proinflammatory cytokine TNF-α

In this thesis work a functional test was applied to the epithelial barrier established on PLLA membrane by exposing our transwell cultures to the proinflammatory cytokine TNF-α in order to asses any effects on epithelial barrier permeability even in presence of Dexamethason. We exposed the apical (upper well, epithelial side) side of the culture to TNF-α (300 U/ml) and determined the effects on TEER at 24 h. This concentration was chosen

because it causes a significant detachment of adhesion molecules as reported in literature [9]. After 24h of the apical exposure of H441 transwell culture to TNF-α, there was significant effect on TEER compared to untreated control (see figure 8).

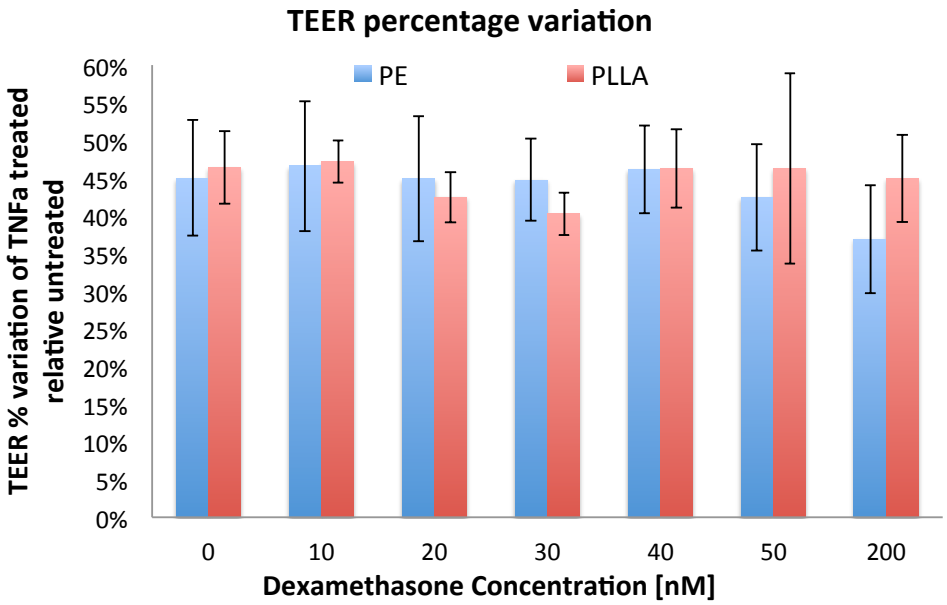

Figure 8: TEER percentage variation after 24h treatment with TNF-α.

The TNF-α treatment induced an increase in epithelial barrier permeability leading to a decreas of 42±5% in TEER values after 24h both in PLLA and PE membrane culture

Considering that TNF-α is an important and multifunctional mediator of inflammation process in different disease including asthma [11], its downstream target human Interleukin 8 (IL8) by Enzyme-Linked Immunosorbent Assay (ELISA) was decided to investigate. IL8 is produced by different cell types including epithelial cells and it is a potent chemokine and stimulator of neutrophils [12]. IL8 ELISA was performed on apical and basolateral medium of H441 transwell cuture in order to evaluate the effect of TNF-α on the release of IL8.

ELISA is a popular format of "wet-lab" type analytic biochemistry assay that uses a solid-phase enzyme immunoassay (EIA) to detect the presence of a substance, usually an antigen, in a liquid sample or wet sample.

Interleukin 8 is a chemokine produced by macrophages and other cell types such as epithelial cells, airway smooth muscle cells and endothelial cells.

TNF-α treatment in PLLA membrane produced an increase of IL-8 concentration from 1.246,6±44 mg/mL to 23.267,1±666,3 mg/mL in basolateral (bottom) side and from 1.320,1±281,7 to 23.951,1±1.130,5 in apical (top) side for 0 nM dexamethasone concentration (see figure 9a and 9b).

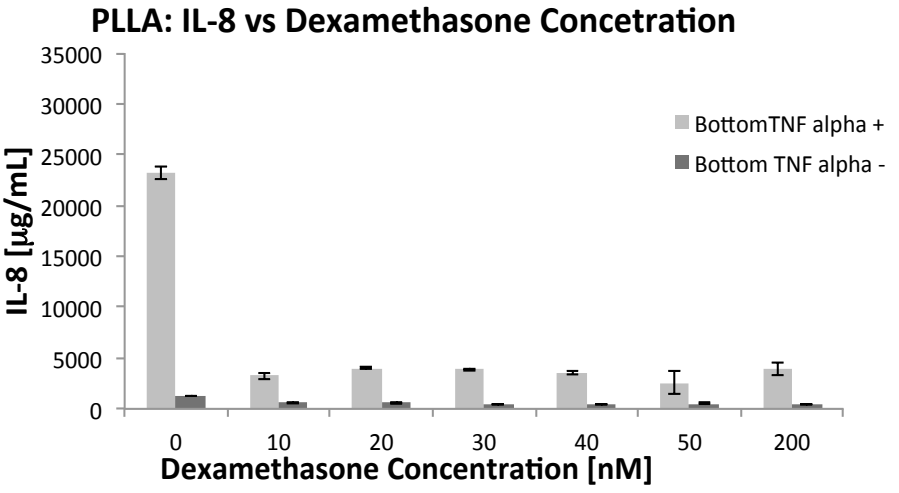
PLLA: IL-8 vs Dexamethasone Concetration
IL-8 [µg/mL]
35000
30000
25000
20000
15000
10000
5000
0
BottomTNF alpha +
Bottom TNF alpha -
0
10
20
30
40
50
200
Dexamethasone Concentration [nM]

a)

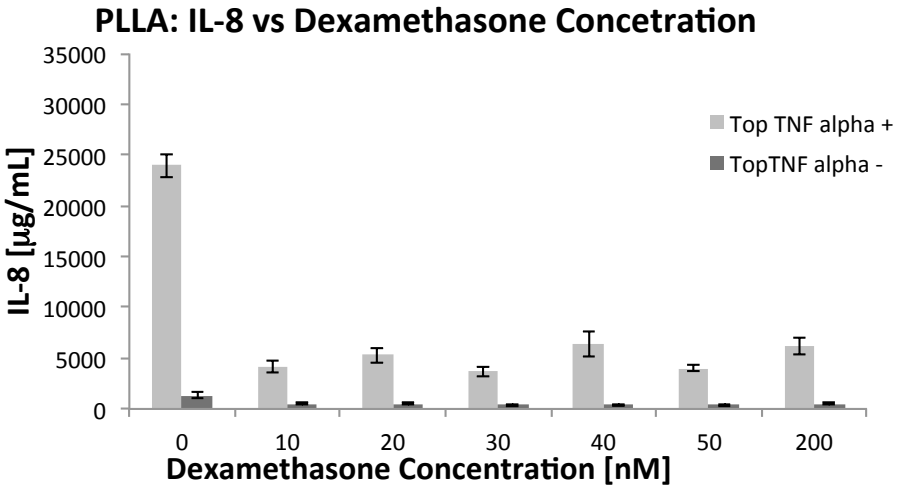
PLLA: IL-8 vs Dexamethasone Concetration
IL-8 [µg/mL]
35000
30000
25000
20000
15000
10000
5000
0
Top TNF alpha +
TopTNF alpha -
0
10
20
30
40
50
200
Dexamethasone Concentration [nM]

b)

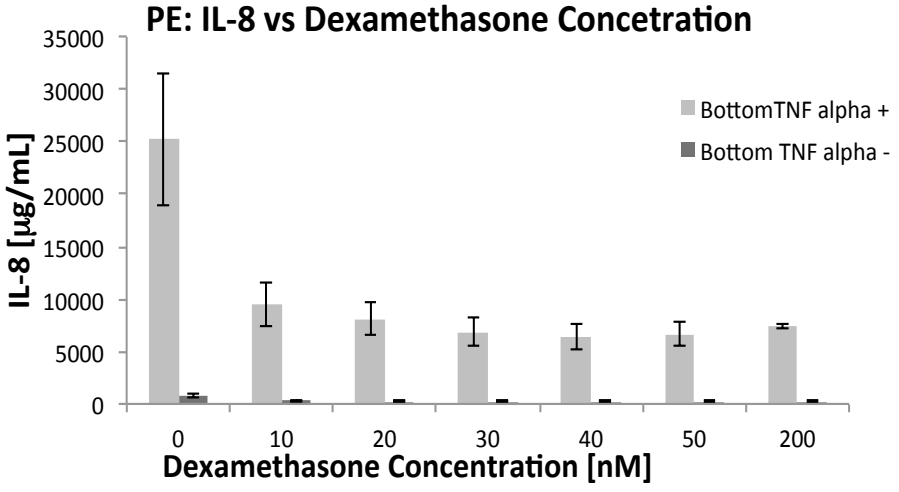
PE: IL-8 vs Dexamethasone Concetration
IL-8 [µg/mL]
35000
30000
25000
20000
15000
10000
5000
0
BottomTNF alpha +
Bottom TNF alpha -
0
10
20
30
40
50
200
Dexamethasone Concentration [nM]

c)

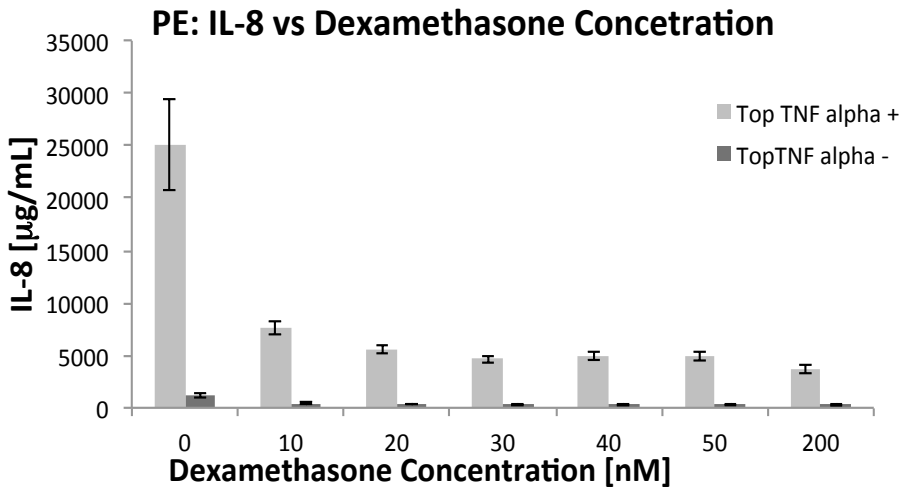

d)

Figure 9: ELISA analysis of: a) Bottom of PLLA membrane with and without TNT-α, b) Top of PLLA membrane with and without TNF-α, c) Bottom of PE membrane with and without TNF-α, d) Top of PE membrane with and without TNF-α.

In PE membrane, IL-8 concentration increased from 762,2±142 mg/mL to 25.274,4±6.332,6 mg/mL in basolateral side and from 1.123,5±281 to 25.124,9±4.362,2 in apical side for 0 nM dexamethasone concentration (see figure 9c and 9d).

IL-8 concentration in apical and basolateral side decreased in culture medium whit dexamethasone (between 10 and 200 nM) in both membranes.

In PE membrane the IL-8 concentration was higher in apical side than basolateral side without TNF-α and lower with TNF-α.

In PLLA membrane IL-8 concentration was higher in apical side than basolateral side with TNF-α and the same concentration was detected without TNF-α. Collected data are summarized in Table 1.

Table 1: Il-8 concentration on apical and basolateral side with and without TNF-a in PLLA and PE membrane.

	PE membrane							
	Bottom TNF-α -		**Bottom TNF-α +**		**Top TNF-α -**		**Top TNF-α +**	
Dex [nM]	Value	Error	Value	Error	Value	Error	Value	Error
0	762.2	142.0	25274.4	6332.6	1123.5	183.4	25124.9	4362.2
10	266.6	61.3	9449.4	2041.1	404.6	84.6	7583.4	669.7
20	240.5	52.8	8072.7	1582.8	327.6	65.9	5632.4	434.6
30	238.0	53.3	6870.6	1338.1	274.1	52.2	4652.8	362.8
40	217.8	49.3	6450.0	1247.4	262.1	52.1	4957.8	395.5
50	215.9	48.6	6643.6	1157.0	282.4	51.5	4915.2	429.0
200	221.0	77.2	7336.3	227.0	256.3	76.3	3664.9	366.7
	PLLA membrane							
	Bottom TNF-α -		**Bottom TNF-α +**		**Top TNF-α -**		**Top TNF-α +**	
	Value	Error	Value	Error	Value	Error	Value	Error
0	1246.6	44.0	23267.1	666.3	1320.1	281.8	23951.1	1130.5
10	576.0	35.6	3220.7	295.1	476.1	121.3	4154.2	559.4
20	562.9	56.7	3958.2	117.0	516.5	101.6	5272.9	778.9
30	460.9	48.9	3879.6	114.8	381.0	112.3	3708.3	496.2
40	409.8	33.1	3541.1	149.6	377.0	72.3	6311.9	1238.1
50	534.2	54.3	2505.0	1129.7	381.4	106.0	3990.9	273.7
200	357.7	10.8	3909.0	628.9	502.5	91.9	6143.0	811.8

This effect was attributed at the permeability different between PLLA and PE membrane.

H441 - MRC5 co-culture

The last step of this study was the setup of H441-MRC5s co-culture on PLLA membrane. Co-culture systems are critical to study the interactions between different cell types and are of particular interest for bioengineering in order to study complex multicellular systems. This experimental model has the potential to create a better biomimetic environments for the development of artificial tissues and therefore representing an human in vivo-like tissue model closer to animal models. Considering the cytocompatibility of PLLA membrane obtained with our system and the possibility to change surface morphology, the realization of co-culture on PLLA membrane could be a good support for the formation of a proper extracellular matrix (ECM) that helps to improve the formation of the tissue microenviroment. Co-culture didn't produce increase in TEERs value compared to monoculture and PLLA and PE membrane TEER resulted comparable (see figure 9).

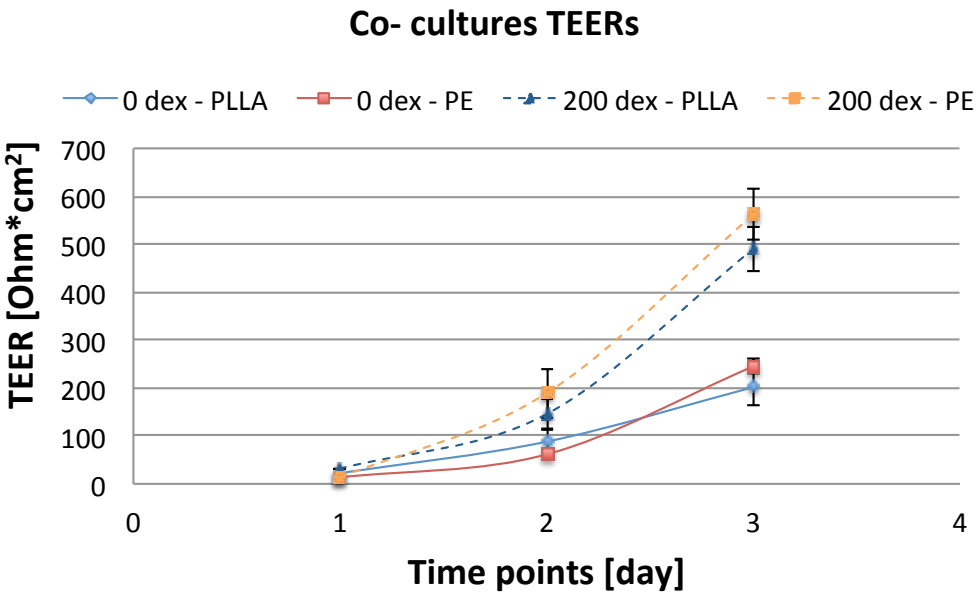

Figure 10: Co-culture TEER values were measured in ohm*cm^2 and corrected for the background value contributed by the transwell membrane alone. Data are mean ± SD.

Immunocytochemica staining was realized on H441-MRC5s co-culture with dexamethasone 200nM. The junctional occluding staining appeared easy detectable as in monoculture (see figure 11).

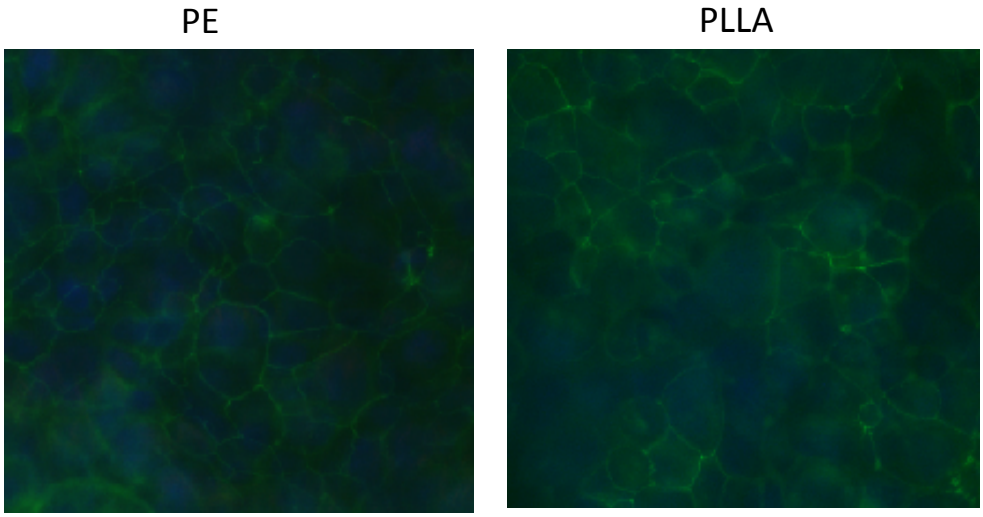

Figure 11: Immunofluorescence images showing tight junctions immunostained using an anti-occludin 488 Alexa Fluor conjugated antibody. Cells were cultured for 4 days on a PLLA membrane (RIGHT) or a PE membrane (LEFT) in transwells with dexamethasone treatment (200 nM).

Immunocytochemistry of MRC5s on PLLA membranes was investigated (using 1:2000 TRITC – Conjugated Phalloidin dilution of the relevant primary antibodies in the blocking buffer) to investigate the morphology of the basolateral side monolayer.

In figure 11 is shown MRC5s monolayer where nuclei and filamentous actin were stained in blue and red respectively. After 4 day, the stained basolateral side show an homogeneous MRC5s monolayer with good morphology.

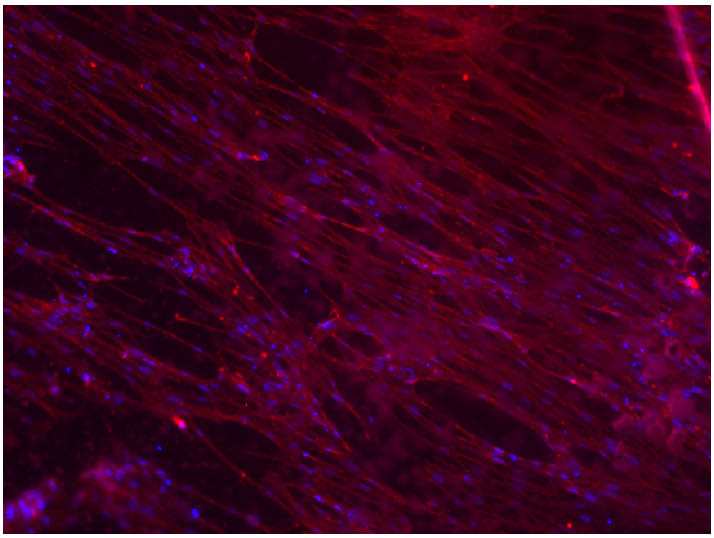

Figure 12: Immunofluorescence images showing filamentous actin immunostained using an 1:2000 TRITC – Conjugated Phalloidin (Temecula California, MILLIPORE) dilution of the relevant primary antibodies in the blocking buffer. Cells were co-cultured for 4 days on a PLLA membrane in transwells with dexamethasone treatment (200 nM).

Conclusion

Our results show that a functional epithelial barrier can be reproduced on such porous biodegradable PLLA membrane. This fact may be useful in tissue engineering applications requiring bio-absorbable membranes in lung tissue or organ regeneration. Moreover, as PLLA membranes can be produced with different morphologies and mechanical properties, there are manyfold potential possibility for the development of 3D scaffolds to improve and control tissue regeneration.

The results obtained provide new insights into the application of PLLA membranes. This might address new applications in tissue regeneration of bioabsorbable membranes. Further investigations, still in progress, are aimed to evaluating and modelling the fabrication process of the membranes and to use PLLA membrane as scaffold for organs regeneration.

References

[1] E. Donna Davies, Epithelial Barrier Function and Immunity in Asthma, Ann Am Thorac Soc Vol 11, Supplement 5 (2014) pp S244–S251.

[2] M. Amanda Marchiando, W. Vallen Graham and R. Jerrold Turner, Epithelial Barriers in Homeostasis and Disease, Annu. Rev. Pathol. Mech. Dis. (2010) 5:119–44.

[3] Y. Cao, J.P. Vacan, K.T. Paige, Transplantationon of chondrocytes utilizing a polymerKcell construct to produce tissueKengineered cartilage in the shape of a human ear. Plastic Reconstruct Surg (1997) 100:297.

[4] M. Zuwei, G. Changyou, G. Yihong, J. Jian, S. Jiacong, Immobilization of Natural Macromolecules on PolyKLKLactic Acid Membrane Surface in Order to Improve Its Cytocompatibility, J Biomed Mater Res (Appl Biomater) (2002) 63:838–847.

[5] S. Montesanto, G. Mannella, F. Carfì Pavia, V. La Carrubba, V. Brucato, Coagulation bath composition and desiccation environment as tuning parameters to prepare skinless membranes via diffusion induced phase separation, Journal of applied polymer science (2015) 132, 42151.

[6] J.J. Salomon, V.E. Muchitsch, J.C. Gausterer, E. Schwagerus, H. Huwer, N. Daum, C. Lehr and C. Ehrhardt, The Cell Line NClKH441 Is a Useful in Vitro Model for Transport Studies of Human Distal Lung Epithelial Barrier, Mol. Pharmaceutics (2014) 11, 995−1006.

[7] M. Popielarska-Konieczna, M. Kozieradzka-Kiszkurno, J.S.́wierczyńska, G. Góralski, H. Ślesak, J. Bohdanowicz, Ultrastructure and histochemical analysis of extracellular matrix surface network in kiwifruit endosperm-derived callus culture, Plant Cell Rep, DOI 10.1007/s00299-008-0534-9.

[8] V. La Carrubba, F. Carfì Pavia, V. Brucato, S. Piccarolo, G. Ghersi, PLLA biodegradable scaffolds for angiogenesis via Diffusion Induced Phase Separation (DIPS), Int J Mater Form (2008) Suppl 1:623–626.

[9] M.I. Hermanns, R.E. Unger, K. Kehe, K. Peters, C.J. Kirkpatrick, Lung epithelial cell lines in coculture with human pulmonary microvascular endothelial cells: development of an alveolo-capillary barrier in vitro, Laboratory Investigation (2004) 84, 736–752.

[10] M.I. Hermanns, S. Fuchs, M. Bock, K. Wenzel, E. Mayer, K. Kehe, F. Bittinger, C.J. Kirkpatrick, Primary human coculture model of alveolo-capillary unit to study mechanisms of injury to peripheral lung, Cell Tissue Res (2009) 336:91–105.

[11] K. Suresh Babu, E. Donna Davies, T. Stephen Holgate, Role of tumor necrosis factor alpha in asthma, Immunology and allergy clinics of north America (2004) Volume 24, Issue 4, Pages 583–597.

[12] Y. Osawa, M. Nagaki, Y. Banno, Tumor Necrosis Factor Alpha-Induced Interleukin-8 Production via NF- κ B and Phosphatidylinositol 3-Kinase/Akt Pathways Inhibits Cell Apoptosis in Human Hepatocytes , Infection and Immunity (2002) 70(11):6294-6301. doi:10.1128/IAI.70.11.6294-6301.2002.

Chapter 5

Basic architecture of microfluidic chip to culture human alveolar epithelial cells

Microfluidics provides the opportunity to effectively study cells on both a single- and multi-cellular level with high-resolution and localized application of experimental environment with biomimetic physiological conditions [1]. Microscale cell cultures are promising supports for high-throughput experimentation in many fields, such as drug screening tests and complex biological studies [2]. Furthermore culturing cells at microscale allows more precise control of the extracellular microenvironment [3]. Microfluidics has the potential for revolutionize the way to approach cell biology research and one of the key benefits of microfluidic for basic biology is the ability to control parameters of the cell microenvironment at relevant length and time scales [4,5].

Microfluidic cell culture platforms combine the advantages of miniaturization and real time microscopic observation with the ability to pattern cell culture substrates [6], to vary the composition of culture medium over space using gradient generators [7] and to create cell culture conditions that are more close to physiological one than those found in other in vitro systems, in terms of nutrients exchange rates and of mechanical stimulation [8]. Microfluidic cell systems are applied to many different situations, from 2D and 3D cell culture systems [9]. These systems differ on how cells are seeded: as monolayer on a substrate surface (2D systems), or on 3D scaffolds (3D systems). 3D cell-culture models have recently garnered great attention because they often promote levels of cell differentiation and tissue organization not possible in conventional 2D culture [10]. A number of 3D microfluidic perfusion culture systems have been developed recently for application in complex biological processes such as in vitro organ development [11]. For tissue types that are highly perfused in vivo, such as the liver and kidney, microfluidic perfusion culture may mimic more accurately the in vivo microenvironment, where cells are in close proximity with the microvascular network [12, 13]. Automated cell culture screening systems based on a microfluidic chip are recently built including valves, mixers and pumps, capable of controlling fluid [14].

As regards ex vivo tissue, in the past the common method to incubate ex vivo biopsies was to place them in medium filled well plates [12]. However, in this in vitro system the medium

was usually refreshed every 24 hours resulting in decreasing concentration of nutrient and accumulation of metabolites and waste products. To prevent this behaviour, some systems used a different approach, consisting of a perfused bioreactor in which the biopsy is closely maintained in a perfused chamber [13]. In this work of thesis, a microfluidics device was designed and tested as platform to use for human bronchial and colorectal mucosa regeneration. Soft lithography technique was used to build silica mold and an electrical characterization technique was developed to monitor the tissue growth.

Experiment and Discussion

Soft Lithography Technique

Soft lithography technique was used to produce polydimethylsiloxane (PDMS) slabs from silicon masters. SU8-2100 negative photoresist was spin coated (about 5 mL) at 500 rpm for 10 s and then 1500 rpm for 30 s. Therefore a transparency layer was placed over the wafer. The coated wafers were then soft-baked for 5 min at 65°C followed from 40 min at 95°C, before exposing the photoresist through an UV light (OAI). Used exposing time was 15 seconds. Then, the substrates were baked post exposure for 5 min at 65°C followed from 10 min at 95°C. Subsequently, the mold was developed for 15 min with methoxy-methacrylate.

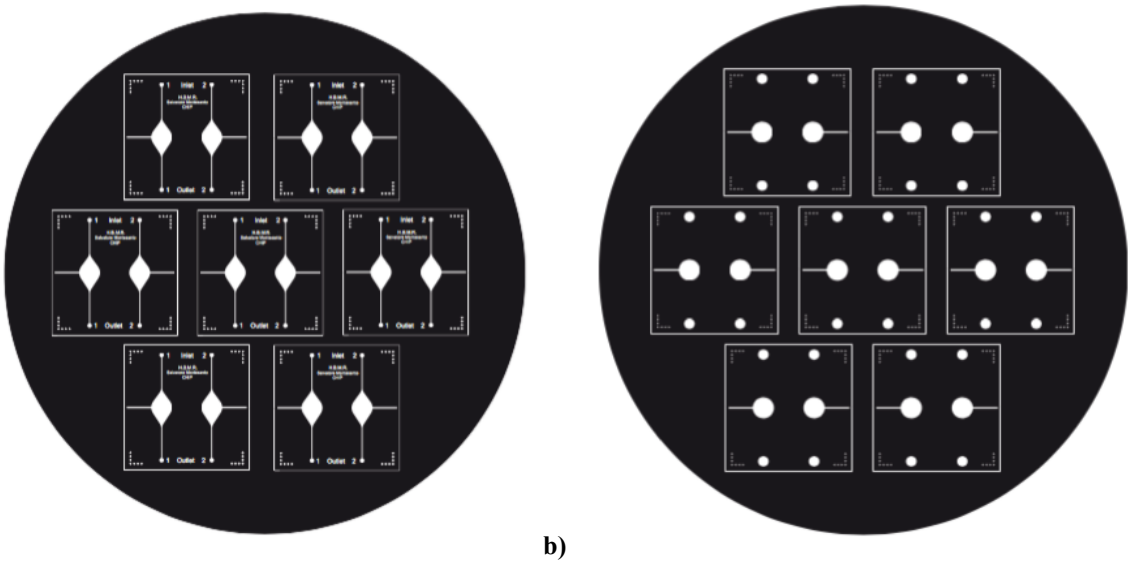

a) **b)**

Figure 46: Chip masks: a) down slide, b) top slide.

Finally, a Hard bake was made at 160°C for 2 hours. The protocol was preformed for a 200 μm thick slab. Bottom and top template (pattern in SU-2100 photoresist on Si wafer) surface was exposed to trimethylchorosilane vapour for more than 20 min in a desiccator room temperature to prevent unwanted bonding. PDMS slabs was prepared by mixing Sylgard 184

(Ellsworth Adhesives) bulk polymer with curing agent in a 10:1 ratio, which was degassed and cured at 70°C for 4 hours. To define the area where the light is free to illuminate the photoresist and where is stopped by absorption or reflection, a mask is employed. Lithographic mask is placed between the substrate and the UV source, made of UV-transparent and absorbing regions. All the masks employed in this work were designed by CAD software, which were processed with Adobe illustrator software before and after printed by high-resolution laser printer (see figure 46). All Soft lithography technique step are showed in figure 47.

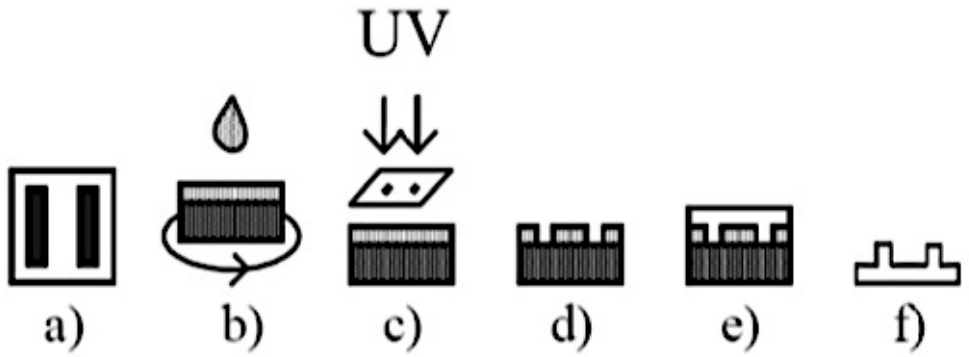

Figure 47: Soft lithography technique step: (a) Mask design; (b) Deposition of photoresist on Si wafer by spin-coater; c) UV-exposing; (d) Develop of the master; (e) PDMS deposition on master; (f) Final PDMS layer.

Microfluidics Device

The construction of the microfluidic device involves two PDMS slabs as shown in Figure 48. The bottom and top PDMS layer of the microdevice have channels whose dimensions are 200 μm wide by 200 μm tall, which were prepared using standard soft lithographic techniques as described above. At one end of each channel, inlets and outlets were punched, and in the centre of each channel, a 4 mm hole was punched to act as a well. The bottom and top slab were performed to realizing two culture chamber. The top and bottom PDMS layer have an electrode abode another to contain two hole wells. Porous membranes were cut to dimensions roughly larger than the culture wells and sandwiched between the two layers of PDMS constructed as detailed in figure 49. Then, the wells punched in the centre of each channel, and one inlet and outlet channel were aligned, where liquid PDMS (1:5 ratio of curing agent to prepolymer mix) was used to seal the layers together.

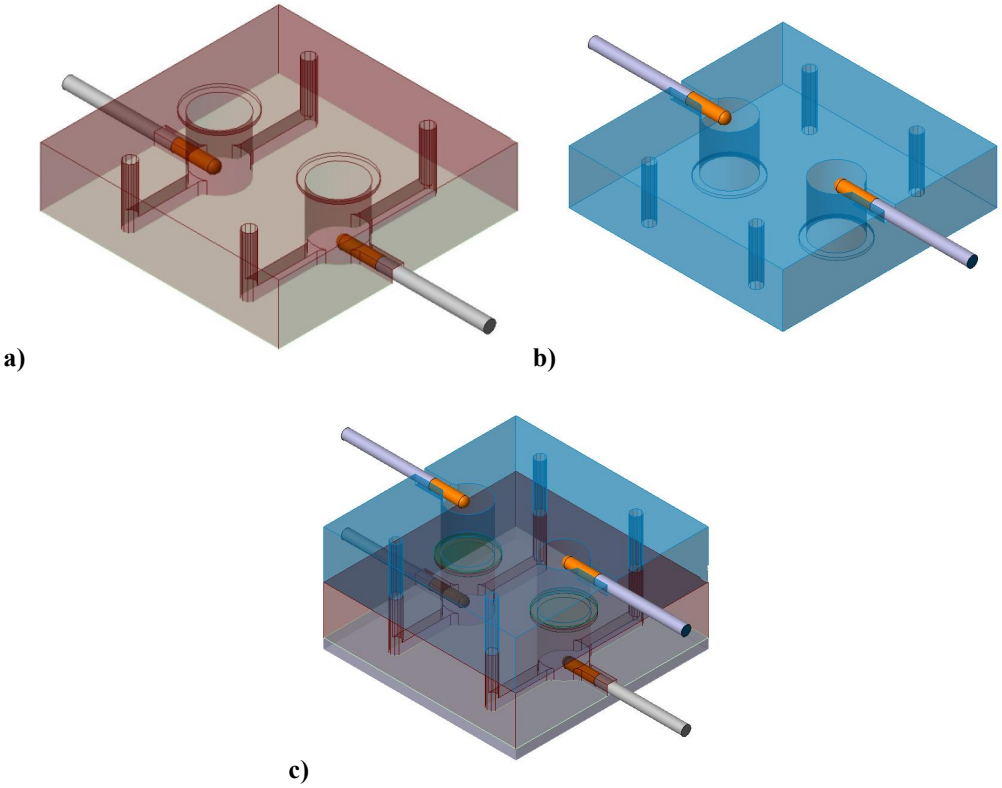

Figure 48: Picture of CAD microfluidic chip: a) bottom layer, b) top layer and c) microfluidic chip.

A slow and soft cure at 40°C for 4 h was performed to seal the sandwiched layers. Porous PET and PLLA membranes with 0.4µm and 10µm size pores, described above, were used in this work. The lower bottom layer surface was then O_2 plasma-sealed to a glass slide by exposure to O_2 plasma for 2 min at room temperature, and heated in an hotplate at 40°C for an hour.

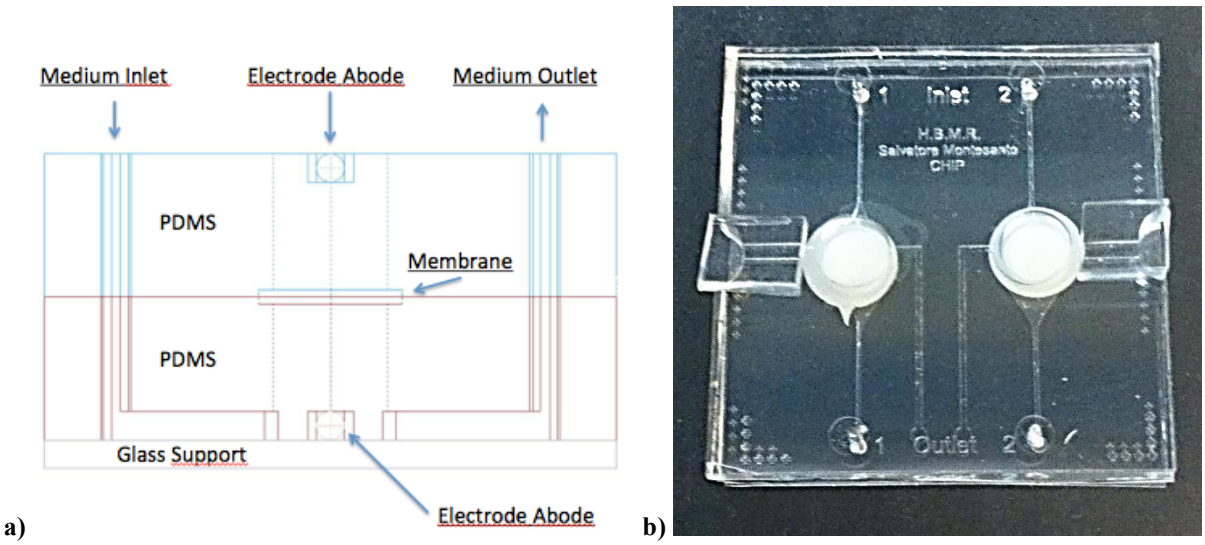

Figure 49: Pictures of: a) microfluidic device perspective, b) microfluidic chip.

Ag or Pt recording electrodes with a diameter of 200 and 250 µm, respectively after described, were fit into the electrodes abode 300 µm × 200 µm side channel, which were held by elastomeric tension. The recording electrodes were put in biochip equidistant than porous membrane. Liquid PDMS with 1:5 ratio of curing agent to prepolymer mix, was used to seal the electrodes at the chip.

TEER (Trans-Epithelial Electrical Resistance) Characterization

A characteristic feature of epithelial cell layers is the formation of intercellular junctions resulting in a tight cellular barrier separating the apical (luminal) from the basolateral (abluminal) side. These cell layers form selectively permeable interfaces between compartments of different chemical composition, thus controlling diffusion along the paracellular way as well as transport processes through intracellular pathways (figure 50). This is guaranteed by the so-called tight junctions (intercellular connections) that seal the intercellular cleft [15]. An intact barrier is crucial for the physiological activities of the corresponding tissue. However, the barrier is not static but can be modulated by specific stimuli to open and close it selectively, thus allowing controlled passage from the apical (luminal) from the basolateral (abluminal) side or vice versa.

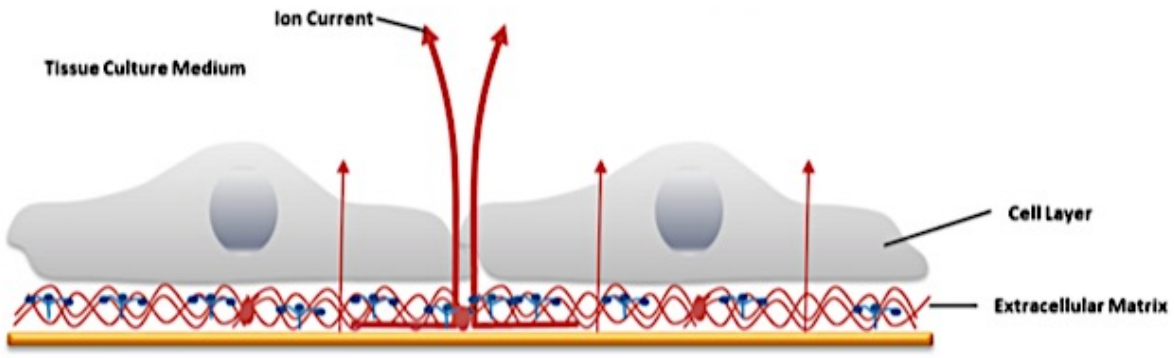

Figure 50: Picture of epithelial cell layers in the electrical characterization.

A straightforward method, which establish to growth of functional tight junctions and thus the differentiation status of polarised epithelia, is the measurement of the Trans-Epithelial Electrical Resistance (TEER). In this thesis two different TEER measurements methods were elaborated to monitor the tissue growth: Electrochemical Impedance Spectroscopy and electrical measurements. However, cyclic voltammetry was elaborated to choose the recording electrodes.

Cyclic voltammetry electrode characterization

Cyclic voltammetry is a commonly used method of measuring the reduction potential of a species in solution. Cyclic voltammetry provides additional data that can be interpreted to make conclusions about the reduction / oxidation reaction and the stability of the species resulting from the electron transfer. In cyclic voltammetry, where an electric potential is applied at the working electrode at a specific sweep rate (in volts / second), while the current through the circuit is recorded. When the voltage reaches a point at which a reduction/oxidation is induced, current begins to flow. A cyclic voltammogram is a plot of current versus applied voltage [16]. In this thesis, cyclic voltammetry was chosen to evaluate the wires system for use as electrodes to measure of EIC and current. In these experiments two wires systems were evaluated: Platinum/Iridium (Pt) and Silver (Ag) wires (Advent Research, UK, diameter of 0.25 mm). A medium (DMEM High Glucose with L-Glutamine without Sodium Pyruvate [Euroclone – ECM0102L] added of Fetal Bovine Serum 10%) and PBS 1X was used as electrolyte for the cyclic voltammetry experiments.

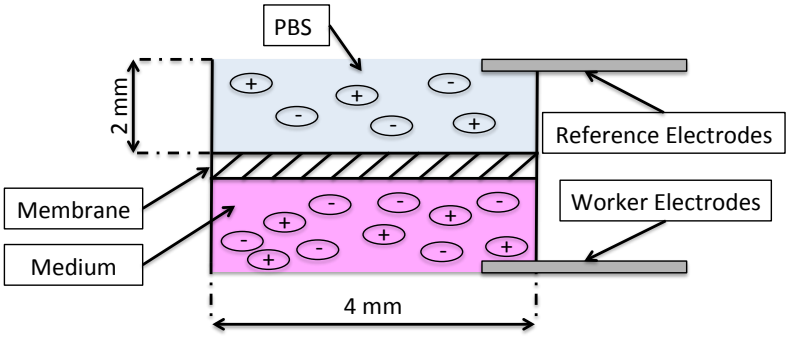

Figure 51: Picture of measurement system scheme.

The electrode put in direct contact with the medium in the lower chamber was chosen as the work electrode while the electrode in direct contact with PBS was chosen as reference electrode (see figure 51 and 52).

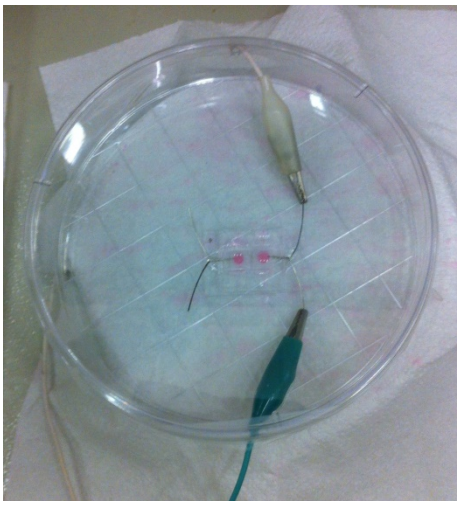

Figure 52: Pictures of microfluidic device.

To eliminate inter-electrode potential difference, a preconditioning time of 30 minute was awaited before measurements, The cyclic voltammetry experiments were performed in two electric potential range: -1 ÷ +1 V and -0.3 ÷ +1 V, at a specific sweep rate of 50 mV/s, for Pt and Ag wires system respectively. The results of such experiments are shown in figure 53.

a)

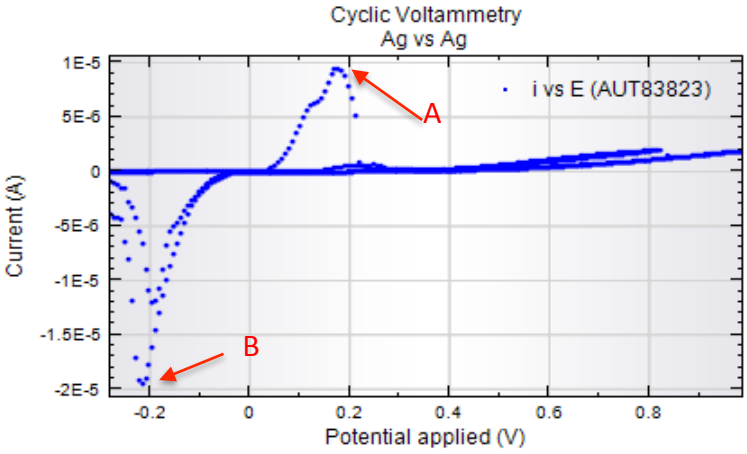

b)

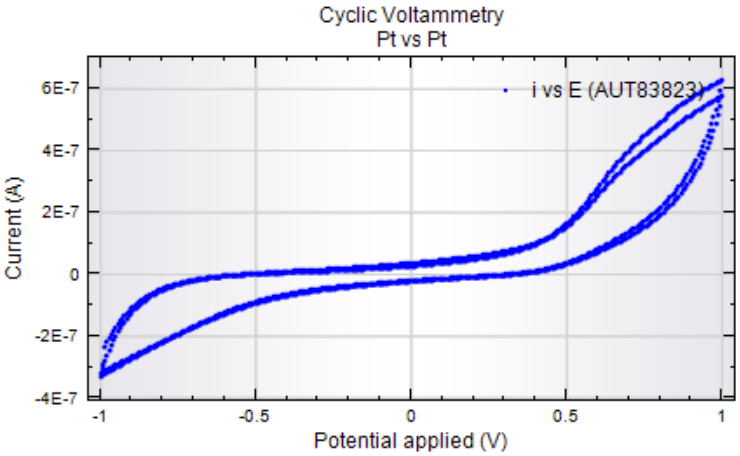

Figure 53: Cyclic voltammetry: a) Ag vs Ag, b) Pt vs Pt.

The Ag wires system presented a Faradic current flow as the voltage reaches the range between -0.3 ÷ -0.1 V and 0.1 ÷ 0.3 V, respectively (figure 25.a). A and B point in cyclic voltammetry are called "anodic and cathodes peak potential" respectively, where redox reaction take part on the Ag wire surface as follows [17]:

$$Ag^0 \rightleftharpoons Ag^+ + e^-$$

The Pt wires system, which doesn't show an increase of current flow in the cyclic voltammetry, result more much stable than Ag wire between -1 and 1 V (figure 25.b). Pt wires system lend themselves as possible candidate for EIS and electrical measurement.

Electrochemical Impedance Spectroscopy

Electrochemical Impedance Spectroscopy (EIS) is a powerful technique for understanding electrochemical systems. Briefly, this technique involves a determination of cell impedance, in response to a small (-5 mV amplitude) AC signal at any constant DC potential, over a span of frequencies ranging typically from 10^5 kHZ to10^{-3} Hz (hence the term impedance spectroscopy). From the measured cell impedance in the form of real and imaginary components and phase angle, it is possible to examine and qualitatively determine several processes such as the electronic/ionic conduction in the electrode and electrolytes, interfacial charging either at the surface films or the double-layer, charge transfer processes and the mass transfer effects, if any. The time constants for these different processes being different, their features will show up at different frequencies in the EIS spectra. The advantage of this technique is rapid and easy measurement method as presently possible with the advent of computer-controlled equipment such as potentiostats and frequency response analysers and appropriate software, which enormously simplify the data collection as well as subsequent analyses. The limit of this technique, on the other hand, is mainly related to the difficulty in interpreting the data. In this work, EIS technique was used to determined electrical equivalent circuit to represent of the microfluidic system described above and quantitatively define the relevant electrical parameters that would help the understanding of the response of system. However, this technique wasn't used to determine TEER value because the frequency from 10 Hz to 1000 Hz are harmful for biological system. Impedance spectra were taken using an Autolab potentiostat/galvanostat (EcoChemie). Alternating current of amplitude 0.2 V in OCP was passed between the two embedded Pt electrodes in the frequency range from 100 Hz to 10^6 Hz, yielding a total of 60 impedance measurements (10 per decade spaced logarithmically).

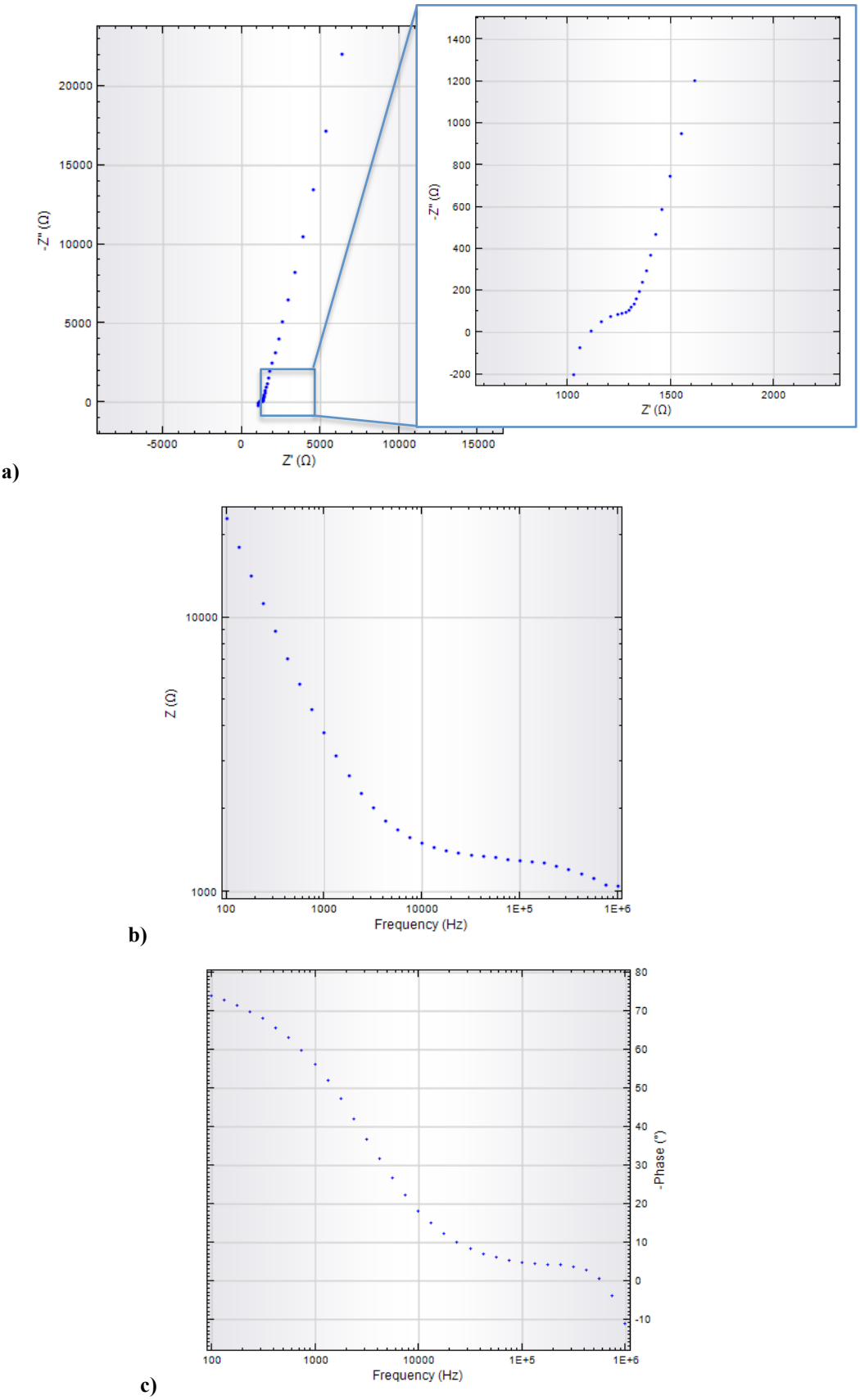

Figure 54: EIS plot of the microfluidic platform, with Pt recording electrodes and integrated PET membrane: a) Nyquist graphic, b) Bode Modulus graphic c) Bode Phase graphic.

The total time for a single frequency scan was approximately 5 min. In the EIS experiment

was used the same system and conditions of cyclic voltammetry.

A typical EIS plot of the microfluidic platform with integrated PET membrane is shown in figure 54.

An equivalent lumped element circuit model (as shown in Figure 55) was used to fit the microfluidic system electrical behaviour. The circuit is constituted by four components, where R_E, R_M, C_M and CPE (Constant Phase Element) represent electrolyte and membrane resistance, membrane capacitance and double layer capacitance of the electrodes, respectively [18, 19]. In this model, CPE is in series with the resistance of the medium (R_E) and the porous membrane system, which is denoted as a membrane resistance (R_M) and a membrane capacitance (C_M) in parallel.

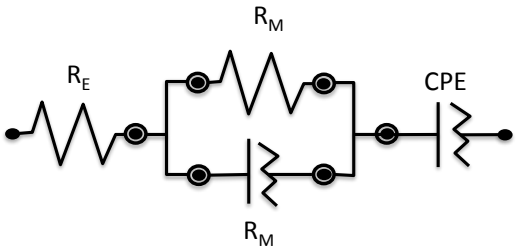

Figure 55: Equivalent lumped element circuit model.

In order, to resolve the value of each component Nova software was used. In the data fitting, the objective was minimizing the absolute difference between the simulated and experimental impedance values under various frequencies. In the figure 56 is showed the data fitting of EIS analysis showed above.

However, while the fitting of the low frequency range (150-300 Hz) and high frequency range (10^5 Hz) provide CPE and R_E value, respectively, the fitting of media frequency range (10^3 – 10^4 Hz) provide R_M and C_M value. For this reason many authors, on the other hand, prefer the fitting of some of the above mentioned frequency range than all frequency spectra [19, 20].

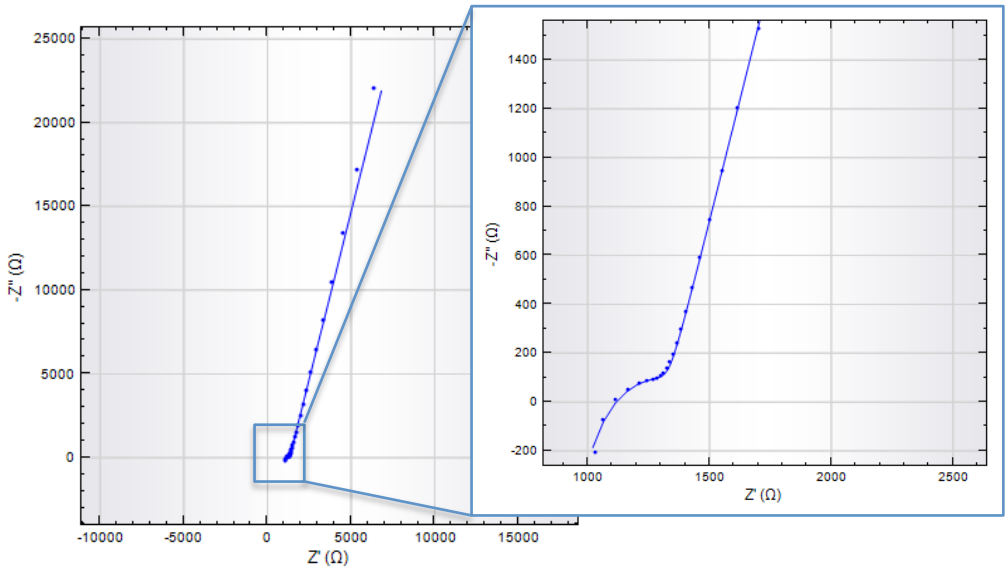

a)

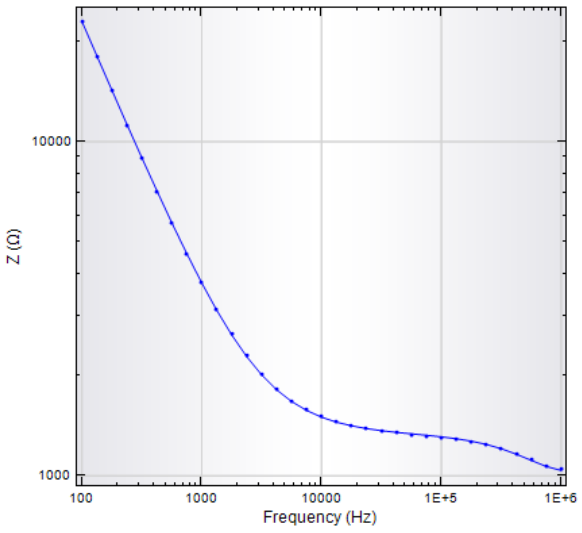

b)

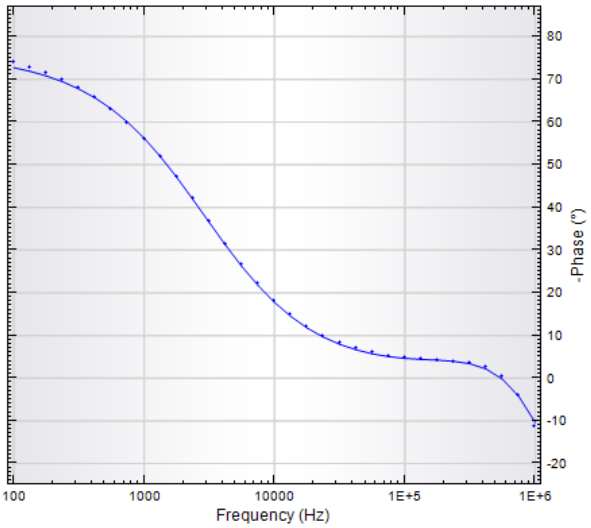

c)

Figure 56: EIS data fitting plot of the microfluidic platform, with Ag recording electrodes and integrated PET membrane: a) Nyquist graphic, b) Bode Modulus graphic c) Bode Phase graphic.

The advantage of this strategy is a rapid and easy fitting method and lower fitting error; the limit of this method, on the other hand, is mainly related to the exclusion of several frequency ranges, which can provide several information. In this work, an overall frequency fitting was achieved. The following table are reports the fitting value of the model components.

Table 4: Fitting value of the model components with PET membrane.

	RM [ohm]	RE [ohm]	CM [F]	CPE	
				Y0 [Ω-1 *sN]	N
Average	$5.34*10^{2}$	$1.33*10^{3}$	$7.28*10^{-10}$	$1.09*10^{-7}$	0.868
Dev. Standard	$3.41*10^{2}$	$5.69*10^{2}$	$3.01*10^{-10}$	$6.62*10^{-8}$	$2.29*10^{-2}$
Error [%]	4.5	1.8	10.8	1.9	0.3
Dev. Standard	0.51	0.10	1.14	0.47	0.065

First, relatively large variability in impedance between different chips was found, due to variance in the distance between the two electrodes than membrane position. Another variability in impedance was due to variance in exposed electrodes surface caused by the positioning of the electrodes into the upper and lower channel. Finally, variability in impedance was due to variance in membrane area caused by alignment variation in the upper and lower chamber [18, 19, 20].

However R_E and CPE, which were affected by alignment and exposed electrode surface variation, presented a error percentage lower then R_M and C_M components which were affected also by the membrane area variation (table 4). Variability between different measurements within a single chip (where the electrodes remain fixed), however, was minimal (see figure 57).

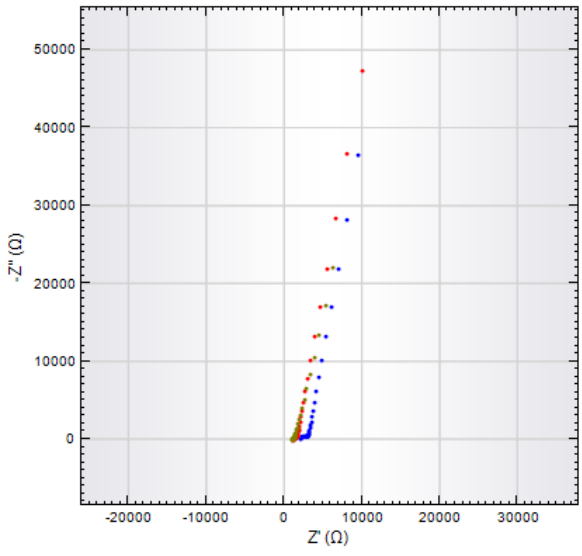

a)

b)

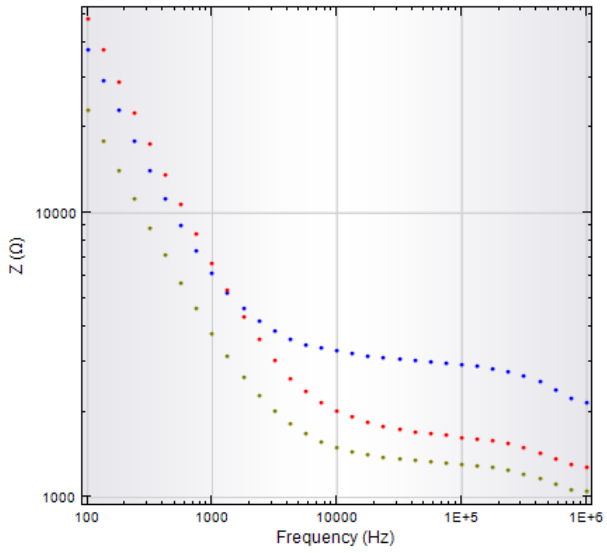

c)

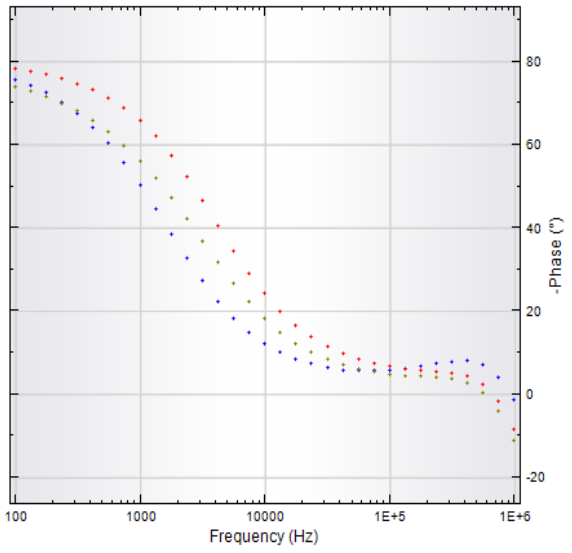

Figure 1: Variability between different measurements within a single chip: a) Nyquist graphic, b) Bode Modulus graphic c) Bode Phase graphic.

EIS experiment were made also for Ag wires system. In these measurement PLLA and PET membrane were integrated into the microfluidic device and investigated. It wasn't possible determine an equivalent lumped element circuit model for PET membrane. The reason is a membrane resistance lower than charge diffusion phenomena on electrode surface, which dominate (see figure 58).

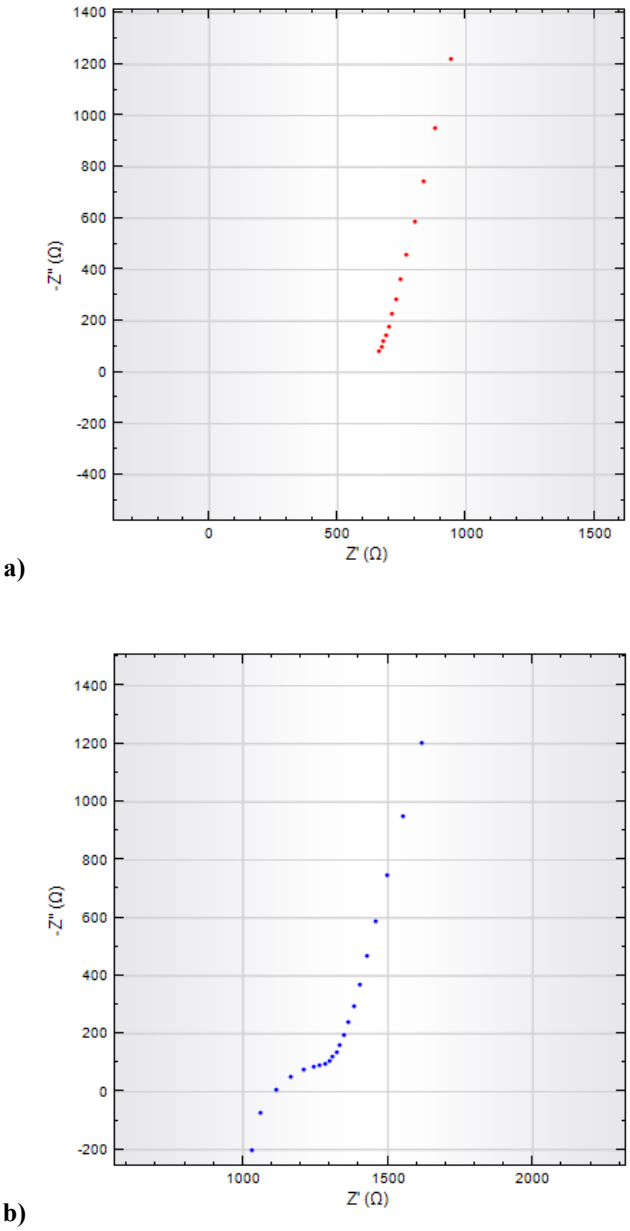

Figure 58: Nyquist graphic with PET membrane: a) Ag wires system, b) Pt wires system.

In the Nyquist graphic (see figure 58) it is possible to see as charge diffusion phenomena starts at higher frequencies in Ag wires system than in Pt wires system where no charge diffusion phenomena are present. On the other hand, different outcome were obtained with PLLA membrane. In this experiment was possible determine an equivalent lumped element circuit model, which was the same to that obtained with Pt wires system and PET membrane. A typical EIS fitting plot of microfluidic platform, with PLLA membrane and Ag wires system integrated, is shown in figure 59.

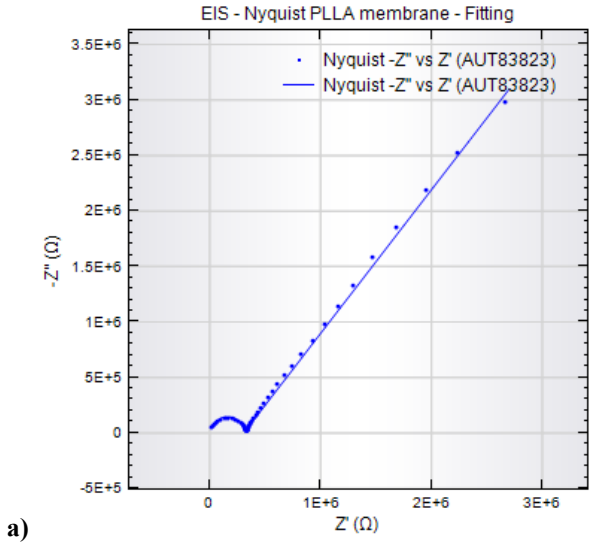

a)

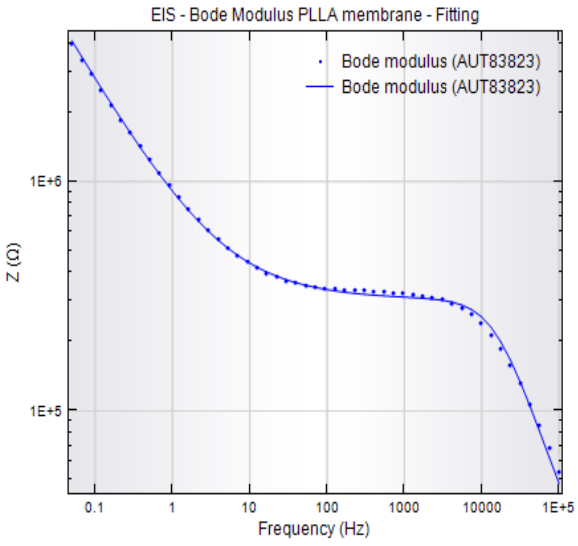

b)

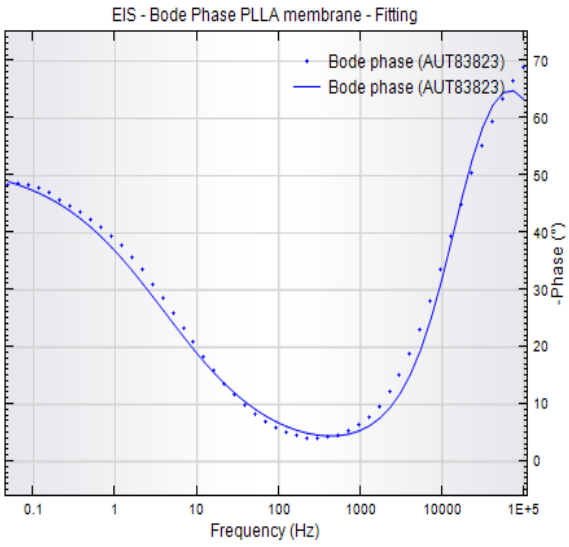

c)

Figura 59: EIS data fitting plot of microfluidic platform with PLLA membrane and Ag wires system integrated: a) Nyquist graphic, b) Bode Modulus graphic c) Bode Phase graphic.

In this case, highest values of membrane resistance than charge diffusion phenomena on electrode surface (high frequency), allow the data fitting. In Nyquist diagram (figure 59) it is possible to see also that for lower frequency the charge diffusion phenomena became dominant. The model components values obtained with PLLA membrane were different than PET membrane. Initially, these variations were associated to thickness, pore size, pore interconnection and pore density difference between the two membranes. As a matter of fact, the PLLA membrane, which is thicker and with interconnected pores, show an R_M upper than PET membrane, while showing a lower C_M due to larger pore density and pore size. The electrolyte resistance in devices with PET membrane was lower than devices with PLLA membrane (see figure 60). The R_E value increased from 10^2 to 10^6 Ohm. This increase can not be associated to the system. Therefore, higher values were associated to the hydrophobic nature of PLLA membrane and then to the presence of air into the membrane. To overcome the problem, the microfluidic chip was submerged into a water-ethanol mixture (70% v/v) and then degassed in vacuum chamber. The results show a decrease of the values but they remains high and long degassing time induced the detachment of the PLLA membrane. In the following table are reported the fitting value of the model components of the microfluidic device with integrated PLLA membrane.

Table 5: Fitting value of the model components with PLLA membrane.

	R_M [ohm]	**R_E [ohm]**	**C_M [F]**	**CPE**	
				Y_0 **[Ω^{-1} *s^N]**	N
Average	$1.25*10^5$	$1.10*10^4$	$5.17*10^{-11}$	$4.72*10^{-7}$	0.60
Dev. Standard	$1.34*10^5$	$3.53*10^3$	$2.10*10^{-11}$	$4.89*10^{-8}$	$4.46*10^{-2}$
Error [%]	1.9	14.6	3.9	1.6	1.0
Dev. Standard	0.46	2.21	1.56	0.29	0.41

Electrical measures were elaborated to improve TEER measurement in chip with PLLA membrane. Finally, Pt wires system were chosen as recording electrodes for EIS and a baseline impedance of each individual chip was implemented.

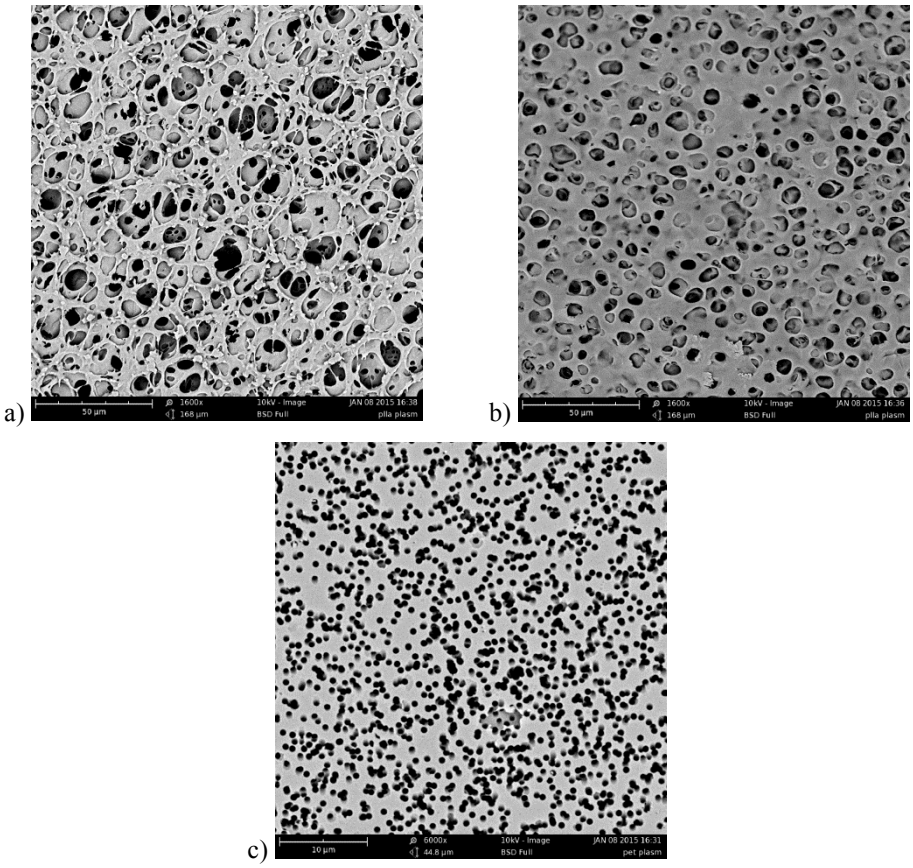

Figure 60: SEM pictures: a) basolateral surface morphology of PLLA membrane, b) apical surface morphology of PLLA membrane, c) PET membrane morphology.

Current measurement to evaluate Trans-epithelial electrical resistance

An alternative approach to determine the TEER (trans-epithelial electrical resistance) is the electrical measure in the time domains. A typical TEER device (see figure 61) is composed of a small volume cup that contains a membrane. This insert then sits in a larger well; when both are filled with liquid (e.g., a physiological buffer), a voltage can be applied and the current passing through the membrane can be measured. In addition, a standard TEER measurement is performed with a four electrode system and consists of an instrument that applies a potential through a battery-powered square wave generator at approximately 12 Hz. Additional sensing electrodes are employed to measure the resulting current through a built-in traditional multimeter.

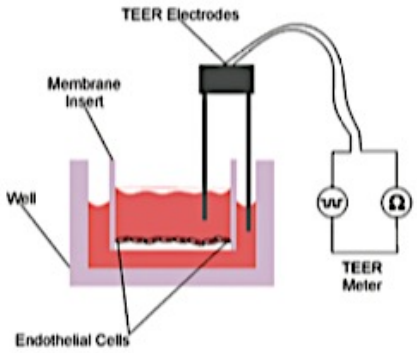

Figure 61: Traditional TEER Measurement.

To simplify the fabrication of this device and eliminate the need of four electrodes, the device with two recording electrodes described in microfluidic device paragraph was designed. A custom Nova program was written and implemented to perform TEER measurements by electrical measurements. The software applies a square wave at constant frequency and magnitude vs OCP across the membrane through Autolab potentiostat/galvanostat (EcoChemie).

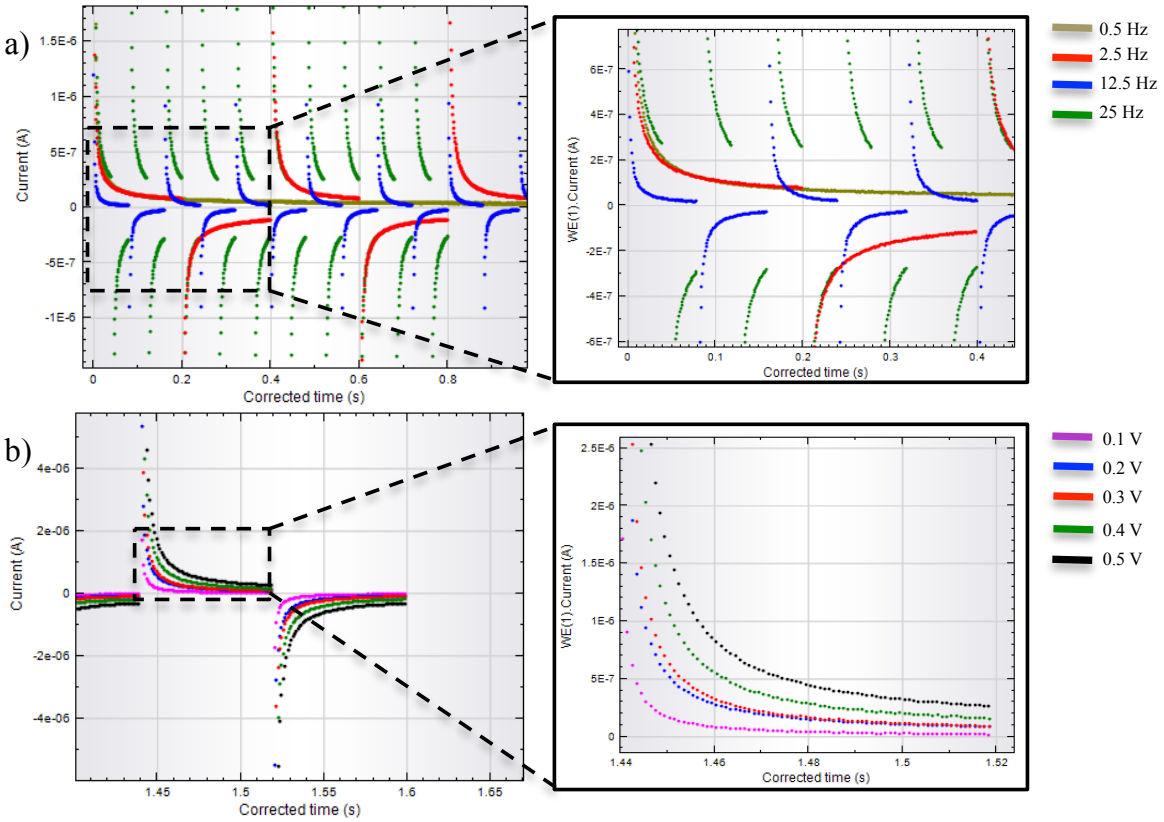

Figure 62: Blank Tests of microfluidic device with PET membrane: a) variable frequency tests b) variable voltage tests.

A total of 1980 current measurements (99 per decade spaced) were recorded. The resultant

current signal is then detected and analysed via MATLAB (Mathworks) or Nova software for the TEER determination. The same measurement condition, described in EIS paragraph, were used to do electrical measurements. Preliminary tests were implemented to choose the optimal frequency and voltage value. Therefore, blank test at frequencies between 0.5 and 25 Hz (constant voltage) and voltage between 0.1 V and 0.5 V (constant frequency) were realized (see figure 62) in microfluidic devices with PET membrane.

It was possible clearly identify (see figure 62a) that a suitable charge and discharge time was obtained at 12.5 Hz while an increase of the current was observed when the potential was changed from 0.1 V to 0.5V. In addition, the current profile was further analysed .Assuming the final current value being the plateau (see figure 62b), current values were plotted vs corresponding voltage (see figure 63).

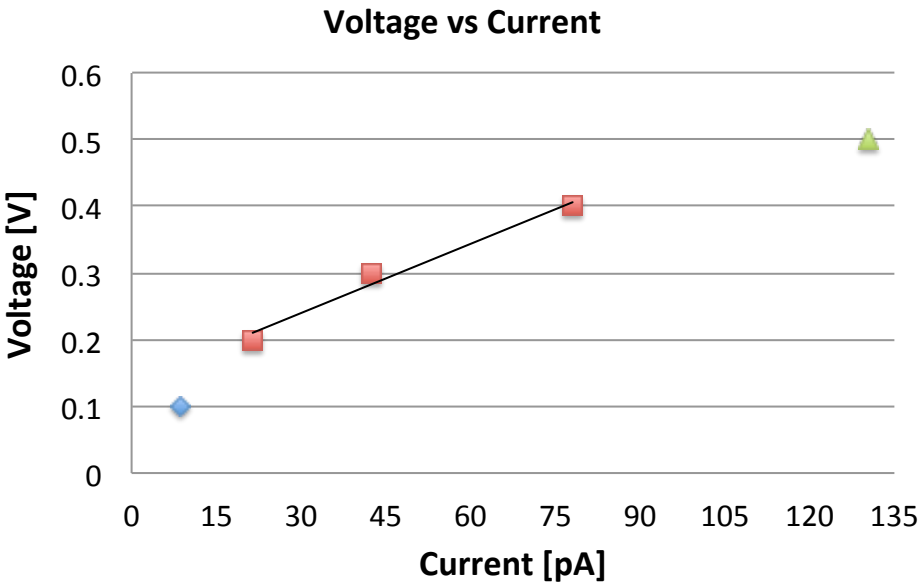

Figure 63: Potential vs Current (Ohm's law).

It was possible to clearly identify in figure 32 that the voltage is reasonably linear to the current in 0.2 V – 0.4 V range. The slope is system resistance. The potential of 0.2 V was chosen as working voltage for it is into validity range of the Ohm's law:

$$R_t = \frac{V}{I} \qquad \textbf{(10)}$$

where V is the applied voltage and I the current through the system.

In addition, when the system is in operation with added electrolyte solutions and a tissue layer on the PET or PLLA membrane, it can be modelled as an RC circuit, which was demonstrated also whit EIS analysis [6].

$$\boldsymbol{I = I_0 e^{-\frac{t}{RC}}} \qquad \textbf{(11)}$$

Where I is the passing through current, I_0 is the initial current and RC is the time constant of the system. With these resultant current profiles, an exponential curve could be fit to the data, and the time constant and conductance could be determined. Numerical integration of data with respect to time is the charge passed through the circuit in that pulse.

$$\int \boldsymbol{I\partial t} = \frac{\partial \boldsymbol{Q}}{\partial \boldsymbol{t}} + \boldsymbol{c} = \frac{\boldsymbol{V}}{\boldsymbol{R}} \qquad \textbf{(12)}$$

Since equation 12 and conductance (G) is the reciprocal of resistance (R), we may conclude that, for a constant potential, charge (Q) is proportional to conductance.

$$\boldsymbol{Q} \propto \boldsymbol{G} = \frac{\boldsymbol{1}}{\boldsymbol{R}} \qquad \textbf{(14)}$$

$$\boldsymbol{R_t} = \boldsymbol{R_E} + \boldsymbol{R_M} + \boldsymbol{R_{load}} \qquad \textbf{(15)}$$

Additionally, in two-electrode system the electrochemical cell resistance include the electrolyte, membrane, and load resistances. The square wave pulse and resulting current profile are plotted as a function of time in Fig. 64.

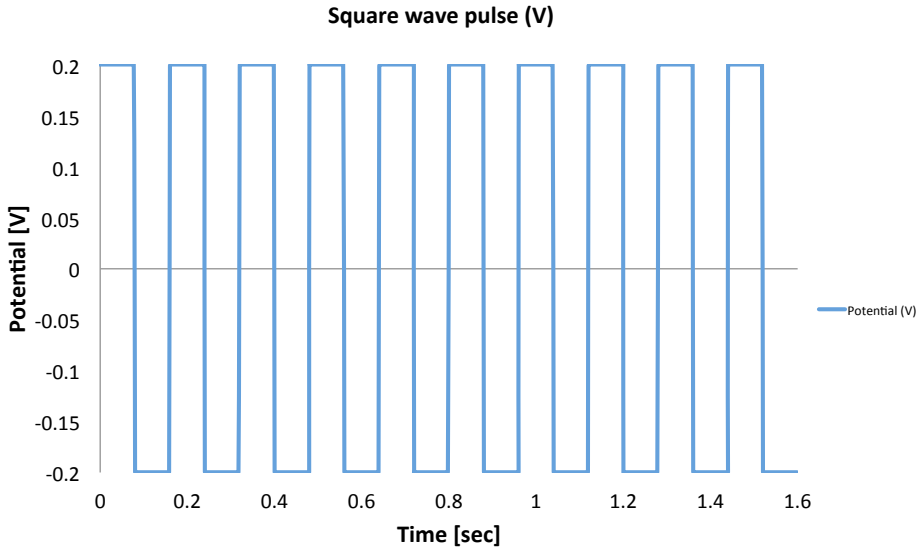

a)

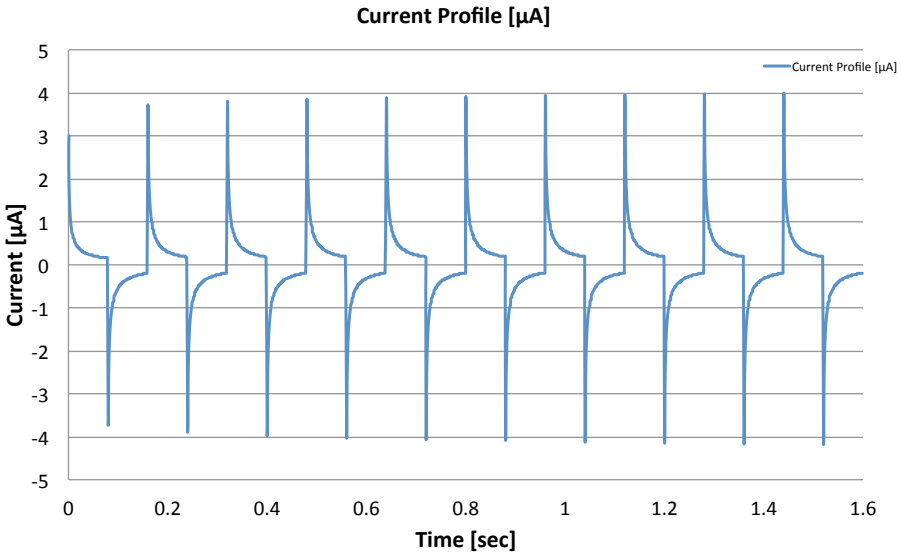

b)

Figure 64: Description of TEER measurement technique: The square wave pulse of 0.2V at 12.5 Hz for applied across the membrane of the TEER device is shown in (a). The resulting current profile for a PBS and medium solution, which into up and down membrane respectively, is shown in (b).

The currents obtained via electrical measure (~0.12 mA) were lower than 0.5 mA as reported in literature [21]. Therefore, the R_M values of microfluidic devices with PET membrane resulted higher than EIS values (R_t = ~ $2.5*10^5$ Ohm). This technique resulted to depend on measure system. In this system, the working electrodes coincide with measure electrodes. The measure systems at two electrodes are less sensitive than measure systems at four electrodes [22]. However, A549 cells were cultured in microfluidic devices with PET membrane and electrical and EIS measures were performed. The PLLA membranes were integrated in microfluidic chips but them weren't used for A549 cultures. A new method to remove the air into the membrane is under development.

A549 culture in microfluidics device

Human alveolar epithelial cells (A549, ATCC) were cultured in DMEM supplemented with 10% fetal bovine serum (FBS, Invitrogen) and 1% antibiotic. Cells were grown in T-75 culture flasks (Corning), which were maintained in a cell culture incubator at 37°C with 5% CO_2 and 95% humidity. When the desired confluence was reached, cells were washed with PBS, trypsinized, collected and suspended in complete growth medium, centrifuged down for 5 min at 4°C and 1,000 rpm, and resuspended in an appropriate volume of the culture medium to give a density of 100.000 cells/cm^3 for seeding into the device.

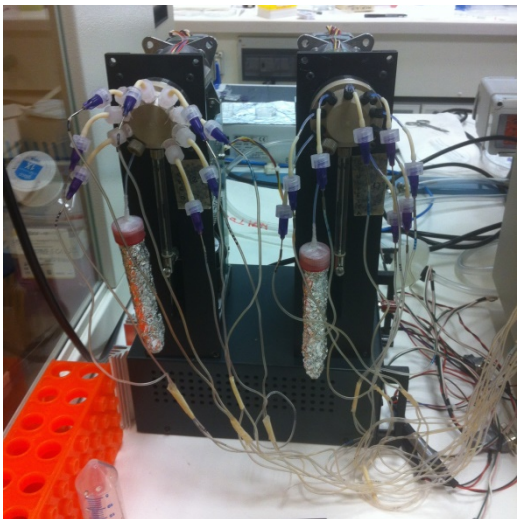

Figure 65: Picture of Tecan CAVRO XR pump.

The medium was fluxed into microdevice system by automatic pump (Tecan CAVRO XR, see figure 65). The automatic pump, through Software Communication, was programmed to replace a volume of 20 µl of growth medium every 12 hours. PDMS microdevices and all microfluidic components (syringes, needles, and tubes) were UV-sterilized prior to use. In addition, all fluidic connections were sterilized with 70% ethanol and rinsed with sterile PBS. The microfluidic channels were filled with cell culture media and allowed to equilibrate for an hour at 37°C and trapped air bubbles were forced out by applying back pressure.

The degree of sealing of tight junctions was assessed from TEER (Trans Epithelial Electrical Resistance) measurements to provide an indication of the integrity of the alveolar epithelial cell monolayers [23]. TEER was determined by electrical and EIS measurements described in the previous paragraph. TEER measurements were performed at regular 1-day intervals, with each data point being a mean of three resistance measurements taken per culture well.
In order to resolve the TEER value from the experimental impedance spectra, the control impedance spectra (taken from the same chip just before cell seeding) was subtracted from the measured impedance spectra (with cells) to eliminate the effect from electrolyte, membrane, and electrode-electrolyte interfaces and simplify the analysis.
EIS of A451 culture on microfluidic chip after 7 days is shown in figure 66.

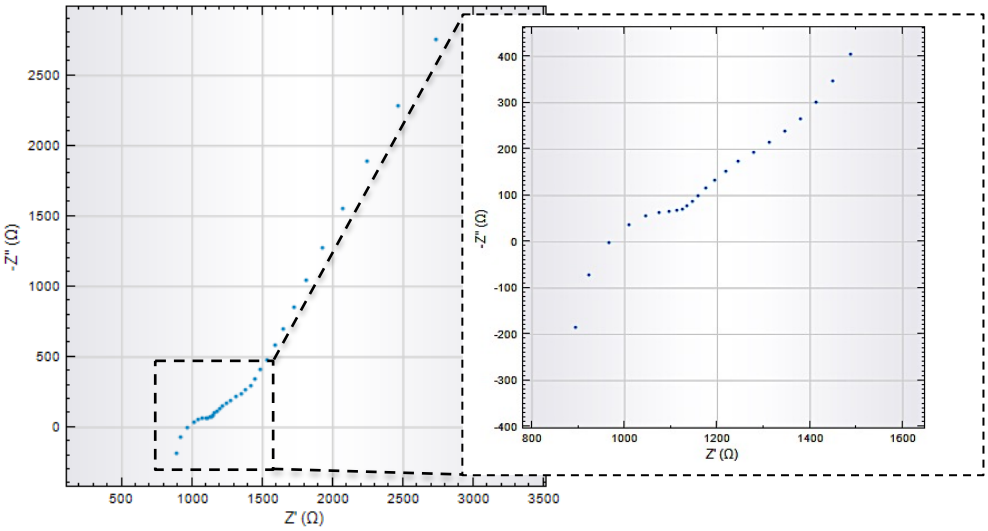

a)

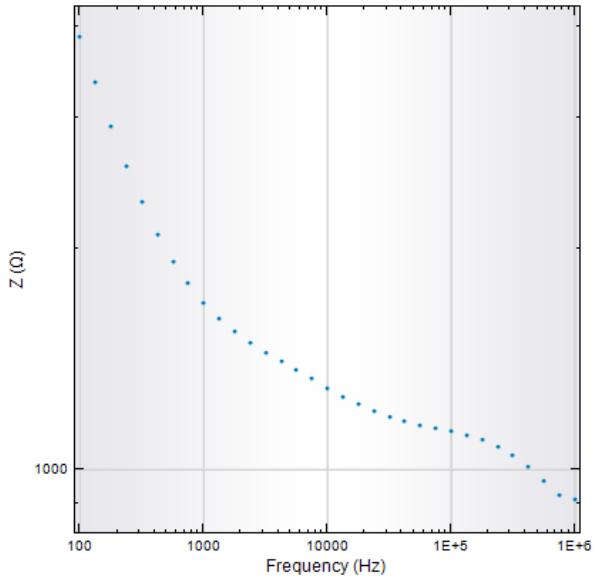

b)

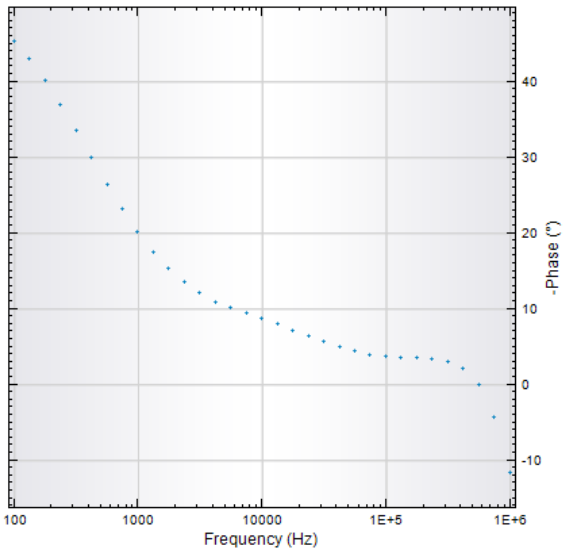

c)

Figure 66: EIS of A549 culture on microfluidic chip after 6 day: a) Nyquist graphic, b) Bode Modulus graphic c) Bode Phase graphic.

An equivalent lumped element circuit model (as shown in Figure 67) was used to simulate the cell monolayer electrical behavior.

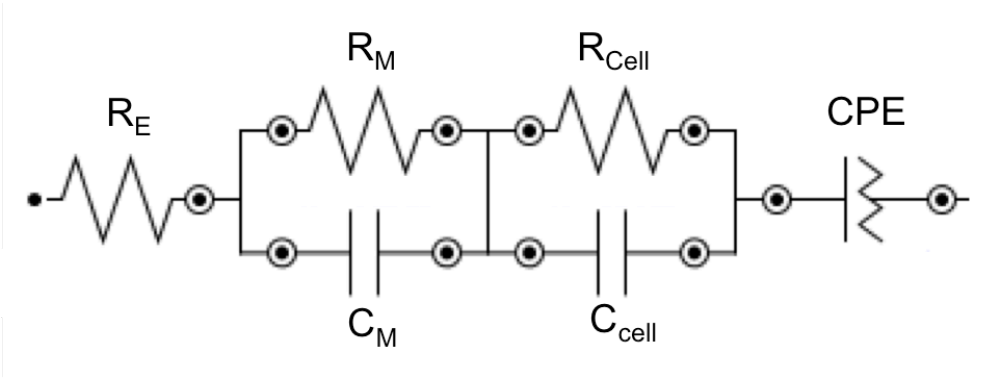

Figure 67: Equivalent lumped element circuit model with A549 cultures.

The circuit is constructed by four components, which were described in previous (R_E, R_M, C_M and CPE), and two new components where R_{cell} and C_{cell} represent extracellular (TEER) resistances and a cellular membrane capacitance, respectively. In order, to resolve the value of each component Nova software was used. In the data fitting, the objective was minimizing the absolute difference between the simulated and experimental impedance values under various frequencies. The TEER value determined by the Nova software was then normalized for surface area of the cell monolayer (specifically 0.125 cm^2) by multiplying the total impedance yielding reported values in units of $\Omega*cm^2$ (see figure 68).

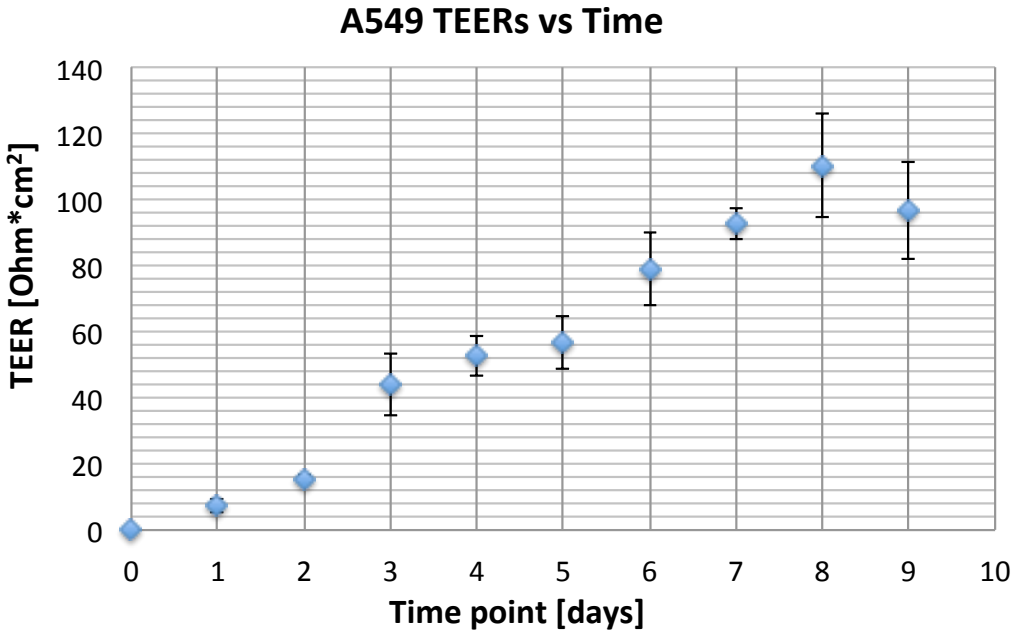

Figure 68: Characterization of A549 cell viability and monolayer integrity. Change in transepithelial electrical resistance of A549 cell monolayer with respect to time. Each data point represents the mean ± SD (n = 4).

TEER was determined at 37°C in cell culture medium (DMEM with 10% FBS) at regular 1 day intervals. The data presented in figure 19 indicates an increase in resistance to flow of current due to decreased gaps in the monolayer which can be attributed to the formation of tight junctions by the cells. The data shown in this paragraph are congruent than that reported in literature, which were recorded by four electrodes measure (EVOM, World Precision Instruments, Houston) [24].

Electrical measures were optimised with same condition described in EIS measures (37°C in DMEM with 10% FBS at regular 1 day intervals). Current measures are shown in figure 69.

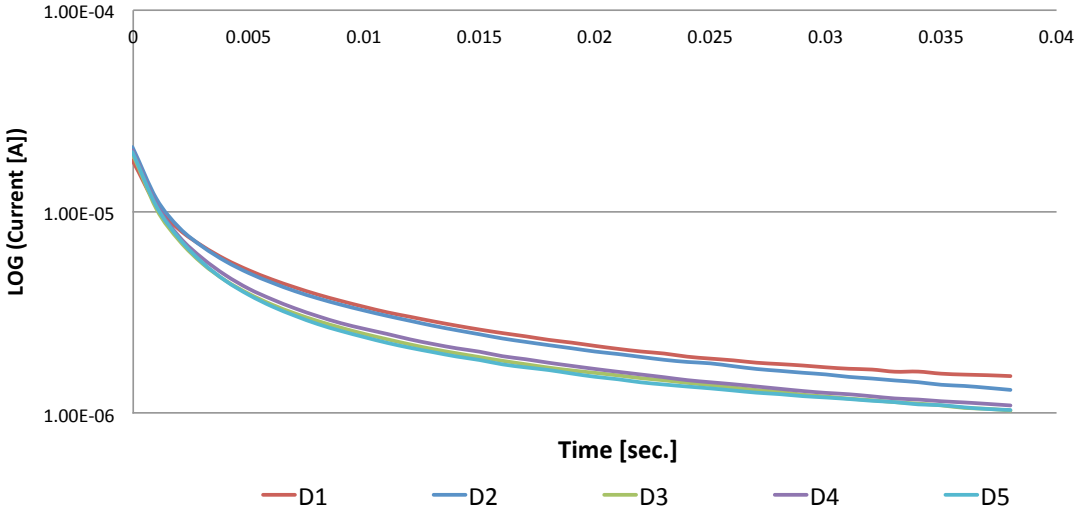

Figure 69: Electrical measure where D indicate the time point.

The data presented in figure 69 indicates a decrease of current with time due to increase of the extracellular resistance in the monolayer, which in its turn can be attributed to the formation of tight junctions by the cells. In the data fitting was used the following equation:

$$y = y_0 + A_1*\exp(-(x-x_0)/t_1) + A_2*\exp(-(x-x_0)/t_2) \qquad \textbf{(16)}$$

Table 6: Fitting value of the model components.

Time point [days]	T_1	T_2	Area	R_{tot} [Ohm*cm^2]
1	4.57E-03	4.56E-03	1.55E-07	1.26E+04
2	4.74E-03	4.69E-03	2.05E-07	1.03E+04
3	2.81E-03	6.44E-03	1.92E-07	1.29E+04
4	2.80E-03	6.29E-03	1.97E-07	1.60E+04
5	2.78E-03	6.51E-03	2.15E-07	1.89E+04

The equation consist of two exponential and then two time constant (T_1 and T_2). This can be attributed a two RC circuit as shown in EIS analysis. In the following table are reported the fitting value of the model components. The resistance values, obtained by electrical measure (reported in table 6) were not comparable to resistance obtained via EIS method.

Conclusion

First of all a microfluidic device was designed and tested to alveolar epithelial cells regeneration. Secondary, a measurement apparatus was investigated and optimized to measure TEER. Finally, a fluxing automatic system was realized to supply growth medium to the tissue into the chip. Preliminary results of alveolar epithelial cells regeneration on PET and PLLA scaffold, which are integrated in microdevice, are awaited.

References

[1] J. El-Ali, K. Peter Sorger, F. Klavs, Review Article Cells on chips, Nature (2006) 442, 403-411.

[2] E.W. Young, D.J. Beebe, Fundamentals of microfluidic cell culture in controlled microenvironments, Chem. Soc Rev. (2010) 39(3):1036-48.

[3] G. Tomaiuolo, M. Barra, V. Preziosi, A. Cassinese, B. Rotoli, S. Guido, Microfluidics analysis of red blood cell membrane viscoelasticity, *Lab Chip* (2011) 7;11(3):449-54.

[4] S.W. Rhee, A.M. Taylor, C.H. Tu, D.H. Cribbs, C.W. Cotman, N.L. Jeon, Patterned cell culture inside microfluidic devices, Lab Chip (2005) 5(1):102-7.

[5] S. Kim, H.J. Kim, N.L. Jeon, Biological applications of microfluidic gradient devices, Integr Biol (Camb) (2010) 2(11-12):584-603.

[6] J. Zhou, L. Niklason, Microfluidic artificial "vessels" for dynamic mechanical stimulation of mesenchymal stem cells, Integr Biol (Camb) (2012) 4(12):1487-97.

[7] C. Kuo, C. Chiang, R. Huang, A. Wo, Configurable 2D and 3D spheroid tissue cultures on bioengineered surfaces with acquisition of epithelial–mesenchymal transition characteristics, NPG Asia Materials (2012) doi:10.1038/am.2012.50.

[8] F. Pampaloni, G. Emmanuel Reynaud, H.K. Ernst, The third dimension bridges the gap between cell culture and live tissue, Nat. Rev. Mol. Cell Biol. (2007) 839-845.

[9] D. Huh, G.A. Hamilton, D.E. Ingber, From 3D cell culture to organs-on-chips, Trends in Cell Biology (2011) Volume 21, Issue 12, 745-754.

[10] K. Domansky, W. Inman, J. Serdy, A. Dash, M.H. Lim, L.G. Griffith, Perfused multiwell plate for 3D liver tissue engineering, Lab Chip. (2010) 10:51–8. doi: 10.1039/b913221j.

[11] Midwound et al, *Intgr Biol*, 2011,3,509-521.

[12] S.K. Fried, N. Moustaid-Moussa, Culture of Adipose Tissue and Isolated Adipocytes, Methods in molecultar Biology, vol 155: adipose tissue protocols, pp 197-212.

[13] L. Sjostrom, U. Smith, P. Bjorntorp, Human adipose tissue maintained in a continuous flow system. Kinetic studies of glycerol release in response to noradrenaline and evidence for the formation of a hormone antagonist, J Biol Chem. (1977) 252:8833–8839.

[14] R. Gómez-Sjöberg, A.A. Leyrat, D.M. Pirone, C.S. Chen, S.R. Quake, Versatile, fully automated, microfluidic cell culture system, Analytical Chemistry 79, no. 22 (2007): 8557-8563.

[15] N.J. Abbott, L. Rönnbäck, E. Hansson, Astrocyte-endothelial interactions at the blood-brain barrier, Nat Rev Neurosci (2006) 7:41–53.

[16] J. Kulys, J.A. Munk, T. Buchrasmussen, H.E. Hansen, The preparation in situ of a silver silver- chloride reference electrode, Electroanalysis 6 (1994) 945-952.

[17] H. Hassan, A.M. Magdy Ibrahim, S. Sayed Abd El Rehim, A.M. Amin, Comparative Studies of the Electrochemical Behavior of Silver Electrode in Chloride, Bromide and Iodide Aqueous Solutions, Int. J. Electrochem. Sci., 5 (2010) 278 – 294.

[18] N.J. Douville, Y.C. Tung, R. Li, J.D. Wang, M.E.H. El-Sayed, S. Takayama, Fabrication of two-layered channel system with embedded electrodes to measure resistance across epithelial and endothelial barriers, Anal. Chem. (2010) 82, 2505–2511.

[19] R. Thuenauer, E. Rodriguez-Boulan, W. Römer, Microfluidic approaches for epithelial cell layer culture and characterisation, Analyst (2014) 139, 3206; DOI:

10.1039/c4an00056k.
[20] L.M. Griep, F. Wolbers, B. de Wagenaar, P.M. ter Braak, B.B. Weksler, I.A. Romero, P.O. Couraud, I. Vermes, A.D. van der Meer, A. van den Berg, BBB ON CHIP: microfluidic platform to mechanically and biochemically modulate blood-brain barrier function, Biomed Microdevices (2013) 15:145–150 DOI 10.1007/s10544-012-9699-7.
[21] P.A. Vogel, S.T. Halpin, R.S. Martin, D.M. Spence, Microfluidic Transendothelial Electrical Resistance Measurement Device that Enables Blood Flow and Postgrowth Experiments, Anal. Chem. (2011) 83, 4296–4301.
[22] H. Xianqiao, L. Xingyu Lin, H. Qiaohong, C. Hengwu, Electrochemical detection of droplet contents in polystyrene microfluidic chip with integrated micro film electrodes, Journal of Electroanalytical Chemistry (2014) 726 7–14.
[23] A. Adson, T.J. Raub, P.S. Burton, C.L. Barsuhn, A.R. Hilgers, K.I.Audus, N.F. Ho, J Pharm. Sci. (1994) 83, 1529–1536 doi:10.1002/jps.2600831103.
[24] D. Divya Nalayanda, C. Puleo, W.B. Fulton, L.M. Sharpe, Tza-Huei Wang, F. Abdullah, An open-access microfluidic model for lung-specific functional studies at an air-liquid interface, Biomed Microdevices (2009) 11:1081–1089, DOI 10.1007/s10544-009-9325-5.

Chapter 6

Fabrication method of natural/synthetic hybrid tissues

Decellularized tissues and organs have been successfully used in a variety of tissue engineering/regenerative medicine applications, and the decellularization methods used vary as widely as the tissues and organs of interest [1]. Several methods for the animal's matrix decellularization are present both in literature and as patents. These methods allow an effective removal from the animal tissue of the antigens, which are responsible of immunological rejection in the human body [2].

The efficiency of cell removal from a tissue is dependent on the origin of the tissue and the specific physical, chemical, and enzymatic methods that are used. Each of these treatments affects the biochemical composition, tissue ultrastructure, and mechanical behavior of the remaining extracellular matrix (ECM) scaffold, which, in their turn, affect the host response to the material [3].

Biologically active three-dimensional scaffold able to support cellular growth and differentiation are produced via freeze-drying and/or electrospinning. Fibers of desired porosity can be obtained from non-structural ECM by this technique which can be useful for numerous tissue engineering applications requiring complex scaffolds [4].

Tracheal tissue is a multi-component structure composed of cartilage, trachealis muscle, mucosa, submucosa membrane and adventitial membrane. Its mechanical properties are essential for an accurate prediction of tracheal deformation, which has a significant clinic relevance [5, 6].

As a matter of fact, the use of a decellularized trachea (natural scaffold), does not ensure stable mechanical properties of the construct, does not guarantee a reproducibility of the internal and external structure and, finally, does not allow a precise control of its biodegradation kinetics.

In this thesis, the efficiency of a given decellularization method or protocol and its effect on the mechanical behaviour of porcine trachea ring was analysed. A coating process with a porous synthetic membrane via a combination of Dip-coating and Diffusion Induced Phase Separation (DIPS) was ~~designed and~~ carried out, in order to build-up a hybrid synthetic/natural construct. Experimental results show that the coating of the ring with the synthetic material helps to recover the mechanical properties lost during decellularization.

Experimental

Materials and methods

The porcine trachea ~~used in this investigation~~ were supplied from Villabate slaughterhouse.

Decellularization methods

Sodium Dodecyl Sulfate (SDS) was used as detergent to the decellularization. The porcine trachea was soaked into SDS bath for 24 h at room temperature. Thereafter, the sample was put in box containing PBS 1X at 4°C until it was analysed.

Tracheal tissue coating

Dip coating consists in the immersion of a biological tissue in a PLLA-dioxane viscous solution (with 8% wt/wt of dioxane) with subsequent extraction at a controlled constant rate. The tracheal ring was first fixed to a glass support and then soak in viscous solution. Via this technique it is possible to control the thickness of the coating layer by varying tissue extraction rate, solution temperature and polymer concentration (see figure 70a). The subsequent pool immersion of the tissue, covered by a continuous layer of a viscous polymer solution, into a coagulation bath, represents the Diffusion Induced Phase Separation (DIPS) step.

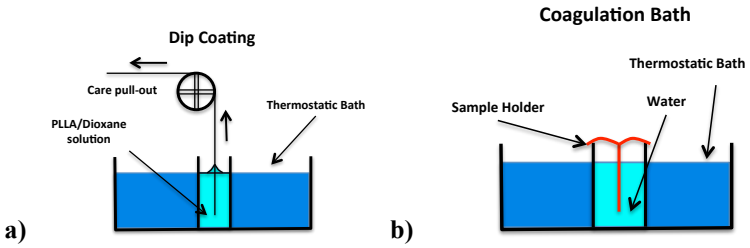

Figure 70: Schematic of the Dip-coating (a) and DIPS (b) processes.

The bath contains pure water. Via DIPS, the simultaneous solvent (dioxane) diffusion out of the polymeric film and counterdiffusion of the non-solvent (water) from the coagulation bath towards the polymeric film will induce the phase separation process. Figure 70b reports a schematic of the two processes. Extraction rate, polymer solution concentration and process temperature were taken constant in all experiments: the extraction velocity was set to 3 cm/min, the polymer solution concentration to 8 wt% PLLA and the temperature to 30 °C. The protocol followed was the same as the one described in chapter 1 for membrane fabrication [7].

H&E staining

Haematoxylin and Eosin (H&E) staining was used to evaluate the efficiency of the decellularizzation process. Same portions of trachea rings, decellularized and not, were heated to a temperature of 65°C for 20 minutes. Afterwards, the samples were soaked in different baths, according to the procedure listed below (see table 7):

Table 7: H&E immersion time and concentration bath.

n°	Immersion time	Concentration Bath
1	10 min.	Xylene
2	10 min.	100% Ethanol
3	5 min.	95% Ethanol
4	5min.	80% Ethanol
5	5 min.	50% Ethanol
6	5 min.	Water
7	3 min.	Hematoxylin
8	10 min.	Water
9	1 min.	Eosin
10	5 min.	Water
11	5 min.	50% Ethanol
12	5 min.	80% Ethanol
13	5 min.	95% Ethanol
14	5 min.	100% Ethanol
15	1 min.	100% Xylene

At the end, the samples were ready for optical analysis.

Masson Tricromica staining

The samples (portions of trachea rings) were washed in distilled water and then 6 drops of a solution A and B (weigert's iron hematoxylin) were added. After 10 minutes, without washing, the samples were drained and 10 drops of reagent C (Picric acid alcoholic stable solution) were added. After 4 minutes, samples were washed quickly in distilled water and 10 drops of reagent D (Ponceau acid fuchsin according to Masson) were added. After washing in distilled water, 10 drops of reagent E (phosphomolybdic acid solution) were added. After 10 minutes, without washing, the drained samples were treated with 10 drops of reagent F (light green solution according to Goldner) for 5 minutes. Finally, the samples were washed in

distilled water and dehydrated rapidly through ascending alcohol concentration. Washed in Xylene, the samples were mounted for analysis.

TEM analysis

To analyze the decellularization effectiveness on the tissue, the as-produced samples (described in decellularization method) were observed via Transmission Electron Microscopy (TEM), by utilizing a JEM-1220 (JEOL, Japan). The TEM analysis and the samples preparation was realized at the "Dipartimento di Biomedicina Sperimentale e Neuroscienze Cliniche (BIONEC)" University of Palermo, in the Prof. Bucchieri's Laboratories.

SEM analysis

To evaluate the coating efficiency and validate to effective polymer adhesion on the biological decellularized tissue, the as-produced samples (natural/synthetic hybrid tissues) were observed via Scanning Electron Microscopy (SEM), by utilizing a Philips SEM quanta FEI, at 10 kV.

Tensile behaviour

Tensile tests were performed to investigate the mechanical behaviour of trachea tissues, PLLA films and hybrid scaffolds (trachea tissue coated with PLLA). For this test force speeds of 0.05 and 0.01N/s were used, while the temperature was taken constant at the value of 30°C. Tracheal samples of 40 × 7.5 mm and thickness in the range of 1.5–3.5 mm were used to determine the stress–strain behaviour by Bose Electroforce Planar Biaxial instrument (figure 71).

Stress–strain behaviour of PLLA films (40 x 7.5 mm and thick 30 μm) and hybrid tissues were tested under the same conditions.

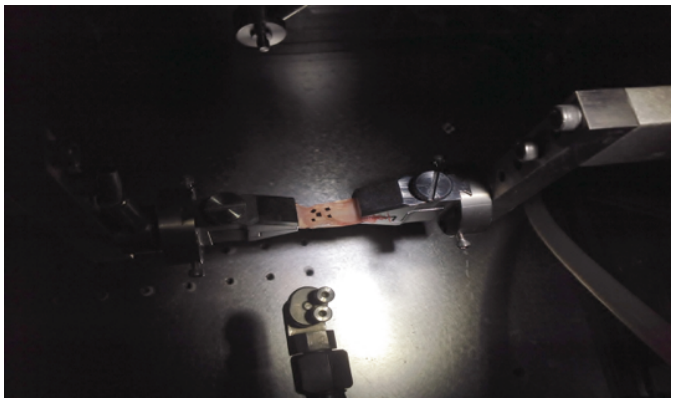

Figure 71: Picture of Stress-strain analysis of tracheal ring.

Shear Stress behaviour

Type III delamination tests were carried out on bioengineered hybrid PLLA-coated cartilage rings in order to validate the effective polymer adhesion on the biological decellularized tissue and specific delamination load. Although the Type I (ISO15024, 2001), the Type II (JIS7086, 1993) and mixed-Type I/II (ASTMD6671-01, 2001) are used to study the delamination process, Type III there is not yet an internationally accepted test.

The test was realized as shown in figure 72. A force speed of 0.01 N/s was chosen, while the temperature was taken constant at the value of 30°C.

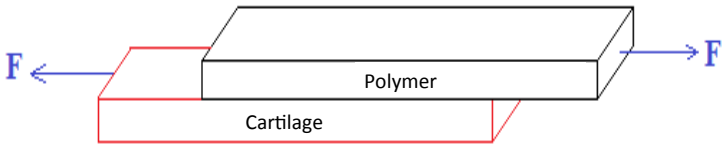

Figure 72: Schematic of type III delamination.

Samples of 40 × 7.5 mm and thickness in the range of 1.5–3.5 mm were used to determine the shear stress delamination by Bose Electroforce Planar Biaxial instrument.

Results and discussion

Tissue decellularization

SDS resulted very efficient in the removal of cellular components from tissue (see figure 73 and 74). Therefore, it tends to disrupt the native tissue structure, and causes a loss of tissue integrity. However, SDS does not appear to remove collagen and/or cartilage from the tissue in such a way to significantly modify the mechanical behaviour of the tissue.

a) 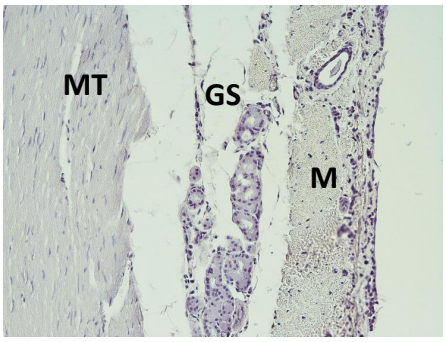

b) 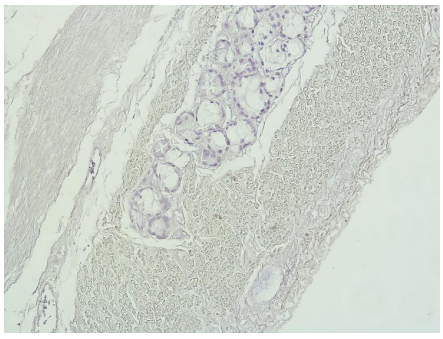

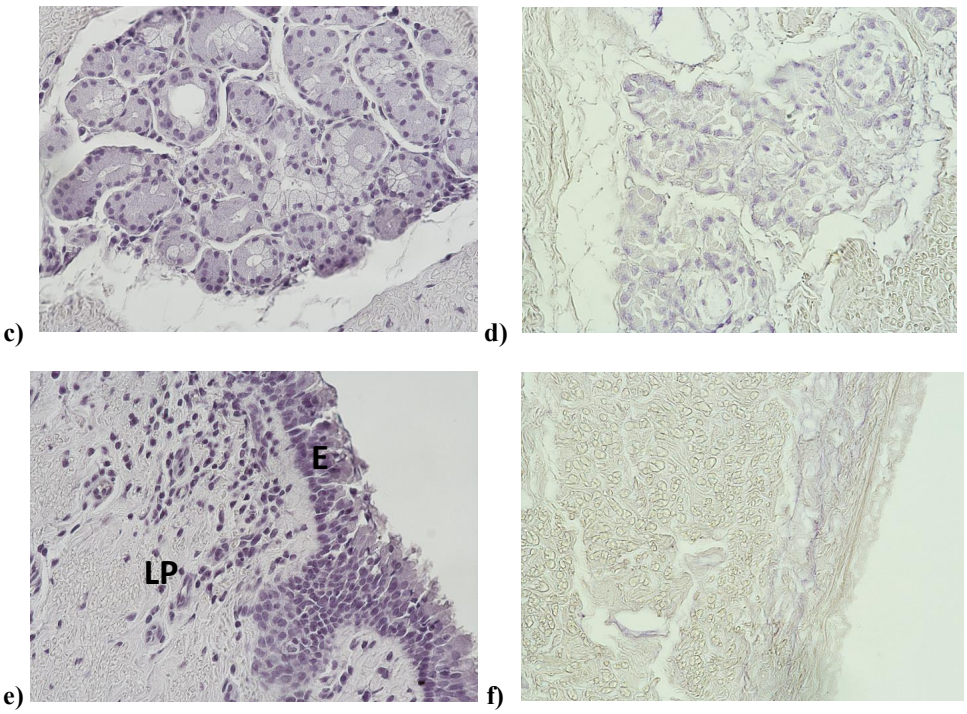

Figure 73: H&E staining of pig trachea, comparison between a native tissue (left side) and a decellularized tissue (right side).

In figure 73 and 74 the letters indicate: (E) epithelial layer, (MT) trachealis muscle, (M) mucosa, (GS) submucosal glands and (LP) lamina propria, (Ca) the cartilage tissue, respectively.

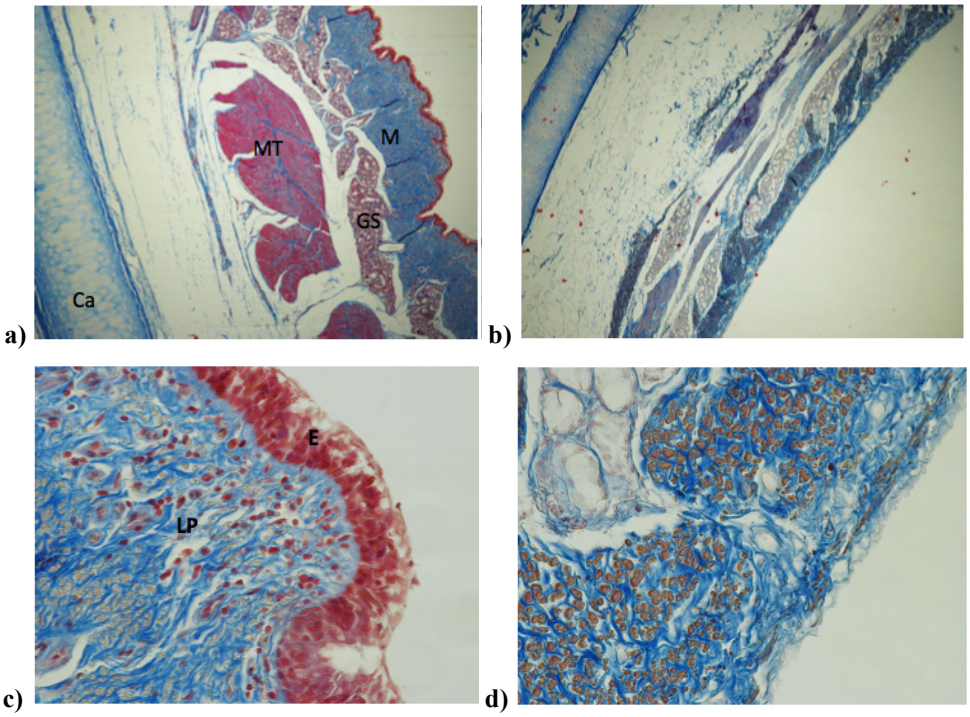

Figure 74: Masson tricromica staining of pig trachea, comparison between a native tissue (left side) and a decellularized tissue (right side).

The cartilage tissue after decellularization process did not become completely cell-free. This effect is ascribable, as reported in literature, to the compact structure of cartilage tissue. Therefore, SDS detergent is not able to deeply penetrate into the cartilage.

Figure 75 shows the comparison between a control pig trachea (a and b) and a decellularized one (c and d). Fibroblasts (F) and numerous bundles of collagen (black arrows) are evident. The control sample shows a well-defined nucleus (N) and cytoplasm (c); in the decellularized sample, instead, both nucleus and cytoplasm are clearly damaged and almost totally displaced. In both samples, bundles of collagen are clearly visible, which maintain their spatial and structural arrangement. Fig. 75 d) shows how collagen bundles maintained their typical banding and structural arrangement.

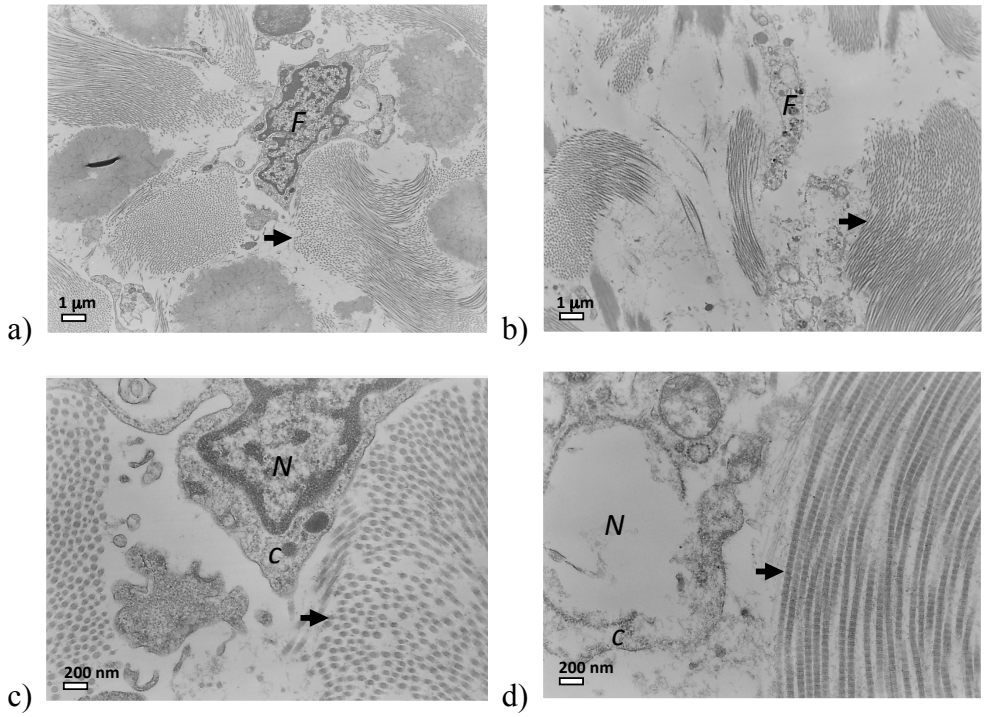

Figure 75: TEM pictures of pig trachea, comparison between a native tissue (left side) and a decellularized tissue (right side).

Tensile behaviour

The use of a natural scaffold, does not normally ensure stable mechanical properties of the construct, does not guarantee a reproducibility of the internal and external structure and, eventually, does not allow a precise control of its biodegradation kinetics. Uniaxial tensile tests were carried out on decellularized and neat (i.e. non-deccelularized) tracheal rings.

Figure 76 shows the representative stress-strain curves for the investigated non-decellularized samples. Tensile curves were characterized by a typical non-linear behavior up to break.

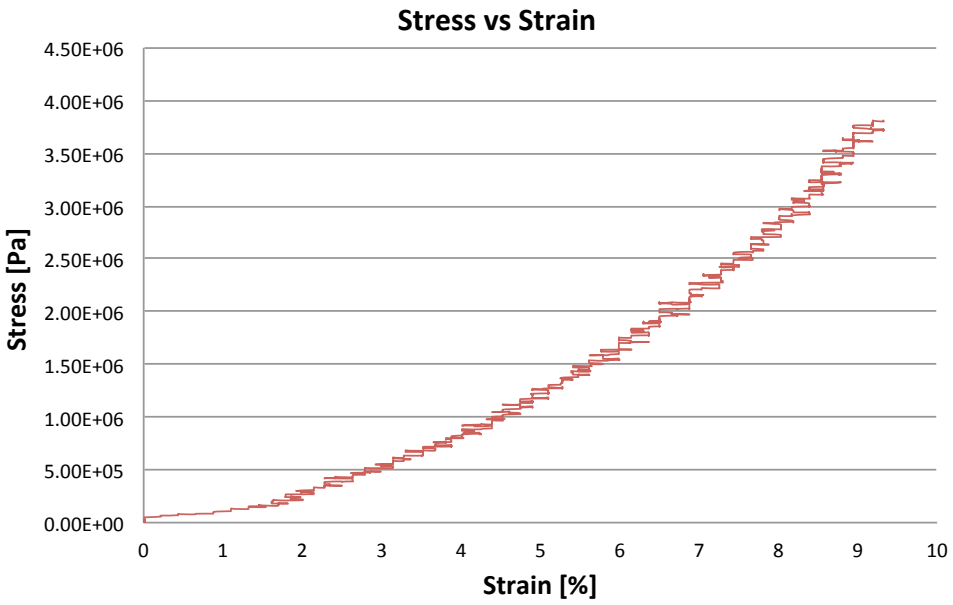

Figure 76: stress–strain curve of no decellularized trachea ring (force speed of 0.05 N/s).

The mechanical properties in tension of cartilage rings made of native porcine tissue are reported and compared with those made of decellularized tissue at the force speed of 0.05 N/s. Figure 77 illustrates the Young's modulus obtained by tensile tests performed on porcine tracheal rings with or without the characteristic tissue layers that constitute this structures.

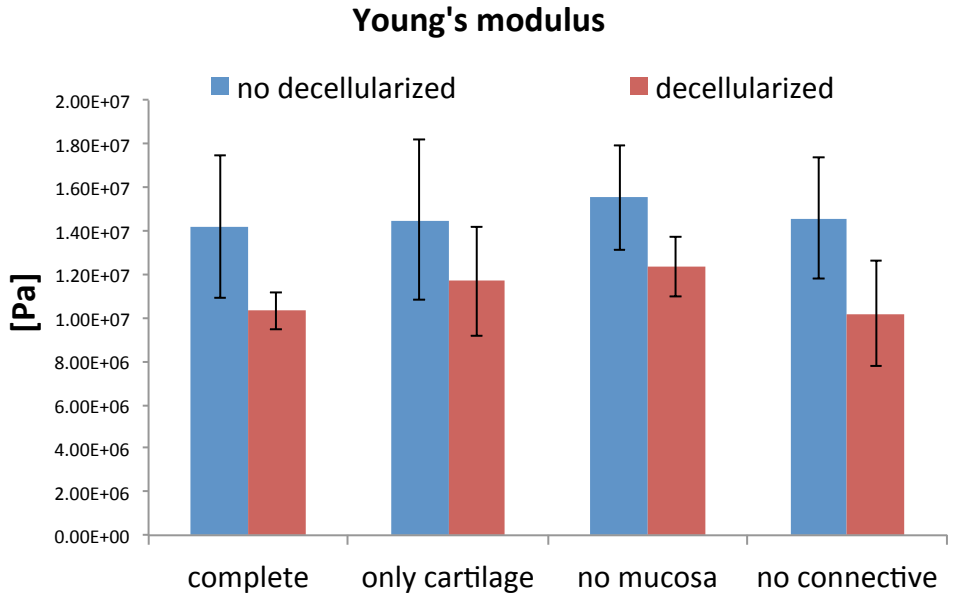

Figure 77: Comparison of mechanical properties of native porcine trachea and decellularized one (force speed of 0.05 N/s).

It can be observed that the decellularization process produces a significant loss of mechanical performance by treatment with SDS (about 30%) and the most relevant controbution to the mechanical strength is provided by cartilage.

Tracheal tissue coating

A coating with a porous synthetic membrane via a combination of Dip-coating and Diffusion Induced Phase Separation (DIPS) was carried out to recover the mechanical properties lost after decellularization.

a) 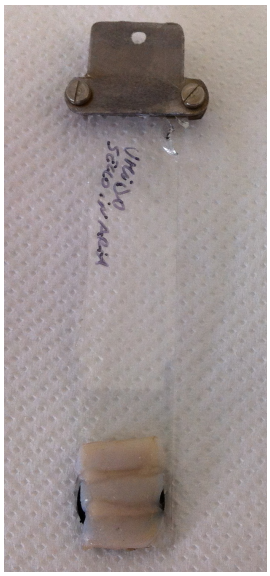 b) 

Figure 78: Tracheal tissue on glass support, a) non-coated, b) coated with a polymeric film.

Figure 78a show a portion of trachea rings fixed to the glass support before of the coating, while figure 78b the same sample coated of polymeric film (PLLA).

In figure 79 SEM micrographs of PLLA film obtained by adopting the described protocol (used to obtain hybrid tissue) is reported. It can be observed that the internal surface (glass support side, figure 79a) is porous, while external surface is closed (without pores, figure 79b). Figure 79c shows the cross section that appears homogeneously porous. The thickness was about 30 μm.

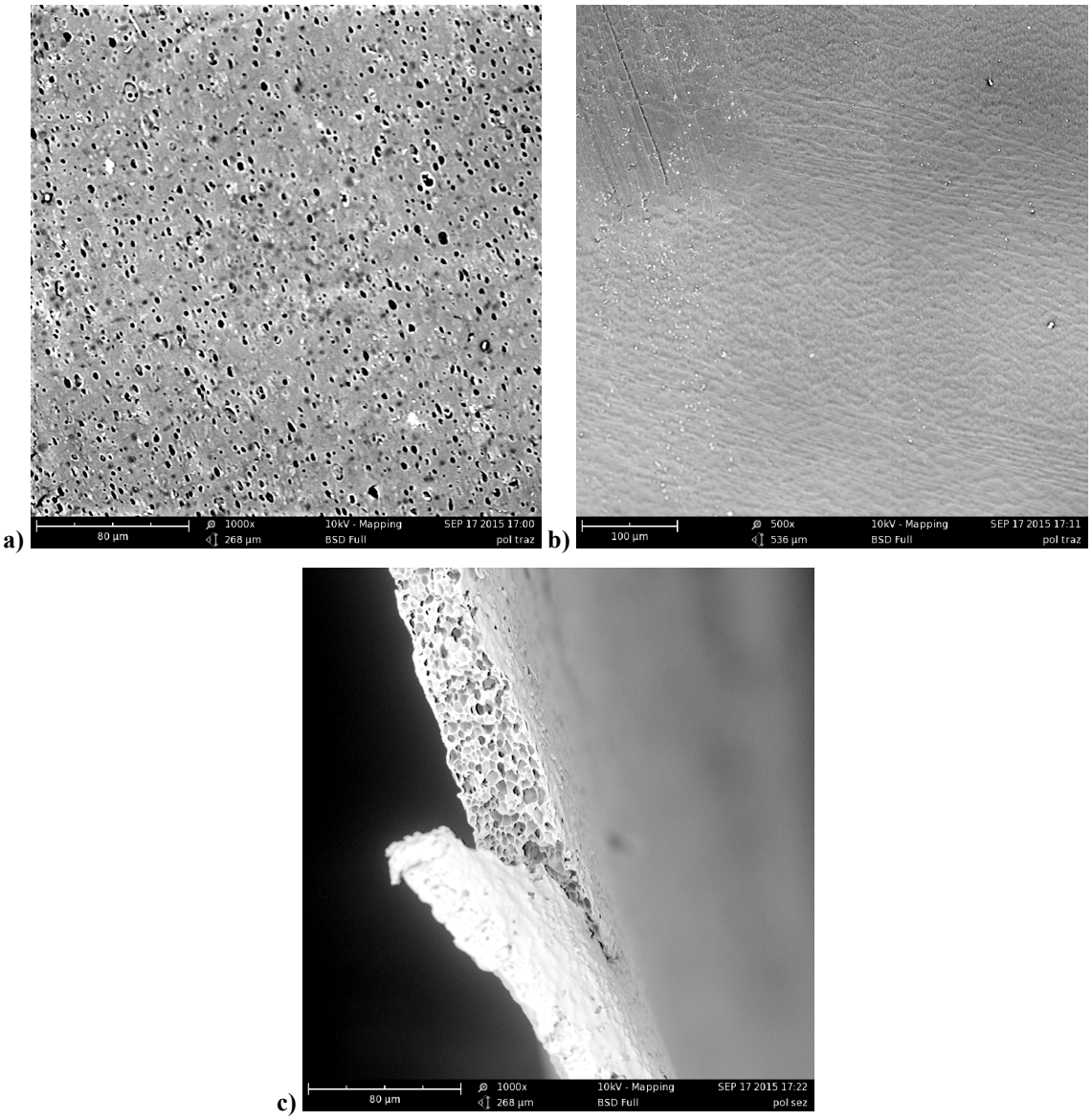

Figure 79: PLLA films obtained with the same protocol used to obtained hybrid tissue: a) internal surface, b) external surface and c) cross section.

Figure 80 shows the stress–strain curves of PLLA membranes at the temperatures of 30°C. Young's modulus measured by tensile tests was 123.9±25 MPa. It is important to underline that PLLA membrane shows stress-strain curves with a concavity opposite to that observed in tracheal ring.

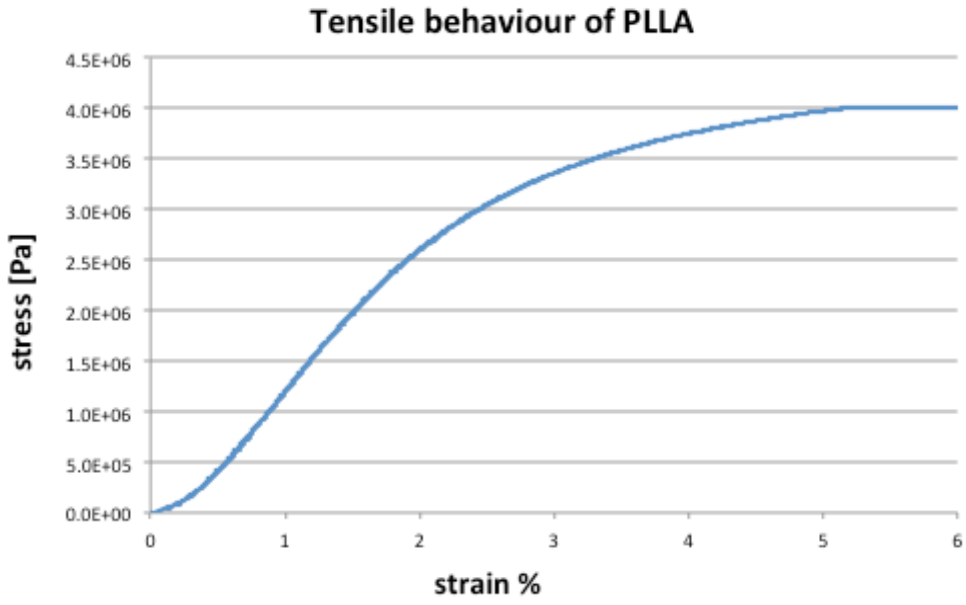

Figure 80: stress–strain curve of PLLA membrane (force speed of 0.01 N/s).

Figure 81 shows two cross sections of hybrid tissue. The adhesion between PLLA film (A) and tracheal tissue (B) is evident. The picture shows a well-defined contact between the PLLA polymeric layer and the natural tissue, where also the connective tissue (C) can be identified.

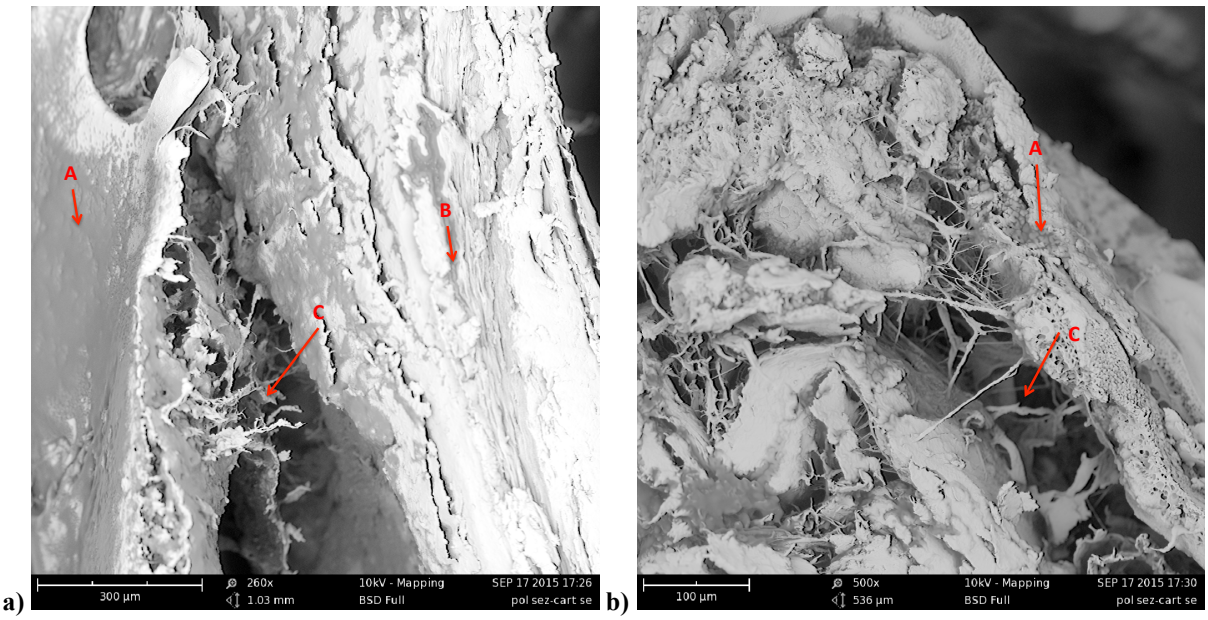

Figure 81: SEM pictures of hybrid tissue.

Mechanical tensile tests on the bioengineered tissue, reported in figure 82, show the recovery of the mechanical properties attained via coating with PLLA. The improvement of the

mechanical performance is evident up to strains as high as 1%, comparable with the physiological deformations of the examined tissue.

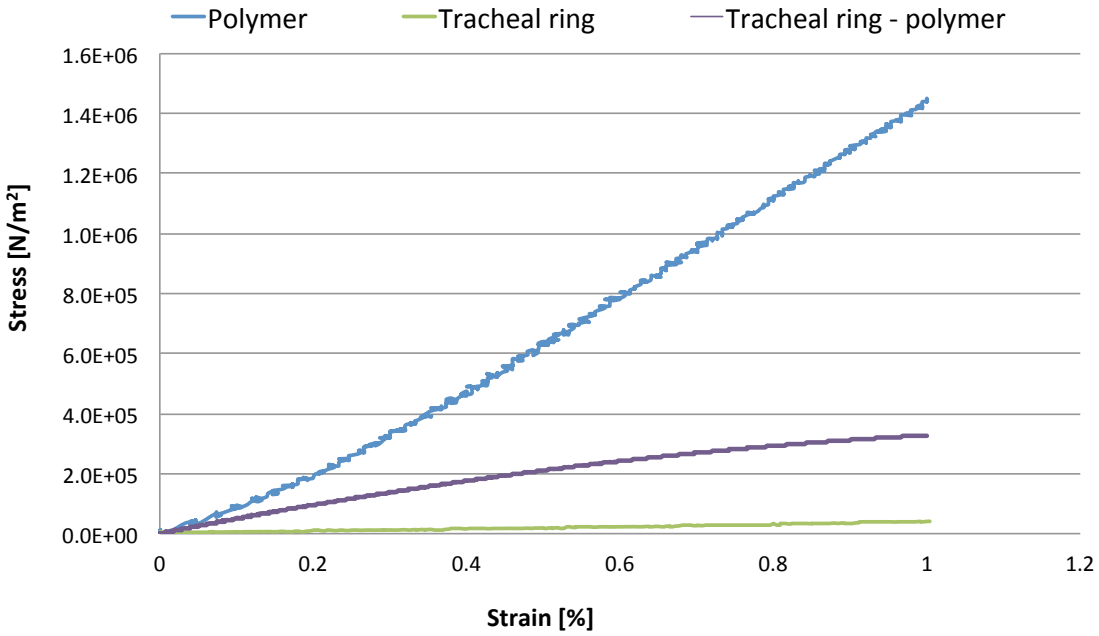

Figure 82: Comparison of tensile mechanical properties of polymer, hybrid tissue and tracheal ring (force speed of 0.01 N/s).

The polymer and natural tissue present a different stiffness and, therefore, the mechanical features of the hybrid tissue resulted halfway between those of synthetic polymer and natural tissue, respectively. Young's modulus obtained by tensile tests performed on hybrid tissue was 35.2±9.7 MPa.

Shear Stress behaviour

The causes of a non-perfect adhesions between PLLA and the natural tissue may be the following :

1. cartilage surface is not perfectly flat;
2. the sample needs to be maintained in solution.

The adhesion surface was estimated in the range 120 - 130 mm^2. Figure 83 shows the shear stress curves of hybrid tissue at the temperatures of 30°C.

It can be observed that the curve exhibits a slope change in correspondence to an elongation of about 0.8% and of a load of 5 kPa: the two surfaces lose adhesion and begin to slide between them. From this point onwards the evolution becomes linear again up to an additional change of slope in correspondence of 25 kPa, where the two layers are completely detached and the test is stopped with a total elongation of about 3%.

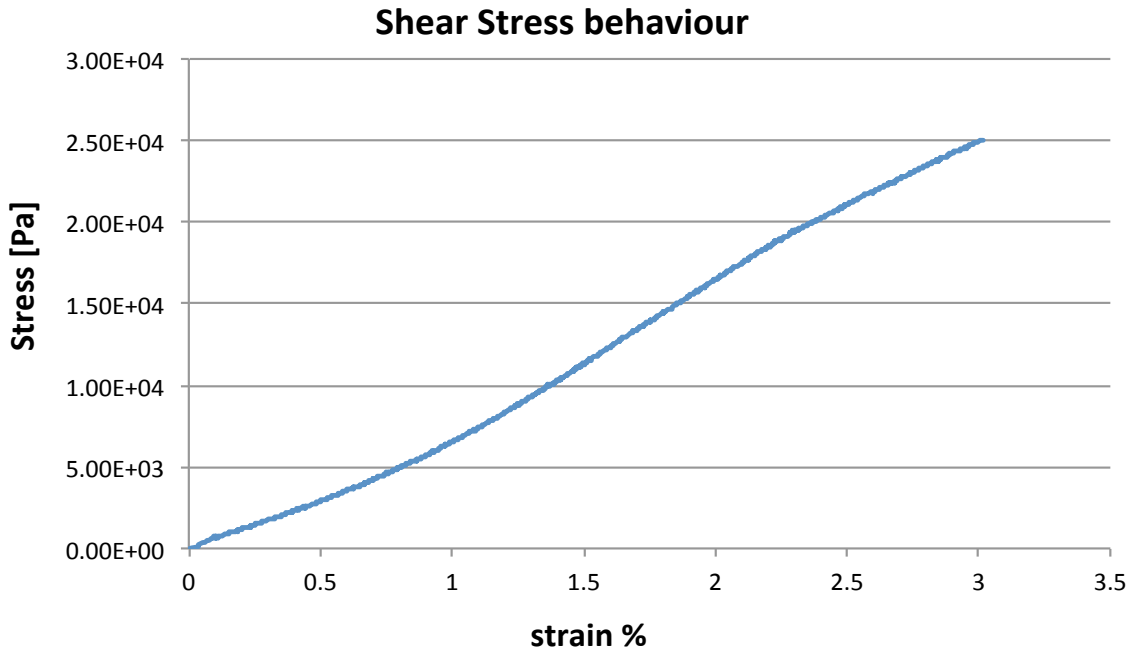

Figure 83: Shear–strain curve of hybrid tissue at 0.01N/s.

A SEM image of the delaminated section is shown in figure 84. It is easy to observe the delamination region of the bioengineered tissue. All things considered, the method seems to be promising for tissue engineering applications, as it provides a route for producing a biohybrid tissue, combining the biocompatibility and bioactivity of the decelluralized tissue with the remarkable and tuneable mechanical properties of the synthetic PLLA coating.

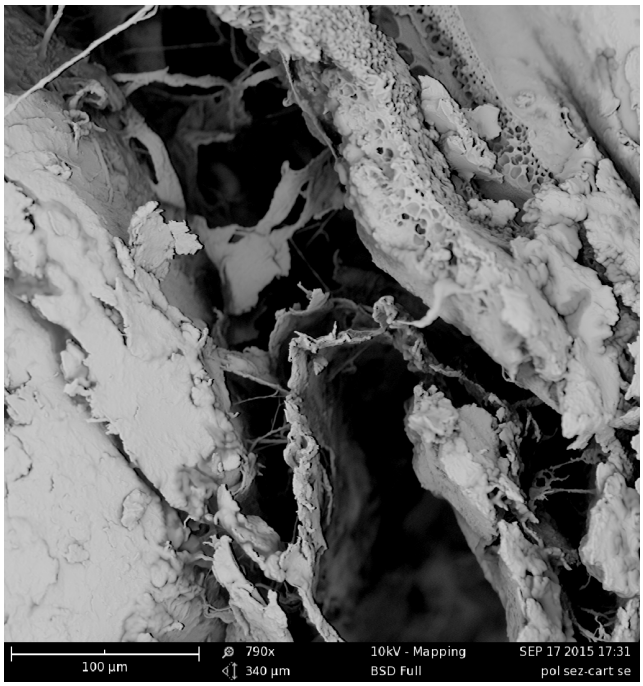

Figure 841: SEM of the delamination section.

Conclusion

The presented results show that SDS treatment is very effective in the removal of cellular components from soft tissues, despite modifies the mechanical properties of the tissue.

Tensile behaviour of native and decellularized tissues shows that the decellularization process leads to a significant loss of mechanical performance of about 30%. Tensile test of PLLA membrane and native tissue exhibit stress-strain curves with a concavity opposite.

A new method for the production of a bio-hybrid scaffolds (natural/synthetic) was designed and optimized. It had as first goal to increase the mechanical properties of decellularized tissue. The technology take advantage of the synthetic component (good mechanical properties) and natural tissue (comfortable environment to the cell growth). Furthermore, natural tissue and PLLA membrane seem to shows a mutual adhesion.

The proposed technological method allows to confer the following properties to the natural/synthetic three-dimensional scaffold:

- obtain a scaffold able to support growth and differentiation of the implanted cells;
- upswing of mechanical property of the biological tissue lost during the decellularization process;
- mechanical support to improve the transplant of the bioengineered tissues;
- maintains an internal aseptic environment when the tissue is exposed to outdoor environments.

References

[1] T.W. Gilbert, T.L. Sellaro, S.F. Badylak, “Decellularization of tissues and organs,” Biomaterials, vol.27, pp.3675-3683, 2006.

[2] L. Zhigang; L. Xinhua; Method for preparing an animal decellularized tissue matrix material and a decellularized tissue matrix material prepared thereby; Application number: WO2014CN78737 20140529.

[3] R.W. Grauss, M.G. Hazekamp, F. Oppenhuizen, C.J. van Munsteren, A.C. Gittenbergerde Groot, M.C. DeRuiter, “Histological evaluation of decellularised porcine aortic valves: matrix changes due to different decellularisation methods”, Eur J Cardiothorac Surg, vol. 27, pp. 566- 571, 2005.

[4] L. Peter I; L. Mengyan; P. Anat; P. Honesto; L. Philip; Three-dimensional scaffolds for tissue engineering made by processing complex extracts of natural extracellular matrices; Application number: US201414546534 20141118.

[5] R.B. Hirschi, R. Tooley, A. Parent, K. Johnson, R.H. Bartlett, “Evaluation of gas exchange, pulmonary compliance, and lung injury during total and partial liquid ventilation in the acute respiratory distress syndrome”, Crit. Care Med., vol. 24 pp. 1001-1008, 1996.

[6] O. Trabelsi, A.P. del Palomar, J.L. Lopez-Villalobos, A. Ginel, M. Doblare, “Experimental characterization and constitutive modeling of the mechanical behavior of the human trachea”, Medical Engineering and Physics, vol. 32 pp.76–82, 2010.

[7] S. Montesanto, G.A. Mannella, F. Carfì Pavia, V. La Carrubba, V. Brucato, “Coagulation bath composition and desiccation environments tuning parameters to prepare skinless membranes via diffusion induced phase separation,“ J. Appl. Polym. Sci., vol. 132, 2015.